Selected puzzles of tropical atmospheric variability

Gilles Bellon

Habilitation à Diriger des Recherches

Quelques mystères de la variabilité atmosphérique tropicale

(Selected puzzles of tropical atmospheric variability)

Gilles Bellon

Soutenue le 20 juin 2023

Jury :

Caroline Muller	Rapporteure
Cathy Hohenegger	Rapporteure
Fabio D'Andrea	Rapporteur
Jean-Philippe Duvel	Parrain
Jean-Pierre Chaboureau	Président

Université :	Université Paul Sabatier
École Doctorale :	Sciences de l'Univers, de l'Environnement et de l'Espace
Unité de recherche :	Centre National de Recherches Météorologiques (UMR 3589)

Contents

Summary

Tropical atmospheric climatology and variability is characterized by a strong interaction between diabatic processes and circulations. The main diabatic processes involved in this interaction are associated with clouds and its one spectacular result is how convective clouds often form clusters or ensembles on a wide range of spatial scales. This spatial organization of clouds is responsible for the development of an alternation of dry, subsiding regions and moist, convective, ascending regions in the tropics.

This manuscript reviews current and past research to understand and conceptualize the interaction between atmospheric diabatic processes and dynamics. In particular, it presents attempts to model this interaction in the simplest ways possible.

It also presents a number of tropical atmospheric phenomena due to a spontaneous spatial organization of clouds resulting from this interaction: self-aggregation of convective clouds in models and the intraseasonal modes of variability. The known and debated mechanisms giving rise to these phenomena are detailed.

In some features of the tropical climate, additional external influences or interactions, involving the surface or the extratropical atmosphere, are also at play in the spatial organization of convective clouds. This manuscript presents a few of these features, such as the Hadley circulation and tropical island climates.

Note:

Throughout the manuscript, studies co-authored with students and post-doctoral scientists under my supervision appear in cyan and other co-authored studies appear in teal.

1 Introduction

1.1 The tropical atmosphere in two columns

In middle school, students learn that there are two types of tropical climate: the arid, desertic type and the humid, rainforest type [1]. This basic knowledge already points to a large contrast in hydrologic cycle between different regions of the tropics, with a large degree of horizontal homogeneity within these regions. What middle-school students do not learn is that this contrast in hydrologic cycle is coupled to an atmospheric circulation, with ascending motion in rainy regions and subsidence in dry regions, and that the hydrologic cycle is intimately coupled to atmospheric dynamics. Moreover, this contrast in humidity and hydrologic cycle occurs not only on planetary scales, but also all the way down to mesoscales.

Such a humidity contrast between fairly homogeneous regions is characterized by a probability density function (PDF) of humidity that is bimodal. Indeed, Zhang et al. (2003) showed that the PDF of large-scale climatological *precipitable water* (PW) [2] is bimodal, as shown in Figure 1.1a. Each mode corresponds to one of the regions, dry (low values of PW) or moist (large values of PW). The PDF exhibits two maxima corresponding to the most likely values of PW in each region. This bimodality in the humidity PDF can also be observed at the mesoscale as shown by aircraft measurements (Fig. 1.1b, Zhang et al., 2003).

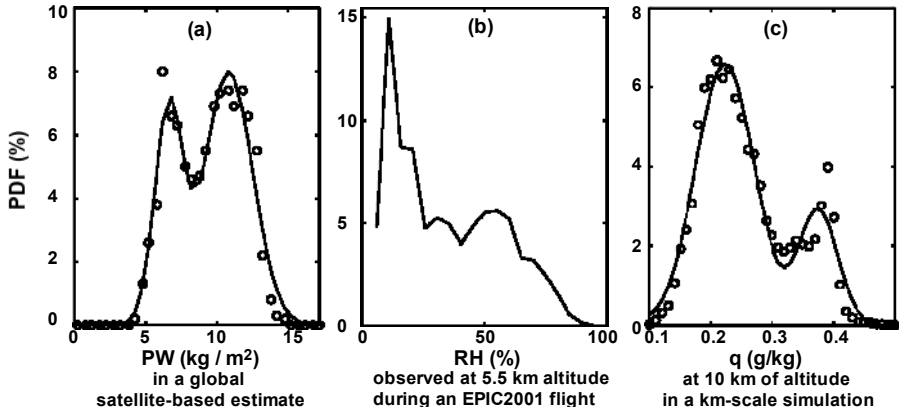

Figure 1.1: Examples of bimodality in the horizontal distribution of humidity: PDFs of (a) climatological March PW based on NASA Water Vapor Project data, (b) relative humidity measured during flights along 95W from the equator to 12N during the Eastern Pacic Investigation of Climate 2001 field campaign (EPIC2001) on 7, 14, 19, 23, 25 September and 2, 9, 10 October 2001, (c) specific humdidity in a simulation of convective self-aggregation from Tompkins (2001), with explicitly resolved deep convection. All panels are adapted from Zhang et al. (2003).

In fact, this bimodality of column humidity is a fundamental characteristic of the tropical atmosphere, at all horizontal scales: moist regions correspond to regions of organized convection and the surrounding regions are significantly drier. Figure 1.2 illustrates the different types of convective organization and the associated space and time scales: mesoscale convective systems (Houze, 2004) are ubiquitous in the deep tropics, synoptic-scale tropical storms and cyclones (Emanuel et al., 2003) are frequent, and equatorial waves, the Madden-Julian Oscillation (MJO), and tropical convergence zones have a planetary-scale signature. Convective organization and the characteristic bimodality of humidity PDF seem to be a little

[1] Sixth-grade curriculum / Programme de sixième, Thème 2 - Habiter un espace de faible densité

[2] PW is the vertically integrated mass of water vapor, per unit area, it is also called *column water vapor* (CWV)

less frequent at intermediate scales between the mesoscale and the synopic scale (Zhang et al., 2003), and between synoptic and planetary scales (Bellon et al., 2006).

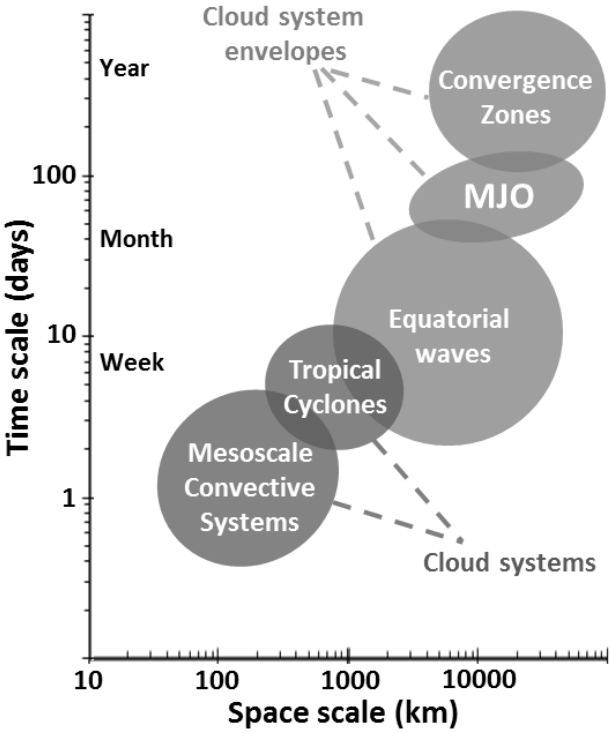

Figure 1.2: Types of convective organization and associated space and time scales; from Bellon & Bony (2020).

Modeling also suggests that the PDF of humidity is frequently bimodal in the tropics. In simulations using different types of models (storm-resolving and general-circulation models), a phenomenon called convective self-aggregation occurs in many configurations (Wing et al., 2018, and references therein): deep-convective clouds regroup in one or a few regions of the domain, moistening these regions and leaving the rest of the domain devoid of deep convection and dry. Meanwhile, an overturning circulation develops, with ascending motion in the moist region and subsidence in the dry region. In these simulations, the PDF of PW or other measures of humidity is bimodal as well, as illustrated in Figure 1.1c (Zhang et al., 2003; Tompkins, 2001; Bellon & Coppin, 2022; Coppin & Roehrig, 2022).

Such observational and modeling evidence supports modeling the tropical atmosphere in two columns, as shown in Figure 1.3: one ascending, moist, and convective, and the other subsiding and dry (Pierrehumbert, 1995; Miller, 1997; Clement & Seager, 1999; Bellon et al., 2003). These models of the tropical climate are essentially thermodynamic, based on the budgets of energy and water of the upper ocean, atmospheric boundary layer (ABL), and free troposphere in each column.

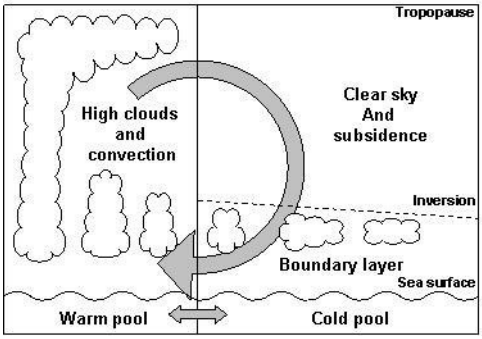

Figure 1.3: Schematic of a two-column model of the tropical climate, from Bellon et al. (2003).

In such models, the moist column is in an unstable state of runaway greenhouse effect: an increase in temperature results in an increase of humidity and cloudiness, which results in a decrease of the top-of-the-atmosphere net upward radiative flux because the increased greenhouse effect more than compensates the increase in cloud albedo. An increase in temperature therefore causes heating of the ocean-atmosphere column and consequently an additional increase in temperature, which yields an instability. The dry column, on the other hand, is very stable: thanks to the dry free troposphere, any increase in temperature is efficiently damped by an increased infra-red emission to space. Such models of the tropical climate explain its stability by the coupling between the columns through the overturning circulation: the excess energy in the moist column is exported to the dry column – mostly in the form of potential energy – where it is radiated to space. In terms of moisture budget, the circulation transports moisture from the dry column to the moist column where it is rained out.

These two-column models of the tropical climate exhibit a strong, robust sensitivity to the relative area of the columns (Pierrehumbert, 1995; Miller, 1997; Clement & Seager, 1999;Bellon et al., 2003): an expansion of the relative size of the dry column has a significant cooling effect on the overall tropical climate. These sensitivities are directly connected to current debates on the expansion of the Hadley cells (Hu & Fu, 2007; Staten et al., 2018) and tightening of the Intertropical Convergence Zone (ITCZ, Su et al., 2017), which correspond to an increase in the relative size of the dry regions in the whole tropics.

In fine, this sensitivity and the potential feedbacks that it provides to the climate system should be evaluated using climate models. But doing so with current models appears challenging, since cloud systems and tropical convergence zones are not particularly well simulated by state-of-the-art models. As an example, Figure 1.4 shows the tropical climatological precipitation simulated by the CNRM-CM6 (which was used to produce the CMIP6 simulations). This model exhibits significant precipitation biases both over land and over ocean, up to half the climatological precipitation, and the spatial distribution of moist and dry regions exhibits significant biases.

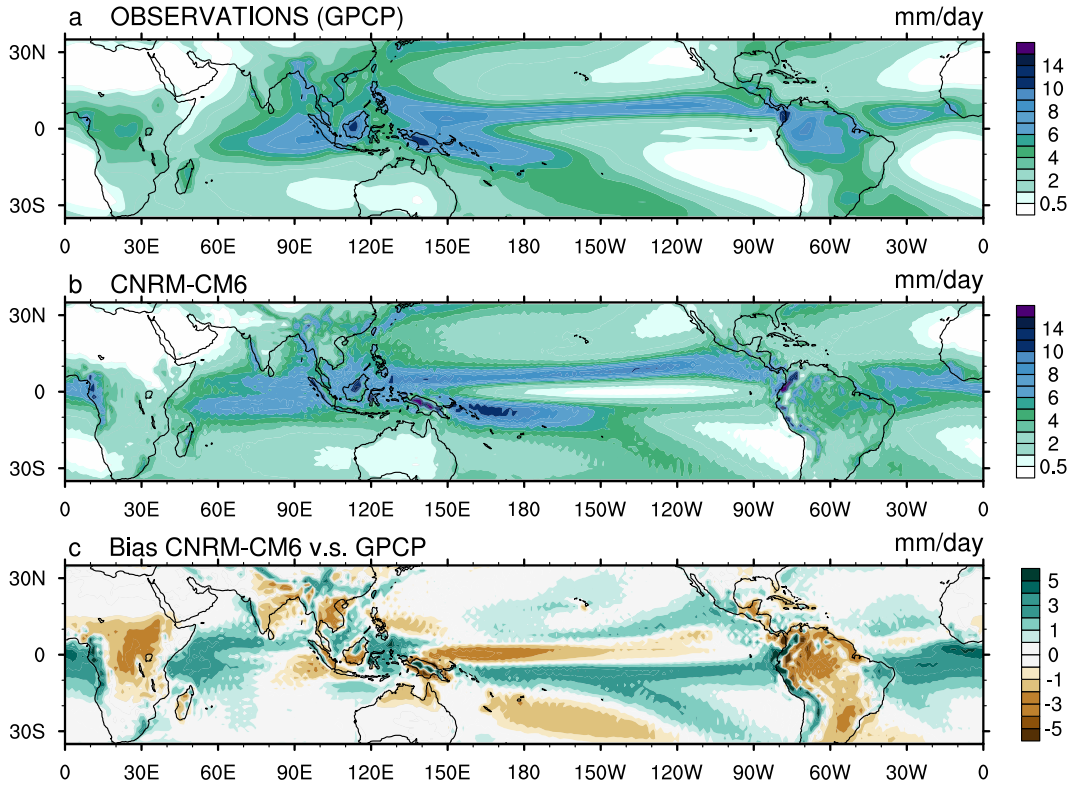

Figure 1.4: Climatological precipitation for the period 1980-2014 in (a) observations (GPCP), (b) CNRM-CM6, and (c) their difference.

My PhD project investigated the sensitivity of a two-column model to perturbations of the radiative properties of the atmosphere and Sun. This work led to the realization that one of the main challenges for these models is to understand what controls the relative area of moist and dry columns. How does the interaction between moist thermodynamics and fluid dynamics determine where the moist regions

start and end, and how does it evolve in time? Unfortunately, the two-column framework is insufficient to address this question [3], which requires an understanding of the basics of tropical geophysical fluid dynamics and cloud thermodynamics and needs to build on a significant existing body of work. The next few sections will attempt to summarize this knowledge.

1.2 A few basic equations

At the scales of interest (meters and larger), the atmosphere can be described using the anelastic equations, which are the Navier-Stokes equations simplified using the fact that the air is not very compressible so that density does not depart much from a reference profile $\rho_0(z)$. Here, we present them in the tangent plane approximation:

- Horizontal momentum equation:

$$\frac{D\mathbf{u}}{Dt} + f\hat{\mathbf{k}} \times \mathbf{u} = -\frac{1}{\rho_0}\nabla p + Q_{\mathbf{u}}, \tag{1.1}$$

- Vertical momentum equation:

$$\frac{Dw}{Dt} + fu = -\frac{\rho}{\rho_0}g - \frac{1}{\rho_0}\partial_z p + Q_w, \tag{1.2}$$

- Continuity:

$$\rho_0 \nabla \cdot \mathbf{u} + \partial_z(\rho_0 w) = 0, \tag{1.3}$$

- Equation of state:

$$p = \rho R_a T_\rho \tag{1.4}$$

- Thermodynamic equation:

$$\frac{D\theta}{Dt} = \frac{\theta}{T}\frac{Q_1}{c_p}, \tag{1.5}$$

with the usual notations: $\mathbf{u}$ the horizontal wind, w the vertical velocity, p the pressure, ρ the density, T the absolute temperature, $\theta = T/\Pi$ the potential temperature with Π the Exner function [4], and T_ρ the density temperature, also called virtual temperature. $\frac{D}{Dt} = \partial_t + \mathbf{u} \cdot \nabla + w\partial_z$ is the total (Lagrangian) time derivative, ∇ is the horizontal nabla operator, $f = 2\Omega \sin\phi$ is the Coriolis parameter (with Ω the frequency of the Earth rotation and ϕ the latitude), $\hat{\mathbf{k}}$ the vertical unit vector, g the acceleration of gravity, R_a is the gas constant for dry air, and c_p is the heat capacity of air. $Q_{\mathbf{u}}$ (sometimes writen Q_3) and Q_w are the terms of horizontal- and vertical-momentum transport at scales smaller than the scales under consideration. In the original Navier-Stokes equations, $Q_{\mathbf{u}} = \nu\left[\nabla^2\mathbf{u} + 1/3\nabla(\nabla \cdot \mathbf{u})\right]$, with ν the viscosity, and Q_w follows the same formulation; in the atmosphere, the effect of viscosity in small except in the surface layer and $Q_{\mathbf{u}}$ and Q_w include turbulent and convective momentum transports. Q_1 is the diabatic heating resulting from phase changes (Q_l), radiation (Q_r), and transport at scales smaller than the scales under consideration (Q_{1t}):

$$Q_1 = Q_l + Q_r + Q_{1t}. \tag{1.6}$$

Q_1 provides the primary coupling between dynamics and hydrologic cycle.

Another effect of the hydrologic cycle on dynamics results from the influence of water species on the density temperature T_ρ, which depends on T, but also on the humidity and water condensate:

$$T_\rho = T\left(1 + \epsilon_1 q_v - q_c\right), \tag{1.7}$$

with q_v the specific humidity, q_c the specific content of water condensate, $\epsilon_1 = R_v/R_a - 1$ with R_v the gas constant for water vapor. Often neglected for large-scale theoretical work and analyses, this effect is significant were buoyancy processes are crucial (Yang, 2018b).

[3] An attempt in Bellon et al. (2006) is less revealing of the physics of this problem than of the naiveté of one PhD student.

[4] $\Pi = \left(\frac{p}{p_{00}}\right)^{R_a/c_p}$ with p_{00} a reference pressure

For moisture, the budget can be written:

$$\frac{Dq_v}{Dt} = -\frac{Q_2}{L}, \tag{1.8}$$

with q_v the specific humidity and Q_2 the latent-heat sink, which results from phase changes (Q_l) and small-scale transport (Q_{2t}):

$$Q_2 = Q_l + Q_{2t}. \tag{1.9}$$

L is the latent heat of phase changes: it is the latent heat of vaporization L_v for condensation/evaporation and the latent heat of sublimation L_s for deposition/sublimation.

These equations (1.1-1.8), or some slightly improved ones (e.g., Durran, 1989) are used in high-resolution models (with horizontal resolutions from meters to kilometers). Kilometer-resolution models that can resolve ensembles of convective clouds or convective storms; this type of models is now called *storm-resolving model* (SRM) [5], in which "storm" is to be understood as a mesoscale storm or thunderstorm, rather than a synoptic storm. I will present some results from such models.

At large scales (synoptic to planetary scales), scale analysis reveals that the terms in blue in Equation (1.2) are negligible. Neglecting them is called the *hydrostatic approximation*: $\partial_z p = -\rho g$, and yields the *primitive equations*, which are the basis of global *general-circulation models* (GCMs), which are the building blocks of climate models. At these scales, the subgrid-scale energy and moisture transport Q_{1t} and Q_{2t} include convective and mesoscale transport and can be very significant. At these large scales, the dominant terms in energy and water budgets (1.5) and (1.8) are between diabatic sources/sinks and vertical advection. In particular, since horizontal temperature gradients are small in the tropical free troposphere, horizontal advection in (1.5) is small as well; neglecting this advective term corresponds to the weak-temperature-gradient (WTG) approximation (a lot more details on this approximation will be given in Section 1.7.4).

From Equations (1.1)-(1.5), we can point out two fundamental differences between extratropical dynamics and tropical dynamics. First, the effect of rotation is weaker: the Coriolis parameter f varies as the sine of the latitude, and is therefore smaller in the tropics than in the midlatitudes. f even changes sign at the equator, which tends to make the effect of rotation more complex than in the extratropics. Second, as the atmosphere is warmer in the tropics, tropical air contains more water vapor and is prone to releasing large amounts of latent heat in clouds: Q_1 can be very large, and diabatic effects on the dynamics are dominant. In terms of theoretical developments, whereas scale analysis provides a balance (geostrophy) and a set of asymptotic equations (quasi-geostrophic equations) for the extratropics, there is no equivalent balance in the tropics, although two asymptotic regimes can be identified by scale analysis (Yano & Bonazzola, 2009) and found for synoptic wavelengths in simplified models (Ahmed et al., 2021): a regime dominated by the variability of temperature (wave dynamics) and one dominated by moisture variability (balanced dynamics/moisture waves).

Finally, the equation for horizontal momentum (1.1) can also be written in terms of divergence $\delta = \nabla \cdot \mathbf{u}$ and vorticity $\zeta = \partial_x v - \partial_y u$, which is the vertical component of the curl of the horizontal wind. Some of our analyses will make use of these equations rather instead of (1.1). Divergence is directly related to vertical motion via the continuity equation (1.3) and therefore to the convective processes; its equation of time evolution is fairly complex:

$$\frac{\partial \delta}{\partial t} + \frac{1}{2}\nabla^2 \mathbf{u}^2 + \partial_z \mathbf{u} \cdot \nabla w + \hat{\mathbf{k}} \cdot [\mathbf{u} \times \nabla(\zeta + f)] - \zeta(\zeta + f) = -\frac{1}{\rho_0}\nabla^2 p + Q_\delta. \tag{1.10}$$

The vorticity equation is simpler, especially if written in terms of the absolute vorticity $\zeta + f$:

$$\frac{D(\zeta + f)}{Dt} + (\zeta + f)\delta - \partial_z \mathbf{u} \times \nabla w = Q_\zeta; \tag{1.11}$$

The second term on the left-hand side is called the stretching term and the third is called the tilting term. Q_δ and Q_ζ result from the momentum transport at scales smaller than the scales under consideration.

1.3 Diabatic heating: the key to large-scale modeling

Although the contribution of water to the density temperature can be significant at cloud-scale and mesoscale (Yang, 2018b), this contribution is smaller and is often neglected at large scales; density

[5] it was called cloud-resolving model for a long time and is also called convection-permitting model

temperature can be approximated by the temperature: $T_\rho \approx T$. This reduces the interaction between the hydrologic cycle and dynamics to the diabatic heating Q_1. Provided accurate initial conditions and accurate Q_1, large-scale circulations can be computed numerically. For GCM development, simulating Q_1 is a major challenge, because most diabatic processes occur on scale smaller than the GCM resolutions.

Clouds are major contributors to Q_1 and its horizontal gradients, because the latent heating Q_l is its largest component and occurs exclusively in clouds, and because clear-sky radiative heating vary more smoothly on the horizontal than cloud radiative heating. Figure 1.5 shows typical Q_l, Q_r, and Q_{1t} profiles associated with different types of clouds.

Low clouds are not usually associated with significant surface rain (except for the deepest cumuli). Among these, stratocumuli are characterized by a large cloud fraction and strong terrestrial cooling at cloud top, somewhat mitigated by solar warming. This cooling powers strong ABL turbulence, which redistributes energy throughout the ABL. In cumulus clouds, shallow convection causes latent heating and compensating mixing; radiation is a second-order term. In congestus and deep-convective clouds, latent heating is dominant, with a maximum at mid-height in the cloud and a large fraction of the resulting condensate precipitates all the way to the surface. Stratiform precipitating clouds are characterized by latent heating in the cloud and latent cooling under the cloud because of the re-evaporation of falling precipitation, which also reduces surface rainfall. Non-precipitating anvil clouds are characterized by small latent heating. The radiative effect of congestus, deep-convective, stratiform and anvil clouds is moderate, dominated by the terrestrial contribution with cooling in the upper part of clouds and warming in the lower part.

The diabatic heating in each cloud creates a circulation with a specific vertical structure, which is given at first order by the vertical structure of the diabatic heating [6]. In particular, the diabatic heating in deep convective clouds creates or amplifies a first-baroclinic, troposphere-deep circulation with ascent in the convective region and descent in the surrounding regions. Stratiform precipitating clouds create second-baroclinic circulations with ascent in the upper troposphere and descent in the lower troposphere in the cloud region and opposite vertical motion in the surrounding regions. Stratiform precipitating clouds occur mostly around deep convective clouds, and the combination of the two cloud types often creates a circulation with maximum ascent in the cloudy upper troposphere, sometimes called "top-heavy" circulations. In non-convective regions, intense cooling at the top of stratocumulus clouds can create shallow circulations which are instrumental in spatially organizing convection in some models (Muller & Held, 2012), although clear-sky effects appear to cause such circulations in other models (Bellon & Coppin, 2022).

From a GCM or large-scale modeler's perspective, a correct simulation of the diabatic forcing Q_1 requires a correct simulation of cloud populations and associated diabatic heating profiles. Correctly simulating the other contributions to diabatic heating, such as the small-scale transport that redistributes the surface forcing to the lower troposphere, is also necessary, as we will see in Section 1.8, but probably not as problematic at this point in time. Theses contributions to Q_1 are computed by the physical parameterizations or "physics" of GCMs while the circulation response is computed by the "dynamics" of the models. The diversity of clouds and complexity of the processes at play in their life cycles hint that the development of physical parameterizations is a challenge. Indeed, current parameterizations are very elaborate but there are still the source of major biases in the state-of-the-art climate models.

[6] assuming the WTG approximation is roughly verified and the vertical gradient of potential temperature does not vary too much on the vertical

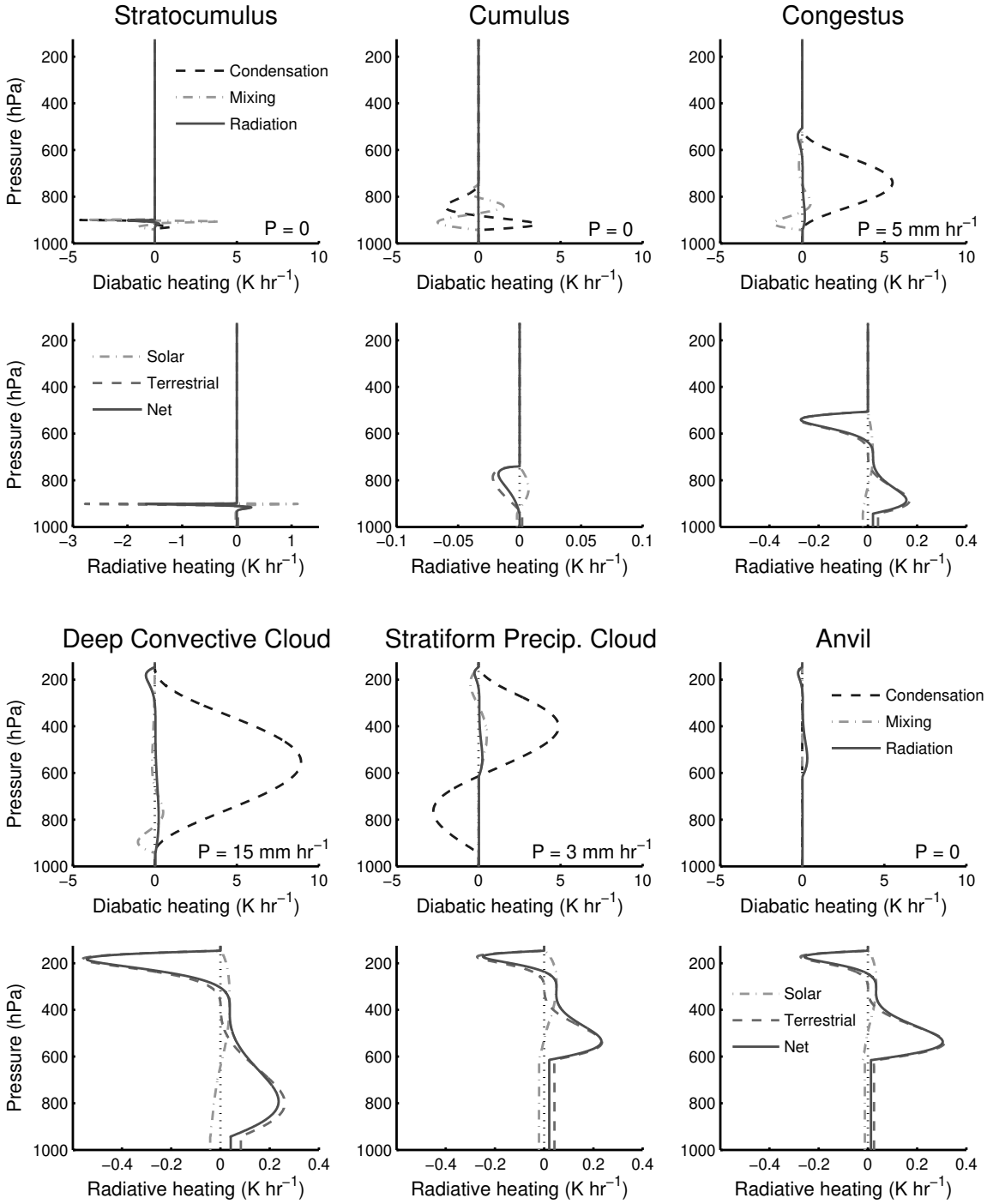

Figure 1.5: Typical profiles of diabatic heating in clouds of different types; first and third rows: latent heating Q_l (dashed lines), small-scale transport Q_{1t} (dash-dotted lines), and total radiative heating Q_r (solid lines); typical surface precipitation rates are indicated in each panel; second and fourth rows: total radiative heating (solid lines), solar (dash-dotted lines) and terrestrial (dashed lines) contributions; adapted from Bellon & Bony (2020).

1.4 Diagnostic tools: Moist static energy and stability

At least for diagnostic purposes, this issue of diabatic heating can be somewhat simplified by considering all thermodynamic energy (thermal plus latent) as one quantity rather than two. This allows us to ignore phase changes, because they cause only latent heating, which is a transfer between the thermal and latent reservoirs.

If the hydrostatic approximation is used and the effect of humidity on density is neglected in the hydrostatic balance, the thermodynamic equation (1.5) can be rewritten in terms of *dry static energy* $s = c_p T + gz$:

$$\frac{Ds}{Dt} = Q_1. \tag{1.12}$$

If we assume, for simplicity, that the only water condensate is liquid, Equation (1.12) can be combined with the humidity equation (1.8) to obtain an equation in terms of *moist static energy* (MSE) $h = s + L_v q_v$ [7]:

$$\frac{Dh}{Dt} = Q_1 - Q_2 = Q_r + Q_{1t} - Q_{2t}, \tag{1.13}$$

with $Q_{1t} - Q_{2t}$ the small-scale transport of MSE. At first sight, the advantage of MSE as a thermodynamic variable is evident: it comprises the thermal, potential, and latent energy of the air and thus is not affected by phase changes or precipitation. In practice, this means that the latent heating Q_l, which is one of the most difficult terms of the heat budget to model, does not have to be calculated or estimated to compute the change in MSE. This might suggest that we can therefore ignore all cloud processes, but it is not quite true, because cloud effects on radiation are significant and included in Q_r and because convective mixing contributes to Q_{1t} and Q_{2t}.

But, since the small-scale transport is almost exclusively vertical, we can write a simple expression for the vertical integral of MSE:

$$\partial_t [h] = -[\nabla \cdot (\mathbf{u}h)] + \Delta R + LHF + SHF, \tag{1.14}$$

with $[\,]$ indicating mass-weighted vertical integration over the atmosphere, ΔR the convergence of radiative flux across the atmosphere (i.e., the difference between surface and top-of-atmosphere net upward radiative fluxes), LHF the surface turbulent latent heat flux, and SHF the surface turbulent sensible heat flux. The vertical integration boils down small-scale transport to the surface turbulent heat fluxes, which are easier to model than local transport terms.

This vertically integrated MSE is a useful metric to describe perturbations in the tropical atmosphere. Indeed, convective disturbances are warmer and moister over the whole depth of the troposphere and are therefore characterized by a local maximum of vertically integrated MSE. If we consider a convective disturbance, its development and propagation can be described using the vertically integrated MSE. And the budget of vertically integrated MSE can be used to identify sources of instability and propagation of the disturbance among a limited set of candidates: transport, radiation, and turbulent surface fluxes.

The horizontal variance of the vertically integrated MSE is also a common metric of the inhomogeneity of a region or domain of interest. In particular, it is used as a metric of convective aggregation. The budget of MSE (1.14) allows us to write the tendency of this variance as the sum of contributions from different physical processes (Wing & Emanuel, 2014):

$$\partial_t \overline{[h]'^2} = -2\overline{[h]'[\nabla \cdot (\mathbf{u}h)]'} + 2\overline{[h]'\Delta R'} + \overline{[h]' LHF'} + \overline{[h]' SHF'}, \tag{1.15}$$

in which we can see that there are contributions from transport, from radiation, and from turbulent surface heat fluxes. The radiative term can be further decomposed into a surface and a top-of-atmosphere components and/or into solar and terrestrial components. This diagnostic is used in particular to analyse convective self-aggregation, since aggregated convection corresponds to much larger horizontal variance of $[h]$ than non-aggregated convection.

Understanding the role of MSE transport has received particular attention, as a way to interpret, understand, and simplify the interaction between the moist thermodynamics and the dynamics of the tropical atmosphere. Because vertical advection is dominant over horizontal advection, the latter is often neglected:

$$[\nabla \cdot (\mathbf{u}h)] = [w\partial_z h] + [\mathbf{u} \cdot \nabla h] \approx [w\partial_z h]. \tag{1.16}$$

[7] If freezing cannot be neglected, a slightly different variable, the *frozen* moist static energy $h = s + L_v q_v - L_f q_i$ can be defined to obtain a similarly simple budget. The main complication is that frozen precipitation cannot be neglected, which is a problem when considering the upper troposphere, but not so much when considering the vertical integral in the tropics since surface precipitation is overwhelmingly liquid.

Furthermore, if the vertical velocity can be assumed to have a fixed profile $\mathcal{W}(z)$, for example a top-heavy profile associated with mature convective disturbances, the vertical velocity can be written $w = W(x, y, t)\mathcal{W}(z)$, with W encapsulating the horizontal and temporal variations of the intensity of vertical motion, and the vertically-integrated MSE transport can be further simplified:

$$[\nabla \cdot (\mathbf{u}h)] \approx [w\partial_z h] = W\Gamma_m, \tag{1.17}$$

$\Gamma_m = [\mathcal{W}\partial_z h]$ is the *gross moist stability* (GMS), first introduced by Neelin & Held (1987) which formalized the finding that the vertical motion in the tropics is constrained by the heat budget of the atmospheric columns.

If MSE horizontal advection is not negligible or if the profile of vertical velocity varies, the definition of the GMS is still possible but more complex. To address the issue of the variability of the vertical profile, this variability can be decomposed into vertical modes, with a GMS for each mode. In the most general case, the *normalized gross moist stability* (NGMS) can always be defined as the vertically integrated MSE export divided by the vertically integrated moisture import $-[\nabla\cdot(\mathbf{u}h)]/[\nabla\cdot(\mathbf{u}q_v)]$ (Raymond et al., 2009).

If the (normalized) GMS is positive, it means that ascent exports MSE from the atmospheric column. Conversely, if the GMS is negative, ascent imports MSE into the column. Since convective disturbances are associated with a maximum of both vertically integrated MSE and ascending motion, the sign of the GMS determines the sign of the feedback of circulation on convection: a positive GMS corresponds to a negative transport feedback (the circulation damps the convective disturbance) and vice-versa.

The typical profile of MSE in the tropics has a minimum in the mid-troposphere because the vertical decrease of latent heat $L_v q_v$ is dominant in the lower troposphere and the increase of potential energy Φ is dominant in the upper troposphere. As a result, the GMS is negative for shallow circulations, with opposite winds in the boundary layer and in the lower free troposphere. Such circulations are observed in some tropical convergence zones (Zhang et al., 2004, 2008) and they are instrumental to self-aggregation in many models (Muller & Held, 2012). As another result, the GMS is negative for second-baroclinic circulations resulting from stratiform heating. Finally, the GMS is generally positive but small for first-baroclinic circulations associated with deep convection, which means that a deep convective perturbation is generally damped by the transport feedback. The evolving combination of shallow, first-, and second-baroclinic circulations throughout the life cycle of a convective disturbance can cause a significant change of GMS and even a change in its sign (Inoue & Back, 2017).

Reasoning based on GMS can become complicated because of horizontal advection and details of the vertical profiles. The simple feedback analysis above also relies on assuming ascent and convection to be colocated, which is mostly the case but the intensity and profiles of ascent may not change in lock with convection. Overall, GMS is a useful analysis tool that bypasses the need to understand or simulate convection and cloud populations in order to estimate or simulate diabatic heating, but it is safer to understand its limitations before using such a tool.

1.5 A few simple solutions to the dynamics equations

Now, what if the diabatic heating were known? As pointed out at the beginning of Section 1.3, this would allow us to integrate the equations of large-scale motion numerically. However, this does not mean that it would allow us to understand tropical circulations in a simple way. Nonetheless, if we consider that winds and temperature perturbations have small amplitudes, the primitive equations (1.1)-(1.5) with the hydrostatic approximation can be linearized about a state of rest with horizontally uniform thermodynamic fields, which have semi-analytical solutions in the form of series.

The linear primitive equations can be projected onto vertical modes [8] and the equations for each mode reduce to the well-known linear Saint-Venant (or shallow-water) equations:

$$\partial_t \mathbf{u} + f\hat{\mathbf{k}} \times \mathbf{u} = -g\nabla h - \epsilon\mathbf{u}, \tag{1.18}$$

$$g\partial_t h + c^2\,\nabla \cdot \mathbf{u} = Q - \mu g h. \tag{1.19}$$

The small-scale momentum transport is modeled as a linear damping term (in blue), called Rayleigh damping. The diabatic heating is transformed into the sum of a mass source Q (in red) and a linear damping term (in blue) called Newtonian cooling. c is the gravity wave speed, which depends on the

[8] Linearized Equations (1.2), (1.4), and (1.5) can be combined into an expression for $\partial_z(\rho_0 w)$ as the sum of a linear differential operator applied to p/ρ_0 and another linear operator applied to Q_1, both involving the reference thermodynamic profiles. The vertical modes are the eigenmodes of the operator applied to p/ρ_0.

vertical mode. In the Saint-Venant equations, this gravity wave speed is related to the reference-state depth H: $c^2 = gH$, so c^2/g is referred to as the effective depth of the mode. The vertical modes can be classified by the number of sign changes n in the vertical profile of the horizontal wind: $n = 0$ is the barotropic mode, $n = 1$ the first baroclinic mode, etc. The first baroclinic mode depicts winds in opposite directions at the top and bottom of the troposphere and therefore deep overturning circulations; for this mode, h is a proxy for the mid-tropospheric temperature, which further explains why the response to deep-convective heating is along this mode, as mentioned in the previous sections. The linear momentum damping term $-\epsilon\mathbf{u}$ can be understood as resulting from small-scale transport, including turbulent transport. If Q is imposed, the linear damping term $-\mu gh$ can be interpreted as the first-order, linear response of the thermodynamics to the imposed heating. The damping rates ϵ and μ depend on the vertical mode. Equations (1.18) and (1.19) are the basis of two seminal theoretical works on the tropical circulation and its variability (Matsuno, 1966; Gill, 1980).

Matsuno (1966) solved the problem of free waves (i.e., with neither heating nor damping) on the equatorial β-plane [9]. He discovered the equatorial gravity waves: Kelvin, Rossby, Mixed Rossby-gravity, and inertio-gravity waves. These have been observed in the stratosphere (Yanai & Maruyama, 1966; Wunsch & Gill, 1976) and ocean (Wunsch & Gill, 1976). More surprisingly, waves with the same structure but coupled to convection are observed in the troposphere (Wheeler & Kiladis, 1999); this means that the coupling between circulation and convection for these phenomena does not modify their structures. Figure 1.6 shows the power spectra of the subseasonal variability of convection in the tropical atmosphere. A large part of this variability follows the dispersion relationships of theoretically derived, dry equatorial waves (red lines).

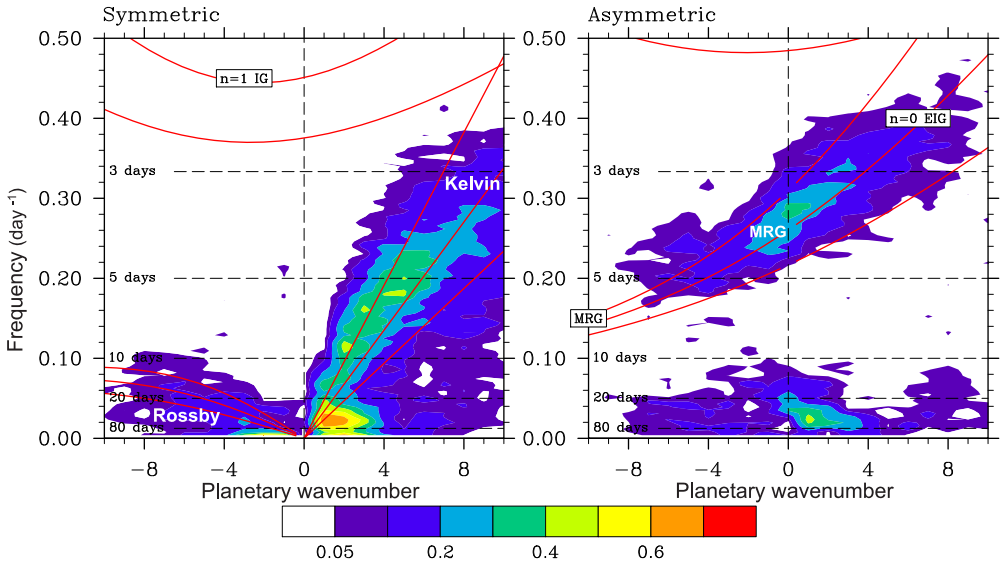

Figure 1.6: Spectra of equatorial (10°S – 10°N) subseasonal variability (on timescales shorter than 3 months, shadings) based on the Outgoing Longwave Radiation (OLR) at the top of the atmosphere and the zonal wind; red lines indicate the dispersion relationships of Matsuno (1966)'s solutions with effective depth of 12, 25, and 50 m.

This similarity between the convectively coupled waves and the dry waves results from: (i) most of the diabatic heating Q_1 in these waves resulting from condensation in clouds and (ii) the main balance in the water-vapor budget (Eq. (1.8)) associated to these waves is between vertical advection and condensation; As a result, $Q_1 \approx -Q_2 \approx Lw\partial_z q$ can be replaced in linearized Equation (1.5), which shows that the effect of humidity is essentially to reduce the effect of thermal vertical stratification, i.e. reduce the phase speed for all modes [10]. This also means that there is little moisture storage ($\partial_t q_v << Q_2$) in convectively coupled equatorial waves: the temperature or thermal-energy variability is dominant over the moisture or latent-heat variability, which corresponds to the wave-dynamics asymptotic regime (Yano & Bonazzola,

[9] A β-plane is a plane tangent to the surface of the Earth at the location of interest on which the Coriolis parameter f is considered to vary linearly with the meridional distance to the point of interest: $f = f_0 + \beta y$; for the equatorial β-plane, $f = \beta y$. Considering a β-plane neglects the curvature of the Earth but retains the variation of the Coriolis parameter with latitude at first order.

[10] Another way to express this is to state that stratification matters in terms of MSE, not in terms of dry static energy

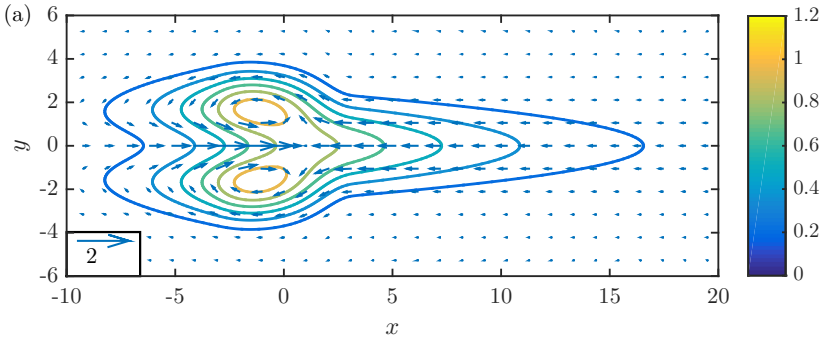

Figure 1.7: Non-dimensional mid-tropospheric temperature perturbation (contours) and low-level winds (vectors) for Gill circulation in response to a diabatic heating symmetric about the equator. x is the distance in longitude from the center of diabatic heating and y the distance from the equator in latitude on the β-plane, in thousands kilometers; adapted from Reboredo & Bellon (2022).

2009; Ahmed et al., 2021).

If the diabatic term Q in (1.19) is modelled as a linear function of temperature (or h) and humidity, and a linear version of the humidity equation (1.8) is added to (1.18) and (1.19), an additional set of solution called *moisture modes* can be identified (Neelin & Yu, 1994; Sobel et al., 2001; Sugiyama, 2009), which are characterized by a significant variability of humidity ($\partial_t q_v$ is not negligible). Some of these solutions are close to the balanced-dynamics asymptotic regime (Yano & Bonazzola, 2009; Ahmed et al., 2021), in which moisture variability dominates temperature variability.

Gill (1980) presented some solutions to the steady, damped flow in response to a steady diabatic heating, i.e. to Equations (1.18)-(1.19) with time derivatives set to zero [11]. One of these solutions is shown in Figure 1.7, for an almost circular heating centered on $(x, y) = (0, 0)$, with a radius of 3,000 kilometers. It features two cyclonic gyres straddling the equator just west of the heating center, with two maxima of temperature at their centers, and easterlies extending east of the heating. The Gill circulation, as this is known, was initially intended to explain the longitudinal asymmetry of the Walker circulation in the Indo-Pacific, powered by mid-tropospheric latent heat release above the warm pool. It has also been shown relevant to the details of the spatial distribution of tropical precipitation (Adam, 2018), to interannual variability in the Pacific (Pazan & Meyers, 1982; Philander, 1983), and to superrotation on tide-locked exoplanets (Showman & Polvani, 2010, 2011; Pierrehumbert & Hammond, 2019).

These simple solutions to simplified dynamical equations have been very useful in understanding and analyzing the observed tropical atmosphere. However, they either neglect or impose diabatic heating and fall short of addressing the interaction between dynamics and moist thermodynamics. To go beyond these simplifications, interactive diabatic heating needs to be modeled. As mentioned above, most of Q_1 and its spatial contrasts results from convective clouds. For a better grasp of cloud heating in the tropical atmosphere, the next section presents basic elements on moist convection.

1.6 Convection basics

Atmospheric convection is a complex phenomenon involving multiple small scales which I do not claim to understand well and is very well explained in other publications (e.g., Emanuel et al., 1994b; Stevens, 2005). This section is only intended to provide some definitions and basic concepts useful to describe the main controls on the development of convection and its intensity, and understand subsequent sections of this manuscript.

Atmospheric convection occurs as a response to the instability of the thermodynamic profiles, i.e., if an air parcel displaced upwards adiabatically becomes more buoyant (i.e., less dense) than parcels at its new altitude. Moist convection occurs as a response to *conditional instability*, i.e. if the thermodynamic profiles are stable to dry adiabatic displacements but unstable to adiabatic displacements that involve phase change. Note that, to simplify, we often assume that vertical displacements are too fast to let the parcel change its energy through diabatic processes.

[11] Gill (1980) also uses the same damping rate for momentum and thermodynamics: $\mu = \epsilon$.

In practice, conditional instability occurs for near-surface air parcels, so that convection occurs either within the atmospheric boundary layer (shallow convection), creating small cumuli, or throughout the troposphere (deep convection), within cumulonimbi, although some convection tops at the level of freezing, creating congesti (Johnson et al., 1999).

Let's consider an atmospheric column with the typical profile of density temperature shown in Figure 1.8 (red profile) a parcel lifted adiabatically from the boundary layer would have the density temperature shown by the black profile. It would follow a dry adiabat up to the *lifting condensation level* (LCL) where it temperature reaches the dewpoint temperature (green profile) and condensation starts. Above, it would follow a moist adiabat which assumes no mixing with the cloud environment occurs and that all water condensate precipitates immediately. In most cases, the adiabatically lifted parcel is less buoyant than the column profile in the lower troposphere. In our example, it becomes more buoyant than its environment, at an altitude called the *level of free convection* (LFC) and it stays buoyant up to the *level of neutral buoyancy* (LNB) in the upper troposphere. Under the LFC, buoyancy force opposes the upward motion of the near-surface air parcel; the work exerted by the buoyancy force on a parcel that rises adiabatically from near the surface to the LFC is proportional to the integral of the difference between the virtual temperature of the parcel and that of its environment. The opposite of this work is called *convective inhibition* (CIN) and it is represented by the area in blue. Above the LFC, the buoyancy force is upward and its work between the LFC and LNB is called *convective available potential energy* (CAPE), represented by the area in orange. Above the LNB, the buoyancy force is downward again.

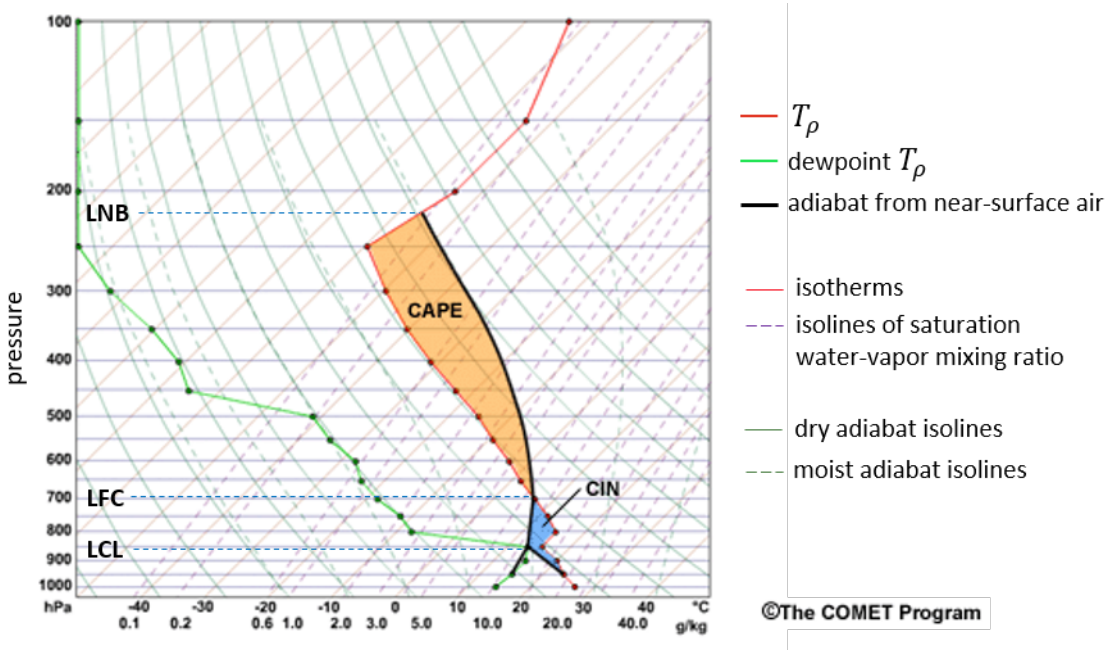

Figure 1.8: Skew-T diagram showing the density temperature profile of an atmospheric column (red line) as well as the density temperature of an adiabatically lifted boundary-layer air parcel (thick black line), as well as the convective inhibition (CIN), the convective available potential energy (CAPE), and the characteristic vertical levels: lifting condensation level (LCL), level of free convection (LFC), and level of neutral buoyancy (LNB); adapted from The COMET Program.

A near-surface air parcel that has an upward vertical speed corresponding to a kinetic energy equal to the CIN can reach the LFC and continue upward to the upper troposphere, accelerating up to the LNB and decelerating above: deep convection occurs. Otherwise, convection is limited to the boundary layer (shallow convection). Turbulence in the boundary layer creates updrafts with some kinetic energy that can overcome a small CIN, but significant CIN efficiently inhibits deep convection. For example, in the trade-wind shallow-cumulus regions, the temperature inversion at the top of the ABL corresponds to a large CIN and these regions seldom experience deep convection. Surface heat fluxes (sensible and latent) increase near-surface buoyancy and decrease CIN (the black line of the adiabat on Fig. 1.8 moves to the right). Large-scale ascent also decreases CIN by cooling the inhibiting layer. Cold-pool, frontal and orographic dynamics can also lift the boundary-layer air and overcome CIN. If deep convection is triggered, the parcel accelerates from the LFC to the LNB, gaining kinetic energy equal to the CAPE.

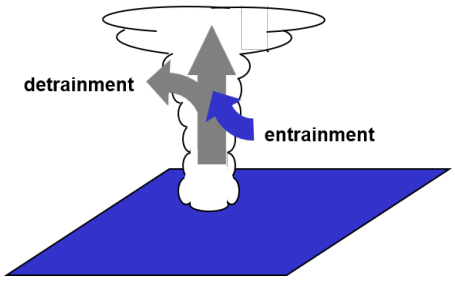

Figure 1.9: Schematic of a cloudy updraft.

Above the LNB, the parcel decelerates in what is called the *overshoot*.

We need to point out the main limitation of this idealized framework, which is the adiabatic and no-condensate assumptions. The overwhelming majority of updrafts are influenced by non-conservative processes, and particularly mixing and precipitation. Above the LFC, entrainment of air from the cloud environment into the cloud reduces the cloud-environment thermodynamic contrast and decreases the in-cloud buoyancy (see Figure 1.9 for a schematic of entrainment and detrainment). Precipitation does not remove water condensate from the convective cloud instantly and condensate's weight reduce the parcel's buoyancy. Assuming that all water condensate precipitates immediately overestimates the cloudy parcel's buoyancy [12]. The CAPE is therefore an upper bound on the work of the buoyancy force between LFC and LNB. By introducing more realistic assumptions on updraft thermodynamic profiles, such as a model for precipitation or entrainment, the quantities CIN and CAPE can be generalized.

1.7 A few theories for dynamics-convection interaction

As noted above, moist convection acts on dynamics by producing most of the diabatic heating Q_1 (latent heating Q_l is the main contribution, but cloud radiative effect and convective transport constitute large fractions of the radiative heating Q_r and the small-scale transport Q_{1t} can be significant). Conversely, dynamics acts on convection via moisture and energy transports. Strong statistical links can be observed between some dynamical variables and convective processes, such as a high correlation between ascending motion and precipitation, which have inspired a variety of theories on the interaction between dynamics and deep convection. But correlation does not systematically express causality (e. g., Mapes, 2000), and some theories have aged poorly.

1.7.1 Convective instability of the second kind

Observation of tropical convergence zones suggests that precipitation occurs in regions of moisture convergence; it was first hypothesized that this convergence was the main control on deep convection. This led to the development of the theory of *convective instability of the second kind* (CISK), which posits that deep convection is controlled by column humidity convergence, both in terms of occurrence (it rains where and when column humidity convergence is positive) and intensity (all or a fixed fraction of the column humidity convergence is rained out). CISK was first proposed to explain tropical-storm development (Charney & Eliassen, 1964; Ooyama, 1964). It was later used to tentatively explain convectively coupled equatorial gravity waves (Lindzen, 1974); it is successful at qualitatively explaining why these waves have the same structure as dry waves (see Section 1.5), essentially because it neglects humidity storage. But it predicts scale selection of the smallest space and time scales for convective disturbances instead of the variety of observed scales.

Based on the observed spatial correlation between humidity convergence and precipitation, CISK introduces a causal link between dynamics and deep convection via humidity transport and ignores the physics of deep convection described in Section 1.6. Theoretical work and model development based on CISK have revealed significant shortcomings. Mainly, convection parameterizations based on this theory (Kuo, 1974) were not very successful at simulating the climatology of precipitation and prone to instability. In fact, by simplifying the column water-vapor budget, CISK adds a constraint on the MSE budget. For moisture modes and large-scale convective disturbances dominated by the variability of humidity, CISK

[12] The quantity obtained with the opposite assumption, i.e. that no water condensate is rained out of the parcel, is called *reversible* CAPE.

imposes a negative GMS in all convective regions, i.e., atmospheric circulation systematically constitutes a positive feedback on any convective disturbances. This is probably too strong a feedback and might explain the instability of CISK-based convective parameterizations.

1.7.2 Convective quasi-equilibrium

An alternative to CISK was introduced by Arakawa & Schubert (1974); it posits that deep convection eliminates conditional instability on short timescales (a few hours), much faster than the adjustment of dynamics. As a result, conditional instability is always negligible: instability created by large-scale forcings (transport, surface fluxes, radiation) is almost instantly consumed by deep convection. This theory is called *convective quasi-equilibrium (CQE)*, because there is a balance between creation of instability by the large-scale forcings (large-scale transport, surface fluxes, and radiation) and elimination by deep convection. This theory is furthered in Emanuel et al. (1994a).

In terms of the physical quantities introduced in Section 1.6, CQE posits that, for large-scales in the tropics:

- CIN is small and atmospheric variability always creates mesoscale regions where CIN is negligible.
- CAPE is negligible because deep convection quickly eliminates any CAPE that large-scale forcings might create.

A consequence of CQE is that in deep-convective regions, the temperature profile is tied to the near-surface entropy or enthalpy, following a reference profile. In the idealized updraft of Section 1.6, this reference profile is the moist adiabat, but more realistic formulations including convective entrainment and condensate loading can also be established. Various physical interpretations can be given to CQE (Yano & Plant, 2012), but CQE essentially presents deep convection as a fast response to the large-scale forcings, which include the large-scale transport.

Over long time scales and large horizontal scales, CQE is verified over oceans (Brown & Bretherton, 1997) and in most monsoon regions (Nie et al., 2010), although the updraft profile does not strictly follow a moist adiabat. There are nevertheless a number of observational limitations to CQE. First, it does not provide any information on convection in dry regions or where deep convection is not intense, such as the upper troposphere of convective regions. In convective regions, CQE theory is better verified in the lower troposphere than in the upper troposphere (Raymond & Herman, 2011; Lin et al., 2015). Holloway & Neelin (2007) even found that cold temperature anomalies are observed above convection in the convective columns, a phenomenon due to transport associated with overshoot in convective atmospheric columns.

Parameterizing deep convection was the first motivation for introducing CQE (Arakawa & Schubert, 1974). Since the observed adjustment of the temperature profile is not instantaneous, this theory was in some cases modified to include a characteristic relaxation time of the thermodynamics profiles towards neutrally stable profiles, such *relaxed CQE* was implemented in a variety of parameterizations (Betts, 1986; Betts & Miller, 1986; Moorthi & Suarez, 1992). Note that this adjustment re-introduces degrees of freedom in the thermodynamics profiles and therefore degrades the tight control of convection by large-scale forcings implied by CQE, which re-introduces more of a two-way interaction between circulation and deep convection.

Mapes (1997, 1998) also criticized the basic tenets of CQE, arguing that convection is controlled by convective inhibition and proposing *activation control* theory (with CIN determining where and when deep convection occurs) as an alternative to CQE. It is true that CIN can be non-negligible over tropical continents and is definitely significant over big midlatitude land masses, which raises an issue for GCM convective parameterizations based on CQE. But over the equatorial oceans, CQE holds well, which shows that atmospheric variability at small and meso- scales is sufficient to overcome CIN at large scales. Mapes (1998) also showed that the scale separation between convective processes and dynamics is insufficiently clear to support CQE: dynamics can eliminate buoyancy anomalies through gravity wave emission in 12 to 72 hours, almost as fast as convection.

1.7.3 Self-organized criticality

Self-organized criticality (SOC) is a property of a dynamical system for which a critical point (i.e., a state of the system at which it changes regime, such as a phase transition) is also an attractor (a state towards which the system tends to evolve). The simplest example of SOC is a horizontal disc on which center rice grains are slowly made to fall (as in this video [13], from timestamp 2:50 to 3:50): a pile of

[13] https://www.youtube.com/watch?v=KnOkkC4QND8

rice forms, eventually assuming a near-conic shape, and avalanches are triggered if the slope of the cone becomes too steep. The addition of rice increases the cone's slope and avalanches reduce it. SOC is characterized by scale-invariant events (in our example, avalanches are events) giving rise to power laws, and noise following a $1/N$ spectrum (with N the frequency).

If precipitation is plotted against PW or *column relative humidity* (CRH) [14], an abrupt transition appears between a non-precipitating regime at low PW/CRH and a precipitating regime at large PW/CRH (Bretherton et al., 2004; Peters & Neelin, 2006; Holloway & Neelin, 2009). This relationship and higher-order statistics suggest to interpret deep convection as a self-organized critical phenomenon (Peters & Neelin, 2006; Neelin et al., 2009): the transition to deep convection is the critical point, the large-scale humidity forcing (evaporation, moisture advection) slowly moistens the atmospheric column and drives it towards the critical point, similarly to the addition of rice grains in our example above and precipitation occurs in convective events analogous to the rice avalanches.

Rather than a theory of the interaction between dynamics and deep convection per se, SOC is a tentative theory of the convection response to the column water vapor (and temperature). It is based on the observed statistics of precipitation and PW or CRH rather than on physical mechanisms and can appear as an alternative to the principles presented in Section 1.6. But one could argue that at small scales humidity has a strong contribution to buoyancy in entraining convective updrafts, and therefore PW is a proxy for convective instability. As a result, the documented relationship between PW and precipitation could be related to convection onset due to CIN/CAPE control of convection; the abrupt transition from weak precipitation to deep convection can be explained physically by CIN becoming negligible in the presence of non-zero CAPE. In this respect, activation control and SOC are compatible.

To many scientists, SOC is rather a flavor of CQE since it also implies a fast convective adjustment to a stability-neutral state. But SOC also includes details on how atmospheric processes eliminate instability. SOC posits non-linear processes and interaction between convective events, a richer and more complex picture than an almost-instantaneous adjustment to neutral stability as postulated by the original CQE theory (Neelin et al., 2009).

However, SOC of convection is not perfectly supported by observations, because different power laws can be extracted from the available data (Peters & Neelin, 2006; Raymond et al., 2009; Yano et al., 2012) and occurrence of very large PW is too rare to properly constrain the analysis (Holloway & Neelin, 2009). Muller et al. (2009) also constructed a simple model with precipitation onset controlled by boundary-layer humidity and precipitation intensity controlled by PW, which reproduced the statistical properties of the relationship between precipitation and PW without involving SOC.

1.7.4 Weak temperature gradient approximation

The WTG approximation (Sobel et al., 2001; Adames, 2022) seeks to simplify the dynamics rather than convection as the theories above attempt to. It is based on the empirical observation that climatological horizontal gradients of temperature are small in the free troposphere, an observation that is explained by the fast redistribution of energy on the horizontal by transient gravity waves (Bretherton & Smolarkiewicz, 1989; Mapes, 1998).

With weak horizontal temperature gradients, the horizontal advection in Equation (1.5) is negligible. In equilibrium or for a slow evolution of temperature, this yields:

$$w\partial_z\theta = \frac{\theta}{T}\frac{Q_1}{c_p}. \tag{1.20}$$

This is the first-order balance in the thermodynamic equation (1.5), between diabatic heating and vertical advection, as pointed out in Section 1.2. The WTG approximation also implies that the vertical gradient $\partial_z\theta$ is uniform on the horizontal in the free troposphere. By essence, it is mostly suitable to large-scale, steady or slowly evolving circulations (Polvani & Sobel, 2002; Bretherton & Sobel, 2002, 2003). Deep convection is a major contributor to free-tropospheric diabatic heating and therefore controls the direction of the vertical motion (upwards where deep convection occurs, downwards elsewhere) and a large part of its amplitude.

The WTG approximation can be used as an asymptote for theoretical developments (Sobel et al., 2001; Bretherton & Sobel, 2002; Polvani & Sobel, 2002; Bretherton & Sobel, 2003) or included in a framework to analyze tropical circulations (Giordani & Peyrillé, 2022). In particular, because the WTG approximation neglects the horizontal anomalies of temperature, it filters out the equatorial gravity waves and can isolate moisture modes (e.g., Sobel et al., 2001; Adames & Kim, 2016). Finally, the WTG approximation can

[14] CRH is the ratio of PW to the column-integrated saturation water vapor mass

be used as a parameterization of large-scale dynamics to represent the first-order feedback of circulation on thermodynamics, as Section 2 will detail.

1.8 Let's not forget the surface

In the previous section, all theories are either about the interaction between convection and large-scale forcing (in which transport is included) or about the interaction between diabatic heating (Q_1) and circulation. Latent, radiative, and convective-transport heating associated with convective clouds is a major contribution to Q_1, overly dominant in the free troposphere. The one other significant contribution to Q_1 is the turbulent fraction of Q_{1t} which occurs on scales smaller than the convective scales and mostly in the ABL, and mostly as a response to the instability created by surface heat fluxes (although, as we have mentioned in Section 1.3, stratocumulus clouds also power strong ABL turbulence via cloud-top radiative cooling). Turbulent heating of the ABL contributes to significant aspects of tropical circulations.

Historically, Lindzen & Nigam (1987) was the first to claim that near-surface winds are controlled by sea surface temperature (SST) gradients because the turbulent redistribution of surface sensible heating throughout the ABL ties the ABL temperature to the SST. This idea came as a counterpoint to the previous viewpoint which assumed that mid-tropospheric latent heating Q_l due to deep convection is the main driver of the climatological tropical circulation as exemplified in Gill (1980). Unfortunately, Lindzen & Nigam (1987)'s study had to include what they named a "back-pressure gradient" in their model to simulate winds with some resemblance to the surface winds. These two studies sparked a debate on what controls climatological low-level circulation, free-tropospheric heating by clouds or SST patterns. This low-level circulation is important for all the theories of the previous section because it transports a lot of water vapor towards regions of low-level convergence, which causes convection (in CISK) or favors it (in CQE, SOC).

Neelin (1989) showed that the two models are mathematically equivalent (essentially, they are linear Saint-Venant models associated to different vertical modes) and physically equivalent if precipitation is modeled as a function of SST. An analysis of interannual variability suggested that the surface-wind variability on these long time scales is driven mostly by convective heating in the zonal direction and by a combination of convective and SST forcing in the meridional direction, the latter being particularly significant in the vicinity of the equator (Chiang et al., 2001). Stevens et al. (2002) showed that a budget of momentum for boundary layer winds including vertical advection of free-tropospheric momentum into the boundary layer could reproduce the climatological low-level winds. Refining this model into the Mixed Layer Model (MLM)-SST in which boundary layer temperature follows the underlying SST, Back & Bretherton (2009) showed that a large part of the low-level convergence is forced by the SST gradients and that the free-tropospheric processes only have a modulating effect. Their findings are generally consistent with Chiang et al. (2001)'s since a large part of convergence results from the latitudinal variation of the meridional winds. Figure 1.10 shows the convergence and winds in the reanalysis ERA40 (Fig. 1.10a) and the SST contribution to this flow in the MLM-SST (Fig. 1.10b). It shows that overall, the climatological low-level circulation patterns follow the surface forcing in the Indo-Pacific. But the influence of free-tropospheric processes appear as a significant damping, particularly in the equatorial eastern Pacific and in the tropical Atlantic. In a way, this approach still needs to take into account a "back-pressure gradient", which includes a large contribution from latent heating in the free troposphere.

Beyond the climatological mean, surface forcing is very significant in the seasonal cycle over the ocean (Back & Bretherton, 2009) and in the case of monsoons (Geen et al., 2020). At longer timescales, the interface between ocean and atmosphere is obviously crucial to interannual coupled variability such as El Niño - Southern Oscillation (ENSO), although this phenomenon also includes feedbacks due to deep convection. On shorter time scales, synoptic and intraseasonal variability are less sensitive to surface forcing. In particular, observed equatorial gravity waves appears to couple almost exclusively to convection (Kiladis et al., 2009). But tropical intraseasonal oscillations involve significant coupled feedbacks due to the fact that the time scales of heat storage in the upper ocean are typically intraseasonal (more details in Section 3.2). On the other hand, the typical time scale of heat storage of land surfaces is sub-daily, this contrast in surface heat capacity is the basis of the diurnal cycle of breezes around tropical islands; but even in this case, convection and cloud processes provides significant feedbacks (more details in Section 4.2).

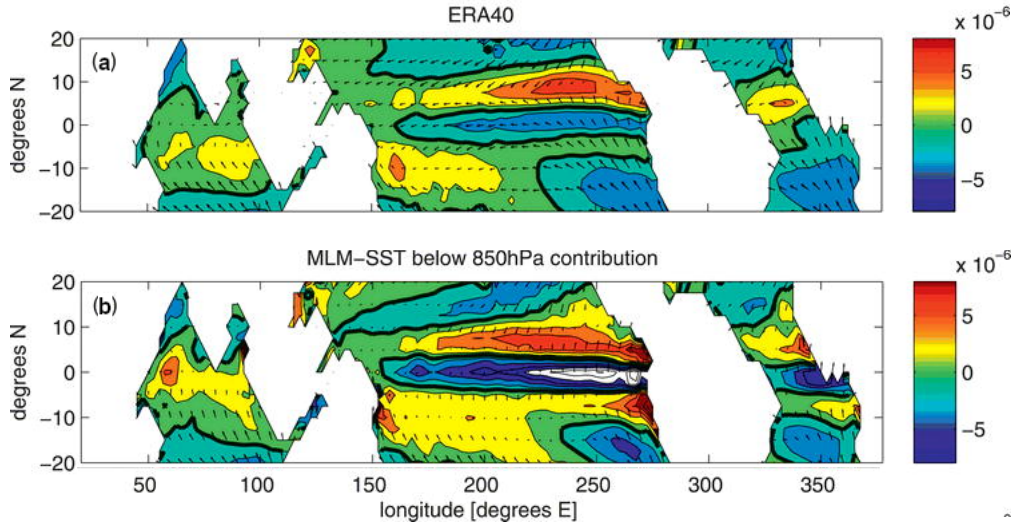

Figure 1.10: Annual-mean surface winds and convergence from (a) ERA-40 and (b) Mixed-Layer Model using SST forcing; 1°arrow length corresponds to 2 m s^{-1} wind and convergence contour interval is 2 × 10^{-6} s^{-1}; adapted from Back & Bretherton (2009).

1.9 Outline

This manuscript will first present efforts to represent large-scale circulation simply and interactively in limited-area models or single-column models in order to simulate the interaction between dynamics and physics at first order (Chapter 2). I will then present a few avenues of research on modes of tropical atmospheric variability that result in spatial organization of convection. Chapter 3 will focus on modes that primarily result from processes internal to the atmosphere (atmospheric dynamics and thermodynamics), and Chapter 4 on modes resulting primarily from the surface forcing. Indeed, in both cases, feedbacks involving coupled surface-atmosphere processes, as well as other atmospheric processes, will be described.

2 Parameterizations of large-scale circulation

The traditional methods of including large-scale forcings in a limited-area SRM or a *single-column model* (SCM) [1] are to impose the large-scale tendency, to impose a relaxation towards a reference profile, and/or to impose large-scale/horizontally averaged vertical velocity. Using the last method, a tendency for large-scale vertical advection can be computed by using the model-simulated vertical gradient. These methods have been used extensively in case studies (e. g., TOGA-COARE [2], Redelsperger et al., 2000; BOMEX [3], Siebesma et al., 2003). As atmospheric scientists noticed the strong influence of the vertical motion on the convective regime (shallow or deep) of the atmosphere, it appeared that imposed circulation might be a strong constraint on the simulated convection. As an alternative, large-scale vertical motion can be parameterized on the basis of the thermodynamic profiles of the model atmospheric column (in an SCM) or horizontally averaged domain (in a SRM), and therefore interact with the SCM's physics or the sub-domain processes of the SRM. These parameterizations enable the study of the first-order interaction between large-scale circulation and the model thermodynamics in a simplified framework.

Two methods have been proposed. In essence, they are very different. The first one uses the weak-temperature-gradient (WTG) approximation (see Section 1.7.4); the second is the damped(-inertio)-gravity-wave (DGW) approximation (Kuang, 2008), which is based on simplifying the momentum equation (1.1).

2.1 Formulations

2.1.1 Weak temperature gradient approximation

The principle of WTG approximation was introduced in Section 1.7.4: it uses the first-order balance in the thermodynamic equation, between diabatic heating and vertical energy advection, to estimate the vertical speed w in the free troposphere. Equation (1.20) shows that this estimate is the ratio of the diabatic source to the vertical gradient of θ. Usually, the profile of w is completed in the boundary layer by assuming uniform divergence there. The parameterized w is used to compute large-scale advection tendencies of water species, horizontal momentum, etc.

In practice, for theoretical developments, we consider that the temperature profile in the free troposphere is constant and set to a reference profile $\theta_{\rm ref}$, which is assumed to be determined by thermodynamic processes, mostly convection, in the convective regions that are away from the location of interest. But, when implemented in single-column models as suggested by Sobel & Bretherton (2000), this type of implementation is prone to numerical instability; to overcome this issue, a *relaxed* WTG approximation was proposed by Raymond & Zeng (2005), in which vertical transport rapidly relaxes free-tropospheric temperature towards a reference profile:

$$\begin{aligned} \partial_t \theta &= \frac{\theta}{T}\frac{Q_1}{c_p} + \frac{\theta_{\rm ref} - \theta}{\tau_{\rm WTG}}, \\ w &= \frac{\theta - \theta_{\rm ref}}{\tau_{\rm WTG}\,\partial_z \theta_{\rm ref}}, \end{aligned} \tag{2.1}$$

with $\tau_{\rm WTG}$ a timescale of adjustment of free-tropospheric temperature that is short ($\tau_{\rm WTG} \leq 1$ day) compared to the timescales of variability of the circulation of interest. Indeed, at equilibrium, the strict

[1] Model of one column of atmosphere without interactive dynamics; often it is one column of a GCM with all its physics but no dynamics.

[2] Tropical Ocean and Global Atmosphere - Coupled Ocean-Atmosphere Response Experiment

[3] Barbados Oceanographic and Meteorological Experiment

WTG approximation of (1.20) is equivalent to (2.1). Physically, the timescale τ_{WTG} can be interpreted as the time necessary for gravity waves to redistribute heat outside the domain of the SRM or SCM, so essentially to propagate outside the domain, i.e., for a domain of typical scale L: $\tau_{\text{WTG}} = L/c$.

More recently, Herman & Raymond (2014) have pointed out that gravity waves' propagation speeds c depend on their vertical structure[4]. The relaxation of temperature anomalies towards the uniform reference profile therefore involves multiple time scales rather than just one as in (2.1). Herman & Raymond (2014) propose to project temperature anomalies onto vertical modes and damp each mode with a characteristic time scale inversely proportional to the propagation speed of the gravity wave with the mode's vertical structure. This approach is called *spectral* WTG.

The WTG approximations presents a fundamental conundrum: being based on thermodynamics, it ignores the equations of dynamics. In particular, it provides no assurance of mass conservation: vertical motion in the domain of interest is supposed to be compensated by opposite motion outside this domain, but there is no specification of where and how this compensating motion occurs and how it can influence the column. This issue can be addressed by coupling two domains with compensating vertical motion (Daleu et al., 2012), but then the respective sizes of the domains are arbitrary. Also, the assumption of no horizontal temperature gradients means that there are no horizontal pressure gradients either (at least in steady state) and therefore nothing to force horizontal motion in the free troposphere, which corresponds via continuity no vertical motion. In fact, small, second-order temperature gradients are enough to force significant horizontal winds in the free troposphere because momentum dissipation is very small there. So the WTG approximation does not contradict mass conservation, it just ignores it.

2.1.2 Damped gravity wave approximation

The DGW approximation (Bergman & Sardeshmukh, 2004; Kuang, 2008) considers that the SCM column or SRM domain is within an extreme phase (either subsiding or ascending phase) of a damped gravity wave forced by the domain-scale temperature anomaly of the model. Large-scale damped gravity waves are solutions to Equations (1.1)-(1.3) linearized about a state of rest with horizontally uniform temperature profile $\theta_0(z)$ [5], with the hydrostatic approximation, and with transport $Q_{\mathbf{u}}$ modeled as a linear damping term $-\epsilon\mathbf{u}$:

$$\partial_t \mathbf{u} + f\hat{\mathbf{k}} \times \mathbf{u} = -\frac{1}{\rho_0}\nabla p - \epsilon\mathbf{u}, \tag{2.2}$$

This approximation is sometimes called the weak pressure gradient approximation (Romps, 2012b,a; Edman & Romps, 2014). Some versions of this approximation neglect rotation (Kuang, 2008; Romps, 2012b,a) or consider the large-scale circulation in quasi-steady state (Kuang, 2008; Romps, 2012b; Blossey et al., 2009). Here, we will present the non-rotating, quasi-steady case for simplicity ($f = 0$ and $\partial_t = 0$). With the hydrostatic approximation, Equations (1.3) and (2.2) can be combined into a partial differential equation for w as a function of temperature:

$$\partial_z \left[\epsilon \partial_z \left(\rho_0 w\right)\right] = -\nabla^2 \rho\, g \approx \frac{\rho_0}{\theta_0} g \nabla^2 \theta_\rho, \tag{2.3}$$

with $\theta_\rho = T_\rho/\Pi$. The last approximation neglects the influence of pressure perturbation on density perturbation in front of the influence of potential temperature perturbation ($\rho'/\rho_0 \approx -\theta'_\rho/\theta_0$).

Equation (2.3) enables a model to compute a large-scale vertical circulation w directly from the horizontally averaged density temperature anomaly, by assuming the SRM domain or the SCM column of interest is located at an extremum of a large-scale damped gravity wave. This requires us to impose the horizontal wavelength of the gravity wave, which can be chosen according to the horizontal scale of the dynamical phenomenon of interest. The thermodynamic anomalies are computed by the model using the complete thermodynamic and humidity equations (1.5) and (1.8) including diabatic terms, sub-domain transport, and vertical advection due to the DGW vertical velocity w (Bergman & Sardeshmukh, 2004; Kuang, 2008).

The DGW approximation also has two caveats. First, the horizontal scale: assuming that only one such scale can represent the large-scale circulation of interest is quite limiting. Second, the rotation: if the DGW approximation can easily include constant rotation (considering a damped inertio-gravity wave rather than a damped gravity wave as we have), this would correspond to wave solutions on an

[4] Gravity waves' vertical structures are the vertical modes used to project the linear quasi-hydrostatic equations (1.1)-(1.5) to obtain the Saint-Venant equations (1.18)-(1.19).

[5] The reference state is in hydrostatic equilibrium and moisture free so a reference pressure profile $p_0(z)$ is linked to ρ_0 and θ_0 via the hydrostatic balance and the equation of state.

f-plane [6]; but, in the deep tropics, wave solutions on a β-plane make more sense: they are known (see the Introduction), but they are more complex than the non-rotating solutions and require knowledge of the latitudinal structure of the perturbation with some precision, additionally to the zonal wavenumber. This requires additional arguable assumptions of the exact location and relative size of the SCM column or SRM domain within the wave.

2.1.3 Comparing WTG and DGW approximations

For the sake of comparing WTG and DGW approximations, we can make further assumptions on the DGW formulation: we neglect the influence of moisture on density ($\theta_\rho \approx \theta$) and consider a DGW with horizontal wavevector $\mathbf{K}$. We also consider a steady-state, linearized, damped version of thermodynamics equation (1.5):

$$w\partial_z\theta_0 = \frac{\theta_0}{T_0}\frac{Q_1}{c_p} - \mu\theta, \tag{2.4}$$

with $T_0(z) = \theta_0(z)\Pi$ the reference temperature profile and μ the temperature damping rate. This damping amounts to considering a deviation from the WTG balance that is linear in θ. We obtain the following relationship between vertical motion and diabatic heating:

$$-\frac{\mu}{\mathbf{K}^2}\frac{\theta_0}{\rho_0 g}\partial_z\left[\epsilon\partial_z\left(\rho_0 w\right)\right] + w\partial_z\theta_0 = \frac{\theta_0}{T_0}\frac{Q_1}{c_p}. \tag{2.5}$$

Compared to (1.20), (2.5) includes an additional term containing the first two derivatives of w; while w in the WTG approximation is directly proportional to the local Q_1, w in the DGW approximation is a weighted integral of Q_1 over the whole atmospheric column, smaller and with smoother features than w in the WTG approximation, which follows $Q_1/(\Pi\partial_z\theta_0)$. To better understand these damping and smoothing, we can further explore the case with uniform damping rates ϵ, μ and constant Brunt-Väisälä frequency N:

$$-\frac{\mu\epsilon}{\mathbf{K}^2N^2}\partial_z^2\left(\rho_0 w\right) + \rho_0 w = \frac{\rho_0 g}{T_0 N^2}\frac{Q_1}{c_p} = M_Q, \tag{2.6}$$

with M_Q the weighted diabatic heating in units of mass flux and

$$N^2 = \frac{g}{\theta_0}\frac{\partial\theta_0}{\partial z}. \tag{2.7}$$

We can further project Equation (2.6) on vertical modes, which, for constant ϵ, μ, and N, amounts to a Fourier decomposition. With the constraint that the vertical speed is zero at the surface ($z = 0$) and at the tropopause ($z = z_t$), the vertical modes are sine functions:

$$\rho_0 w = \sum_{n=1}^{\infty} W_n \sin\left(n\pi\frac{z}{z_t}\right) \quad \text{and} \quad M_Q = \sum_{n=1}^{\infty} M_{Qn}\sin\left(n\pi\frac{z}{z_t}\right), \tag{2.8}$$

with W_n and M_{Qn} the Fourier coefficients for, respectively, $\rho_0 w$ and M_Q.

For WTG, (1.20) yields very simply $W_n = M_{Qn}$ for all n. For DGW, (2.6) yields:

$$W_n = \frac{1}{1 + n^2\pi^2\frac{\mu\epsilon}{N^2\mathbf{K}^2}} M_{Qn} < M_{Qn}. \tag{2.9}$$

This means that the dynamical response to diabatic forcing along the n^{th} harmonics is smaller in DGW than in WTG and increasingly so for increasing vertical wavenumber n or for decreasing horizontal wavevector amplitude $|\mathbf{K}|$. On the vertical, this means that small features projecting on modes with large n (i.e., high-order baroclinic modes) will be damped in DGW compared to WTG, and the vertical profile of w will be smoother in DGW than in WTG. In spectral WTG approximation, high-order baroclinic anomalies will be damped faster than low-order baroclinic modes because gravity-wave propagation speed increases with the baroclinic order, which makes spectral WTG an intermediate approximation between WTG and DGW.

Why is the dynamical response in DGW ($W_n < M_{Qn}$) weaker than in WTG ($W_n = M_{Qn}$) for each vertical mode? Equations (2.4), (2.5), (2.6), and (2.9) all show that WTG is the limit of DGW with no

[6] The f-plane is a plane tangent to the Earth surface at the location of interest, with constant Coriolis parameter f. Considering an f-plane is an approximation that neglects the curvature of the Earth's surface and the change of f with latitude.

dissipation of either momentum ($\epsilon = 0$) or energy ($\mu = 0$). The WTG approximation implicitly neglects dissipation, whereas, in the DGW approximation, diabatic heating forces a temperature perturbation and horizontal wind, which is damped, and vertical motion results from the horizontal wind via continuity. Neglecting the momentum damping in the free troposphere is actually a reasonable simplification in clear sky, less so in convective region because convective momentum damps baroclinic motions. How damping should be modeled in these models is therefore a pending question, which I unpack further in Section 2.3.2.

2.2 Results

Both relaxed WTG and DGW approximations have shown some promise for traditional case studies: a large part of the variability of the precipitation can be reproduced by SRMs in which these parameterizations are implemented instead of prescribing the observed vertical motion (e.g., TOGA-COARE, Bergman & Sardeshmukh, 2004; Wang et al., 2013; CINDY-DYNAMO [7], Wang et al., 2016b; OTREC [8], Raymond & Fuchs-Stone, 2021). The WTG approximation appears to produce vertical profiles of ascent which are too fast in the upper troposphere (i.e., too top-heavy), the DGW approximation w profiles that are not top-heavy enough. In Wang et al. (2016b), the spectral WTG method was also implemented and yielded the best results, intermediate between the WTG and DGW methods.

To better understand the potential and differences between the WTG and DGW methods, an intercomparison program was organized (Daleu et al., 2015, 2016). Coordinated simulations using SCMs and SRMs with both approximations implemented showed that in general the parameterized dynamical responses in SRMs are more robust across methods and models than the responses in SCMs. One robust difference between the two methods is the more top-heavy profiles of vertical motion with the WTG approximation than with the DGW approximation. This a direct consequence of the increased damping of high-harmonics in DGW compared to WTG noted in the previous section: if we consider a top-heavy profile of diabatic heating resulting from a mix of convective and stratiform heating, it can be decomposed into a first-baroclinic component with a mid-tropospheric maximum and a sum of higher-order baroclinic components that move the mid-tropospheric maximum upwards; the WTG dynamical response w roughly follows the heating profile; in the DGW dynamical response, the higher-order baroclinic forcings are damped more than the first-baroclinic component and the maximum w is closer to the mid-troposphere than the maximum heating.

The WTG method applied to an SCM has been used for theoretical purposes: Sobel et al. (2007) showed that the interaction between dynamics and convection can create two stable equilibria over warm waters. Figure 2.1 shows the precipitation at equilibrium as a function of the imposed SST. For SST warmer than 301 K, two equilibria can be obtained depending on the initial conditions: one deep-convective with ascending motion and significant precipitation, the other with convection limited to the ABL, with subsidence and little precipitation. The existence of these multiple equilibria is widespread: they have been documented in multiple SCMs and SRMs (Sessions et al., 2010; Daleu et al., 2015), and are a little more likely with the WTG approximation than with the DGW approximation. These two equilibria can be interpreted as a simple model of the alternation of moist and dry regions, with the deep-convective equilibrium corresponding to the moist regions and the other equilibrium to the dry regions. A theoretical conclusion is that the interaction between circulation, convection and radiation is sufficient to explain the bimodality of the humidity distribution in the tropics: deep convection, or its inhibition, is maintained by the first-order dynamical feedback, creating a regional stability of moist and ascending conditions or dry and subsiding conditions. It was also interpreted as a simplified model of self-aggregation, and more refined models (Emanuel et al., 2014; Beucler et al., 2018; Kuang, 2018) using either WTG or DGW approximations have confirmed that the development of self-aggregation can be explained as a linear instability of the RCE giving rise to either a moistening or a drying of an atmospheric column (with a compensating drying or moistening in other columns). I will expand on self-aggregation in Section 3.1. The bifurcation resulting in these two equilibria in SCMs can significantly impact the large-scale tropical circulation: for example, this bifurcation results in inter-hemispheric symmetry breaking of the Hadley circulation and ITCZ in an intermediate-complexity axisymmetric [9] model (Bellon & Sobel,

[7] Cooperative Indian Ocean Experiment on Intraseasonal Variability in Year 2011 - Dynamics of the Madden-Julian Oscillation

[8] Organization of Tropical East Pacific Convection

[9] In this manuscript axisymmetric means longitude-invariant, i.e., 2D meridional-vertical, with a non-zero zonal wind but no zonal transport.

2010).

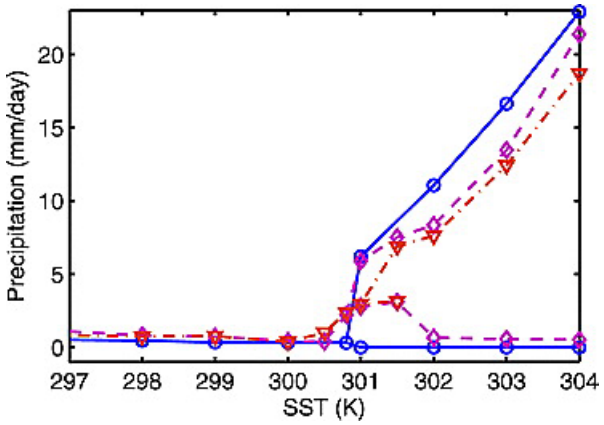

Figure 2.1: Precipitation rate as a function of the imposed SST in the equilibria of an SCM in which the WTG approximation is implemented. The blue line corresponds to neglected horizontal humidity advection, the purple and red lines to horizontal humidity advection parameterized as a relaxation towards a reference RCE profile with relaxation time scales of 6 days (purple line) and 3 days (red line); from Sobel et al., 2007.

More recently, the WTG and DGW approximations have been used in conjunction with a simple model of convection to develop a simple model of the relationship between humidity, stability, circulation and precipitation in the tropics (Romps, 2021; Singh & Neogi, 2022).

On the other hand, these parameterizations of the large-scale vertical motions have a very practical application as a validation tool in the development of physical parameterizations for GCMs. Single-column models using parameterizations of a GCMs and the WTG approximation can, to a large extent, reproduce the convection and vertical motion regimes simulated by the corresponding full GCM (Zhu & Sobel, 2012, Bony et al., 2013). It seems warranted that this framework be used in to evaluate GCM parameterizations (Raymond, 2007), in complement to the usual test cases with prescribed vertical motion. This was also a motivation for the intercomparison work in Daleu et al. (2015, 2016), which showed improvement in the SCMs between the CMIP5 versions and their versions preparing for CMIP6.

The WTG approximation was further used to understand a number of phenomena (list probably not exhaustive):

1. investigate the feedback of circulation on the sensitivity of convection to mid-tropospheric moisture. As noted in Section 1.6, convective entrainment of environmental air into the cloudy updrafts reduces cloud buoyancy more by drying the cloud than by cooling it. Convection is therefore damped and sometimes inhibited by dry mid-troposphere (Derbyshire et al., 2004). This effect is amplified by the circulation feedback (Sobel & Bellon, 2009, Sessions et al., 2015): less convection means less latent heat release and through WTG to less ascending motion, which further dries the free troposphere since ascent brings moist boundary-layer air upwards into the free troposphere.

2. provide a physical explanation for the direct response of the atmosphere to increases of carbon-dioxide concentration (Bony et al., 2013). The change in tropical precipitation projected by climate models can be divided into a thermodynamic contribution due to the surface warming and a dynamic contribution due to a slow-down in the atmospheric tropical circulation. These contributions have the same order of magnitude. The dynamic contribution can be attributed to the direct effect of carbon dioxide on diabatic heating: an increase in carbon-dioxide concentration decreases the radiative cooling of the troposphere (increased absorption dominates increased emission). In dry regions, this causes a decrease in free-tropospheric diabatic cooling and therefore a reduction of subsidence, as shown in Figure 2.2. In moist regions, this causes an increased stability that reduces deep convection and the associated latent heating; this reduces the overall diabatic heating and therefore slows ascent, as shown in Figure 2.2. These circulation changes generally reduce precipitation in moist regions and increase it slightly in dry regions.

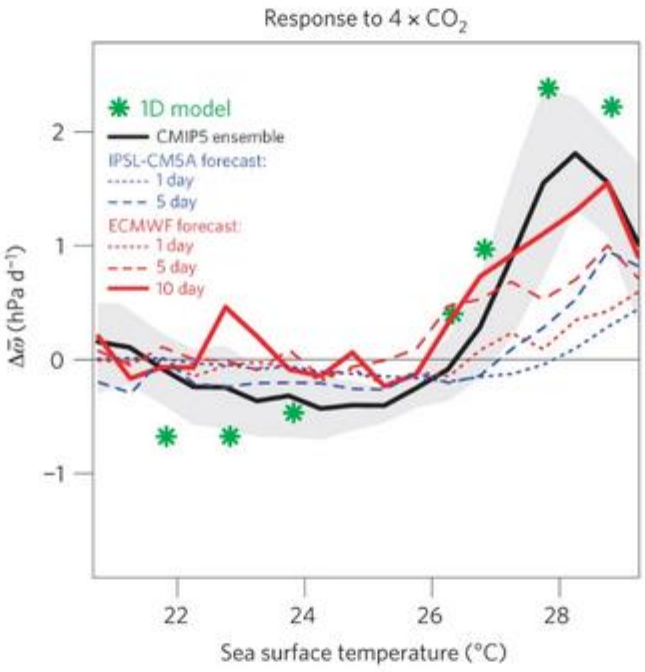

Figure 2.2: Change in mid-tropospheric vertical pressure velocity $\omega = -\rho_0 g w$ for a quadrupling of the atmospheric carbon-dioxide concentration, as a function of SST, for CMIP5 multi-model ensemble (black line) and LMDz SCM with WTG (green markers), at equilibrium (about a century after the increase in carbon-dioxide concentration for the GCMs). Dry regions over cool SSTs experience a slow-down of subsidence, and moist regions over warm SSTs experience a slow-down of ascending motion. The short-term (1-day and 5-day) forecasts aim to illustrate how fast this dynamical adjustment occurs. Adapted from Bony et al. (2013).

3. understand the circulation feedback on the diurnal cycle of convection over the ocean (Ruppert & Johnson, 2016) and the possible role of the interaction between this diurnal cycle and large-scale circulation in the transition between suppressed and active phases of intraseasonal variability (Ruppert, 2016).

4. evaluate the feedback of circulation on aerosol effects (Anber et al., 2019).

2.3 Perspectives

Although these simple parameterizations of large-scale dynamics have been improved over the years and some validation studies have shown their relevance (Kuang, 2008; Romps, 2012b,a) and their potential (Daleu et al., 2015, 2016), their use is still limited to theory aficionados. I would like to further refine these methods in order to make this type of parameterizations useful to represent the effect of large-scale circulation in SCMs and SRMs.

2.3.1 Adding the β effect

Both DGW and WTG approximations neglect the Earth's rotation and the β effect, resulting from the change of the Coriolis parameter f with latitude. Considering that WTG approximation results from a scale analysis of the thermodynamic equation, one can wonder why rotation would impact it. This objection is valid for the strict and relaxed WTG approximations, but for the spectral WTG approximation, temperature perturbations are assumed to be transported away by gravity waves with various timescales resulting from their vertical structures. If a β-plane is considered instead of a non-rotating atmosphere, three kinds of gravity waves arise for each vertical structure: Kelvin, Rossby, and inertio-gravity waves (Matsuno, 1966). Each of these waves has a specific latitudinal structure, specific propagation zonal direction and speed. Rossby and inertio-gravity wave are also dispersive. The effect of rotation can be included in the spectral WTG by projecting temperature perturbations on these waves and damping each

component with the appropriate time scale, but to do so the longitudinal and latitudinal structures have to be known, or hypothesized.

A stationary damped gravity wave on the β-plane with a vertical structure following a vertical mode is a Gill circulation (Gill, 1980). Reboredo & Bellon (2022) and Bellon & Reboredo (2022) show that the vertical motion in the Gill circulation is smaller than in a damped gravity wave and larger than in a damped inertio-gravity wave, which shows that the β effect is not negligible. By projecting density temperature perturbations on the vertical modes similarly to Herman & Raymond (2014), the dynamical response of the tropical, stratified troposphere can be decomposed into transient and steady damped equatorial gravity waves. Again, this decomposition requires knowledge of the longitudinal and latitudinal structure of the temperature perturbation.

2.3.2 Improving momentum dissipation

If we overlook the effect of rotation, I believe that the spectral WTG method takes the WTG approximation to maturity as far as the free troposphere is concerned. As pointed in Section 2.1.3, the WTG approximation neglects dissipation, which is not unreasonable in the clear-sky atmosphere. I think that the major area of improvement of this approach is in the representation of the large-scale dynamics in the ABL, which include surface friction. Indeed, current implementations of the WTG approximation just assume a fixed ABL depth and vertically invariant divergence within the ABL. The weakest of these assumptions is the fixed ABL depth, especially since the vertical motion computed by the WTG approximation at the ABL top depends on the heat budget in a very local layer at the assumed bottom of the free troposphere. Combining the WTG approximation in the free troposphere to a vertically integrated momentum budget of the ABL (e.g., Beare & Cullen, 2019) could improve the representation of ABL dynamics including surface friction and provide a diagnostic of the ABL depth (by ensuring the continuity of w on the vertical between ABL and free troposphere). But conceptually, this approach combining a thermodynamics scaling in the free troposphere to full dynamics of the ABL is a little unsettling. And it would still ignore the turbulent and cloud physical processes which are predominant in determining ABL depth. This issue of how to improve the representation of the ABL under a free troposphere in WTG approximation is certainly challenging.

On the other hand, modeling the dynamical response of the tropical atmosphere as a damped wave presents opportunities that go beyond the current DGW implementations. Most of these implementations model momentum dissipation as Rayleigh damping with a uniform rate ϵ; this is a simple and practical choice, but probably not the most physical. Unrealistic dissipation is not a new issue in simple models of tropical dynamics (Battisti et al., 1999), and in the case of the current DGW implementations, the choice of a uniform ϵ overestimates the damping in the upper troposphere and implicitly underestimates the upper-tropospheric winds, which explains why the parameterized vertical motion is not as top-heavy as expected. An early work on DGW approximation envisioned a vertically varying rate $\epsilon(z)$ (Kuang, 2008), which gives another degree of freedom to adjust the DGW implementation but does not improve its physical basis.

How to represent the combination of surface friction, diffusion, turbulent and convective momentum transport correctly is worthy of more consideration. The effect of air viscosity is negligible everywhere except at the very surface of the Earth; the resulting surface friction is redistributed efficiently throughout the ABL by turbulent transport and the combination of these processes can be well approximated by Rayleigh damping. In the free troposphere, the issue is simpler in some places and more complicated in others: in non-convective regions, dissipation is negligible, but in convective regions, there is significant convective momentum transport: updrafts and downdrafts mix momentum across the troposphere. This results in a damping effect on baroclinic modes to the benefit of the barotropic mode. By mixing momentum vertically, the convective momentum transport also communicates surface friction to the whole troposphere. Convective momentum transport can hardly be parameterized as a Rayleigh damping alone, but if we consider a simple mass-flux convective scheme, it can be modeled as a first-order, linear term proportional to the vertical gradient of momentum $\partial_z \mathbf{u}$. Investigating to what extent dissipation in the tropical atmosphere can be modelled as Rayleigh damping in the ABL and a simple, linear, convective-momentum-transport contribution in convective regions could be a first step in improving the DGW approximation. The implementation of a more complex mass-flux scheme Romps, 2014, e. g., can later be envisioned.

2.3.3 Opportunities for validation and applications

Many datasets are now available for validation of circulation parameterizations. Within the recent intercomparison project RCEMIP (Wing et al., 2018), a number of large-domain, SRM simulations without rotation have been performed and are now publicly available. Over these large domains, large-scale dynamical response to convection is simulated, and these experiments can be used as a benchmark for the WTG and DGW parameterizations, as well as their potential improvements, in particular in terms of momentum dissipation. Furthermore, current computing resources are sufficient to perform global albeit short SRM simulations (Satoh et al., 2018). Cloud-resolving aquaplanet simulations are becoming affordable and available and can be used to evaluate schemes including the Earth's rotation.

Now, improving parameterizations of large-scale circulation can expand the relevance of their applications. It will enable better theoretical developments on all phenomena resulting from the interaction between moist physics and circulation, because these parameterizations capture first-order dynamical response which is often sufficient in simple models. In particular, the WTG approximation is already used in some promising simple models of intraseasonal variability (e.g., Wang & Sobel, 2022) and an improved DGW might be useful to understand the dynamical aspects of self-aggregation (see next chapter).

As these parameterizations are improved to be robust and reliable, their use will expand beyond the theoretical realm to practical matters. They can be implemented in SRMs and SCMs:

- in SRMs, to simulate the first-order large-scale circulation feedback on the atmosphere in the limited model domain. For example, this could be useful to understand the impact of a tropical island on the large-scale circulation and the feedback of this circulation on the island climate, with a configuraion in which the SRM domain include the island and the neighboring seas, and the parameterization of large-scale circulation simulates the dynamical response on synoptic to planetary scales to the local atmospheric processes forced by the island and its feedback on the island climate (see the perspectives in Section 4.2).

- in SCMs, to evaluate GCM physical parameterizations and guide GCM development. In classical test cases with deep convection (TOGA-COARE, CINDY-DYNAMO, OTREC), the parameterizations of large-scale circulation can be used to release the constraint of prescribed vertical motion, which essentially controls convection by constraining the moisture and energy transports, and obtain a finer evaluation of physical parameterizations. Idealized cases can also be developed to compare SCMs with SRMs in the same framework with interactive, parameterized large-scale circulation.

The models necessary for such experiments are available at CNRM: MUSC, the SCM of ARPEGE (GCM), and Meso-NH, used in SRM configuration. Basic versions of the WTG and DGW approximations have already been implemented (Daleu et al., 2015, 2016) in these models, and I intend to further develop these configurations.

3 Spontaneous organization of convection

As mentioned in the introduction, spatial organization of deep convection occurs on a wide range of scales and creates moist regions surrounded by drier regions. In tropical atmospheric variability, organization occurs as a result of the interaction of atmospheric processes only. We will call this type of organization "spontaneous", because no forcing external to the atmosphere is provided.

Spontaneous organization of convection also occurs in models in the simplest of configurations, the *radiative convective equilibrium* (RCE), i.e. with no heterogeneity in the surface or top-of-atmosphere forcings and no large-scale transport or imposed circulation. This phenomenon is named *self-aggregation*. Because it can be thought of as a minimal analog to the observed organization of convection, it has captured the attention of the scientific community working on convection in the last decade. We will cover this topic in Section 3.1.

Convective organization can be observed at mesoscale, synoptic and planetary scales. Mesoscale convective systems (MCS) are cloud ensembles characterized by a transition from shallow to deep convection to stratiform anvils (Houze, 2004; Schumacher & Rasmussen, 2020). At synoptic scales, tropical depressions, storms, and cyclones appear with a significant rotational, cyclonic circulation (Emanuel et al., 2003). The mechanisms of self-aggregation probably contribute to the development of such disturbances (Bretherton et al., 2005; Khairoutdinov & Emanuel, 2013; Muller & Romps, 2018).

As noted in the introduction, some of the observed large-scale tropical variability can be identified as convectively coupled equatorial gravity waves. It is not quite understood why these convectively coupled waves have the same structure as the dry waves except for an adjustment of the gravity wave phase speed. Essentially, it means that moisture perturbations are not significant enough to influence the structure of these modes and the impact of moisture is limited to modifying the effective stratification of the troposphere, i.e., the Saint-Venant equivalent depth. Why it is so is not perfectly understood. And there is still much to understand about the *intraseasonal* tropical variability (on timescales between 10 and 90 days), in which moisture perturbations have a much more significant role than in convectively coupled equatorial gravity waves. This variability is the focus of Section 3.2.

3.1 Convective self-aggregation

3.1.1 Radiative-convective equilibria

Self-aggregation arises in many models in a configuration of radiative-convective equilibrium, i.e., with no heterogeneity of the boundary conditions (at the surface and top of the atmosphere) and no large-scale forcing. The basic RCE configuration has fixed, homogeneous SST and homogeneous solar incoming radiation at the top of the atmosphere. In limited-area SRMs, doubly-periodic lateral boundary conditions are used to avoid any influence of these boundaries. In some configurations, as one would expect, convection develops sporadically everywhere in the domain, and in stationary state precipitation and thermodynamic fields are homogeneous on the horizontal and there is no internal circulation in long-term average: this is a non-aggregated stationary state (I will use, abusively, the term "equilibrium" for "stationary state"). But in many configurations, even if the initial conditions are essentially uniform on the horizontal, convective clouds gather in a region of the domain and an overturning circulation develops between the convective region and the surrounding dry region (Hess et al., 1993; Bretherton et al., 2005): it reaches an aggregated stationary state. This does not occur in all configurations, it is more frequent for larger domains and coarser resolutions (Muller & Held, 2012). In some models, there is a hysteresis: an overlap between the configurations yielding a non-aggregated RCE and an aggregated RCE: both RCEs can be obtained for the same forcing, depending on initial conditions (Muller & Held, 2012; Coppin & Bony, 2015, Bellon & Coppin, 2022). Figure 3.1 shows an example of this multiple equilibria obtained with Meso-NH in RCE configuration.

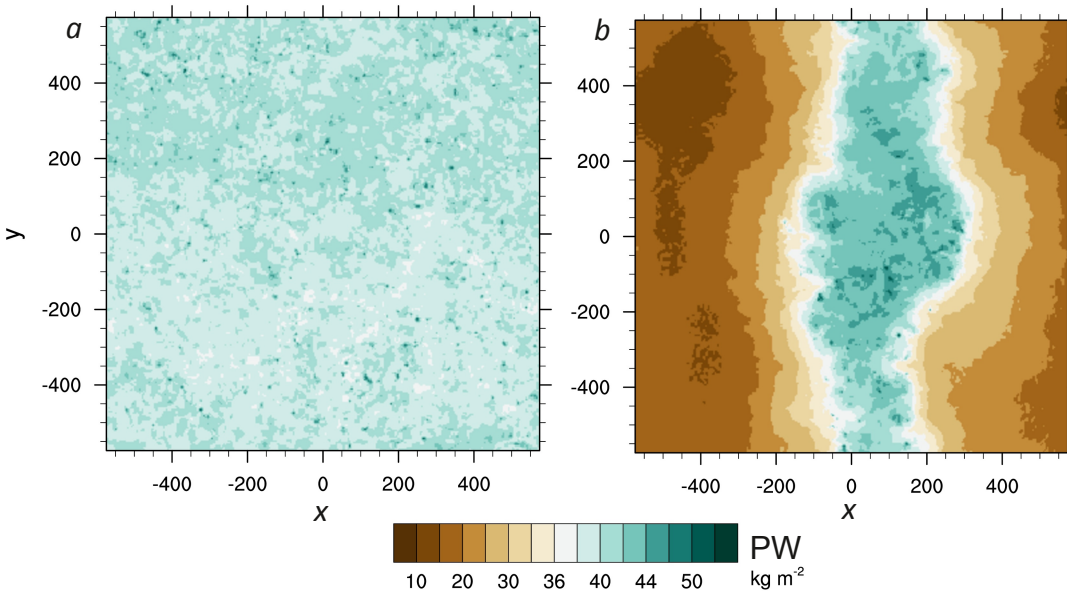

Figure 3.1: Maps of precipitable water averaged over one day in stationary state in the radiative-convective equilibria simulated by Meso-NH (for a square domain of 1152 km and a resolution of 4 km) for different initial conditions: (a) non-aggregated and (b) aggregated stationary states.

3.1.2 Mechanisms

Past studies have focused on mechanisms giving rise to convective self-aggregation in models because these mechanisms could be at play in the development of observed convective disturbances at a variety of scales. These mechanisms vary from model to model and depend on external forcing such as SST (Coppin & Bony, 2015; Becker et al., 2017, Bellon & Coppin, 2022). Nevertheless, the development of self-aggregation in most SRMs and some GCMs is attributed to a linear radiative-convective-dynamical instability of the non-aggregated RCE (Emanuel et al., 2014; Wing & Emanuel, 2014; Beucler & Cronin, 2016; Kuang, 2018; Beucler et al., 2018): the linear response of radiation, convection, and vertical motion to some perturbations of the non-aggregated equilibrium enhance these perturbations (which are the unstable eigenmodes of the linear system).

Because the distributions of PW and vertically integrated MSE $[h]$ are bimodal in an aggregated state and unimodal in a non-aggregated state, variances of PW and MSE are much larger in aggregated states than in non-aggregated ones. Documenting the evolution of the variance of vertically integrated MSE $\overline{[h]'^2}$ is a simple way to measure convective aggregation and analyze the contributions of the different physical processes following Wing & Emanuel (2014) and Equation (1.15). As an example, Figure 3.2 shows the evolution of the variance and the contributions of the different processes to this evolution in a Meso-NH simulation of self-aggregation. We can see that $\overline{[h]'^2}$ increases very significantly from day 30 to day 60 of the simulation (Fig. 3.2a); this is characteristic of aggregation.

Figure 3.2b shows the contributions of the different physical processes, which are overall robust with the results in the literature:

- Radiation is instrumental to self-aggregation (Tompkins & Craig, 1998; Bretherton et al., 2005; Tompkins & Semie, 2017): solar radiation systematically favors aggregation (Wing & Emanuel, 2014, Bellon & Coppin, 2022) and terrestrial radiation generally favors aggregation (Muller & Held, 2012; Muller & Bony, 2015; Coppin & Bony, 2015), although it can at times change sign (Wing & Emanuel, 2014; Wing et al., 2018).

- The contribution of turbulent surface heat fluxes is model dependent: it is the result of the competition between the opposite effects of the wind-induced surface heat exchange (WISHE), favorable to aggregation (Tompkins & Craig, 1998; Wing & Emanuel, 2014; Coppin & Bony, 2015; Becker et al., 2017; Wing et al., 2018, Bellon & Coppin, 2022), and of the air-sea thermodynamic contrast, opposing aggregation (Wing & Emanuel, 2014; Wing et al., 2018, Bellon & Coppin, 2022).

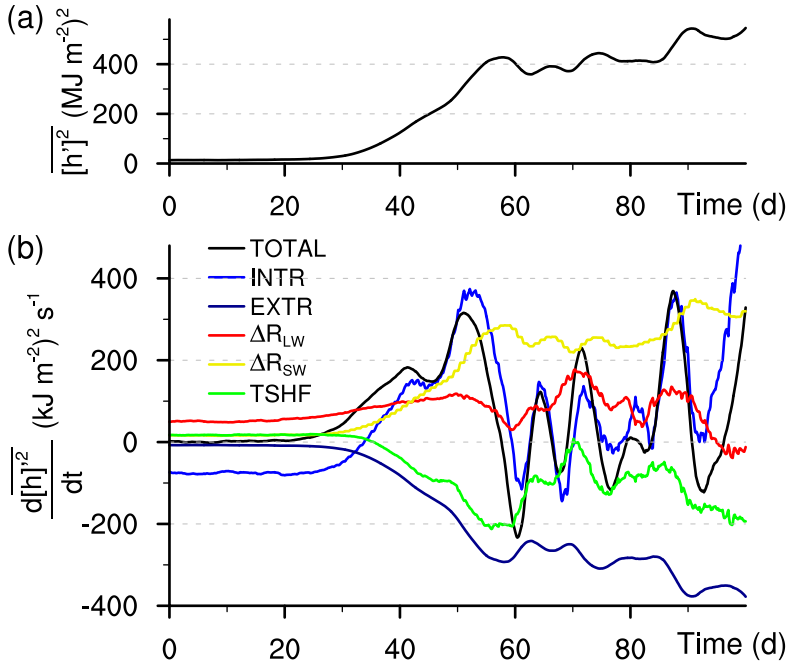

Figure 3.2: Time evolution of (a) variance $\overline{[h']^2}$ of column MSE $[h]$ for days 1-100 of a Meso-NH simulation; (b) corresponding tendency of $\overline{[h']^2}$ (black line) and the contributions from the different processes: transport (INTR, blue line), terrestrial radiation (ΔR_{LW}, red line), solar radiation (ΔR_{SW}, yellow line) and turbulent surface heat fluxes (TSHF, green line). In this particular simulation, a large-scale forcing is added by an imposed homogeneous subsidence which creates an additional transport contribution (EXTR, dark blue line); adapted from Bellon & Coppin (2022))

- Transport of MSE generally redistributes MSE and opposes aggregation (Wing & Emanuel, 2014; Wing et al., 2018, Bellon & Coppin, 2022). But this circulation can be decomposed into a troposphere-deep circulation and a shallow circulation extending from the surface to the lower troposphere. The deep circulation is associated to a positive GMS, transports MSE downgradient, and opposes aggregation. On the other hand, the shallow circulation is associated to a negative GMS, transports MSE upgradient and favors aggregation. This circulation results from terrestrial cooling at the top of the dry-region ABL, often at the top of the ABL clouds, and is instrumental to developing self-aggregation because it develops before the deep circulation (Muller & Held, 2012; Muller & Bony, 2015; Ackerman et al., 2009). The contribution of transport exhibits a large temporal variability in the aggregated state: it is the main source of time variability in $\overline{[h']^2}$ and can change sign depending on the intensities of the shallow and deep circulations.

Another analysis based on a measure of variability in convective instability (available potential energy) also highlights the role of ABL diabatic processes in the development of self-aggregation (Yang, 2018b).

In general, any process that makes convection more difficult favors aggregation. For example, an increase in convective entrainment favors aggregation (Tompkins & Semie, 2017; Becker et al., 2017), and so does the addition of large-scale subsidence to the configuration (Bellon & Coppin, 2022). Convective cold pools can organize convection spatially because ascent occurs at the gust fronts and particularly where these fronts meet, where deep convection can be triggered. As a result, cold pools contribute and might be fundamental to self-aggregation (Tompkins, 2001; Haerter, 2019; Haerter et al., 2020), although the opposite influence was documented in simulations over small domains (Jeevanjee & Romps, 2013).

Fewer studies have documented the mechanisms that dismantle aggregation. Bellon & Coppin (2022) shows that the contributions of the different physical processes are similar: in Meso-NH, disaggregation primarily results from transport, and diabatic processes generally oppose disaggregation, but the contribution of turbulent surface heat fluxes can change sign for some (model) time and contribute to disaggregation.

3.1.3 Scales of aggregation

The shape and spatial scale of self-aggregated convective disturbances vary depending on models and model geometry (Wing et al., 2020). For SRMs over square domains, self-aggregation most often results in one convective patch which scales with the size of the domain up to domain-sizes of a few thousand kilometers (Muller & Held, 2012; Muller & Bony, 2015; Patrizio & Randall, 2019). Sometimes, self-aggregation results in a convective band (as Figure 3.1b above or in Muller & Bony, 2015; Patrizio & Randall, 2019), which seems to happen for similar areas of the convective and dry regions. In simulations over rectangular, "channel" domains, self-aggregation generally creates convective bands parallel to the shortest sides of the rectangle (Wing & Cronin, 2016; Wing et al., 2020). The number of convective bands depends on models (Wing et al., 2020) and increases with SST (Wing & Cronin, 2016). Yang (2018a) proposed a scaling based on the buoyancy budget of the ABL that predicts a typical scale of 2000 km for self-aggregation, which is consistent with a number of model results (Patrizio & Randall, 2019; Wing & Cronin, 2016; Wing et al., 2020). Beucler & Cronin (2019) showed that the different diabatic processes favor different spatial scales: terrestrial radiation organizes convection on large-scales (1000–5000 km), while solar radiation favors smaller scales (500—2000 km), and the wind-induced surface heat fluxes tends to reduce the scale of aggregated convection. The diversity of spatial scales documented in SRMs might result from the differing influences of physical processes on self-aggregation. If an external forcing such as large-scale subsidence is added to the configuration, the scale of the convective region can vary significantly with the forcing, from about 20% to about 80% of the domain area (Bellon & Coppin, 2022).

In terms of time scales, self-aggregation occurs over tens of days (Wing et al., 2018), with the most active aggregation phase between 10 and 20 days in most models (Bretherton et al., 2005; Muller & Held, 2012; Holloway & Woolnough, 2016; Wing & Cronin, 2016; Bellon & Coppin, 2022). This is consistent with the e-folding time of the instability of 9 days found in Bretherton et al. (2005)'s semi-empirical model. For disaggregation, the time scales are similar (Muller & Held, 2012; Holloway & Woolnough, 2016; Bellon & Coppin, 2022).

3.1.4 Relevance to observed convection

The relationship between observed spatial organization of convection and self-aggregation is still a pending question. We see spatial organization of convective clouds at multiple scales in the observations as in model simulations, and the differences between aggregated and non-aggregated convection exhibit some common characteristics in observations and simulations (Tobin et al., 2012; Holloway et al., 2018). Potentially, modeled self-aggregation could be used to understand real-world development of convective disturbances. But it is still unclear if the mechanisms at play in idealized model configurations such as RCE are the same as in the real world and active in the development of MCSs, tropical storms, and/or intraseasonal disturbances. Self-aggregation occurs on multiple spatial scales, making it potentially relevant to all observed modes of organization, but its typical time scales point to a possible role in slow synoptic and intraseasonal disturbances.

Multiple numerical experiments of self-aggregation including more realistic processes have already been performed. Rotation has been shown to transform the self-aggregated convective clusters into tropical cyclones (Bretherton et al., 2005; Khairoutdinov & Emanuel, 2013; Zhou et al., 2014; Shi & Bretherton, 2014; Wing et al., 2016; Merlis et al., 2016; Muller & Romps, 2018). Whether most observed cyclones result from self-aggregation processes is still a matter of debate, however; the time scales of self-aggregation are on the slow side to explain the fastest cyclone intensification and some alternative theories posit dynamical precursors (e.g., Dunkerton et al., 2009).

The influence of, and interaction with, the surface has also been explored. SST contrasts favor self-aggregation and reinforce the stability of the aggregated stationary state (Shamekh et al., 2020a), and convective organization may disregard the symmetry of a prescribed SST field (Müller & Hohenegger, 2020). Coupling with a simple model of the upper ocean slows self-aggregation (Hohenegger & Stevens, 2016; Shamekh et al., 2020b) and the coupled ocean-atmosphere feedbacks can introduce some internal variability because SST cools under the convective region as a result of reduced solar flux due to cloud albedo, and convection migrates towards warmer SSTs (Coppin & Bony, 2017; Tompkins & Semie, 2021).

The influence of large-scale circulation has seldom been explored. A recent study documented the sensitivity of self-aggregation to imposed vertical motion (Bellon & Coppin, 2022). Large-scale motion appears to influence self-aggregation: subsidence favors aggregation and ascent can inhibit self-aggregation. This could explain why convection is more organized before and after the active phase of intraseasonal disturbances, rather than during these active phases (Sakaeda & Torri, 2022). But the sensitivity is

non-linear, including a hysteresis: for a range of subsidence intensity, both an aggregated and a non-aggregated stable stationary states can be obtained depending on the initial conditions, while only the aggregated stationary state is stable for larger subsidence and only the non-aggregated stationary state is stable for weaker subsidence and ascent.

A better understanding of the relevance of self-aggregation to the observed organization of deep convection in the tropics requires a hierarchy of model configurations towards more realistic experiments. One type of phenomena for which self-aggregating processes might be particularly relevant are intraseasonal disturbances because the time scales of self-aggregation are squarely in the intraseasonal range, and also, somewhat opportunistically, because we are still to find a consensus on the fundamental mechanisms of these disturbances.

3.2 Intraseasonal variability

3.2.1 Observations

The most puzzling phenomenon in the tropical subseasonal variability is the *Madden-Julian Oscillation* (MJO, Madden & Julian, 1971; Zhang, 2005). This is an eastward-propagating intraseasonal mode of variability, with a planetary wavenumber between 1 and 2 and a period of about 40 days (i.e., a frequency of about 0.025 day^{-1}). The signal of this mode is clearly visible in the spectrum of symmetric variability in Figure 1.6. Using the MJO index of Wheeler & Hendon (2004), this oscillation can be divided into 8 phases. Figure 3.3 shows this life cycle for the austral summer (November-April). In this season, the so-called *canonical* MJO occurs: a large-scale envelope of anomalous convection develops in the western equatorial Indian Ocean and propagates eastward at a speed of about 5 m s^{-1} all the way to the middle of the Pacific ocean. This convective disturbance is called the *active phase* of the MJO. It is first preceded and later followed by a region of reduced convection, the *suppressed phase*. The winds associated with the active phase are very similar to the Gill circulation (see Section 1.5), with two off-equatorial cyclonic gyres west of the convective envelope and easterlies east of the envelope (Hendon & Salby, 1994; Kiladis et al., 2005). This suggests that the circulation is close to quasi-equilibrium with the diabatic heating in the convective envelope [1]. There is also a Gill circulation associated with the suppressed phase, with anticyclonic gyres and equatorial westerlies, which is superposed onto the main dynamical response to the active phase. An upper-tropospheric dynamical signal can be observed propagating further than the convective signal, with a faster propagation speed (15-20 m s^{-1}); this dynamical signal can complete the circumnavigation and trigger convective intensification anew in the western Indian Ocean. In some cases, an MJO-like convective disturbance develops in the Indian Ocean and starts propagating eastward, but decays over the archipelagos and peninsulas [2] around the equator between the Indian and Pacific Oceans, a region called *Maritime Continent*. The reasons for this occasional decay are still being explored.

In boreal summer, the direction of propagation is north-northeastward, as Figure 3.4 shows. This mode is either called boreal-summer MJO, *boreal-summer intraseasonal oscillation*, or *monsoon instraseasonal oscillation* (MISO); we will use the last name in this manuscript. It is an important modulator of the Asian monsoon, with significant impacts (droughts, floodings) in the region (Kikuchi, 2021).

3.2.2 Theories

There is still considerable debates on the fundamental mechanisms that cause the development and the propagation of MJO disturbances. At this point, six theories (or families of theories) have been proposed (Zhang et al., 2020; Yano & Tribbia, 2017; Ahmed, 2021; Kim & Zhang, 2021), they describe the MJO as:

1. the result of a propensity for synoptic convective activity to organize at large scales (Majda & Stechmann, 2009, 2011; Thual et al., 2014);
2. a moisture mode powered by surface fluxes, zonal and meridional moisture transport (see Section 1.5, Sobel & Maloney, 2012, 2013; Adames & Kim, 2016; Ahmed, 2021; Wang & Sobel, 2022);
3. the result of a trio-interaction between moisture, convection, and ABL frictional convergence (Wang et al., 2016a; Wang & Chen, 2017) (essentially a moisture mode but with a strong role of low-level circulation);

[1] Chao (1987) showed that the circulation associated to a slowly propagating diabatic source is very similar to the Gill circulation.

[2] i.e. : Indonesia, Malaysia, East Timor, Papua New Guinea, etc.

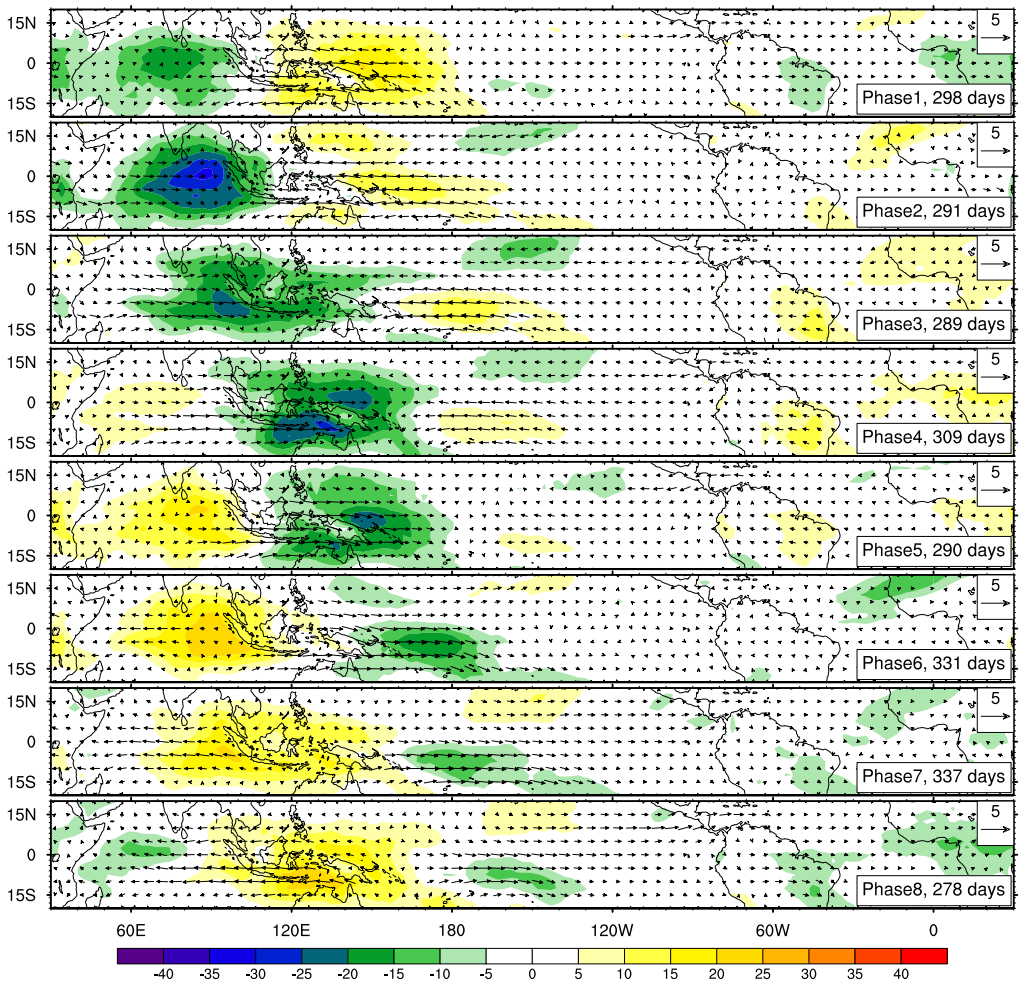

Figure 3.3: Life cycle of the Madden-Julian Oscillation: OLR (NOAA, shadings) and 850hPa wind (ERA-Interim, vectors) associated with the austral-summer (November-April) MJO as identified by Wheeler & Hendon (2004)'s method. (Convective clouds appear as negative anomalies of OLR because of their greenhouse effect.)

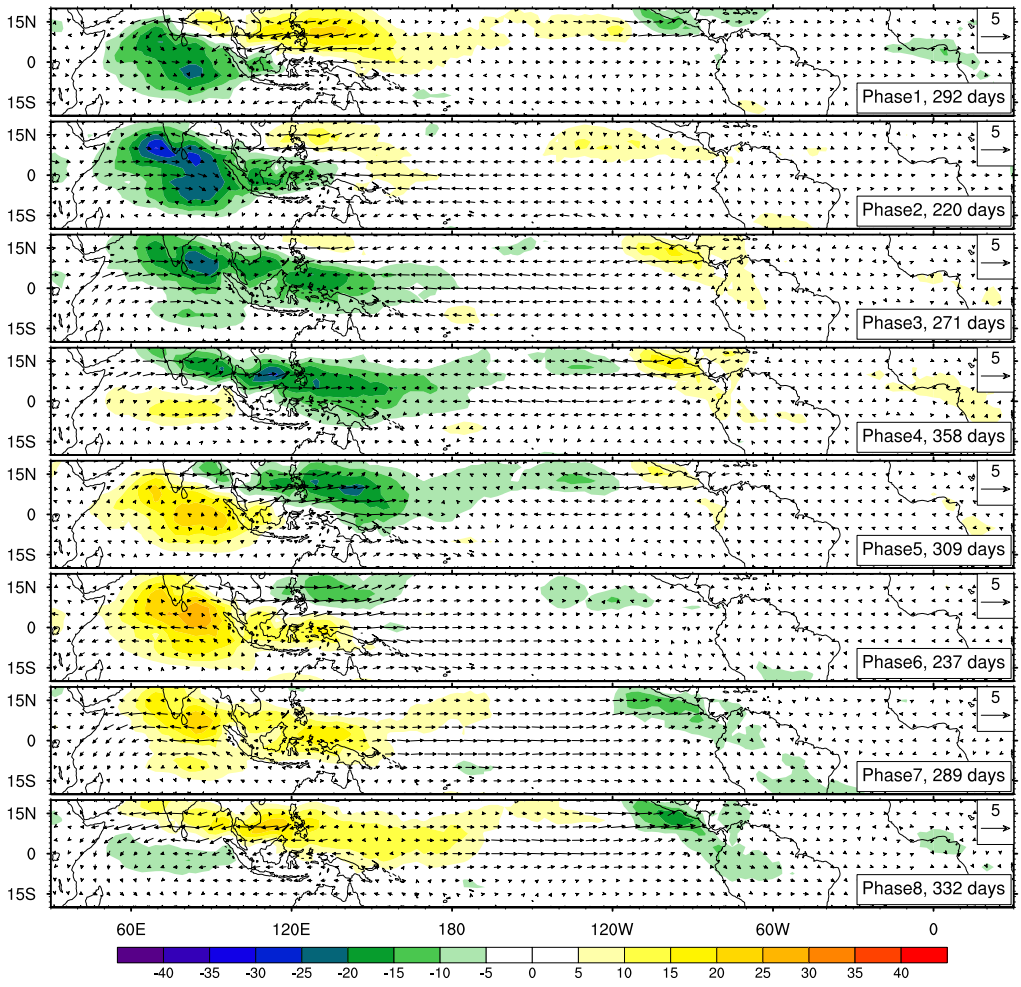

Figure 3.4: Life cycle of the Monsoon Intraseasonal Oscillation: OLR (NOAA, shadings) and 850hPa wind (ERA-Interim, vectors) associated with the MISO, or boreal-summer (May-October) MJO, as identified by Wheeler & Hendon (2004)'s method.

4. a large-scale envelope of westward- and eastward-propagating inertio-gravity waves (Yang & Ingersoll, 2013, 2014).

5. a non-linear free wave called modon (Yano & Tribbia, 2017; Rostami & Zeitlin, 2019);

6. a Kelvin wave modified by momentum damping and caused by resonance in the intraseasonal frequencies stimulated by the stochastic forcing of extratropical variability (Kim & Zhang, 2021, and references therein).

Some of these theories (1, 2) can explain both the MJO and MISO. There is also some convergence between Theories 2 and 3, but overall this list provides a surprising diversity of explanations for a planetary mode of variability identified half a century ago.

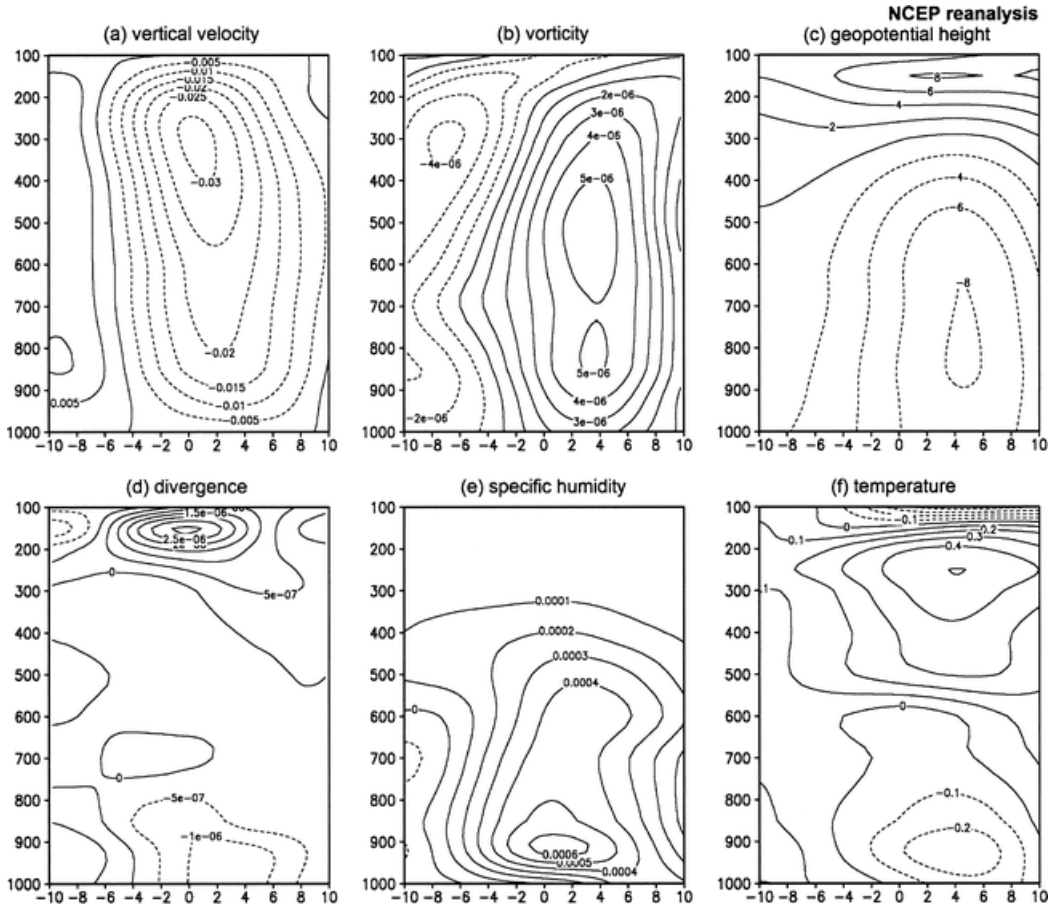

Figure 3.5: Meridional–vertical structure of the northward-propagating MISO mode derived from the NCEP reanalysis: (a) vertical velocity (hPa s^{-1}), (b) vorticity (s^{-1}), (c) geopotential height (dam), (d) divergence (s^{-1}), (e) specific humidity (kg kg^{-1}), and (f) temperature (K). Horizontal axis is the meridional distance (° of latitude) with respect to the convection center, positive northward. The vertical axis is the pressure (hPa). From Jiang et al. (2004).

A few mechanisms for the poleward propagation of MISO disturbances have been independently proposed. They rely on an analysis of the meridional and vertical structure of the disturbances. Figure 3.5 shows a composite of this structure: the intraseasonal disturbance propagates because the low-level atmosphere is moister poleward of the convective center: lower-tropospheric humidity is maximum about 1° poleward of the convective center (Fig. 3.5e); this humidity pattern is caused by ABL convergence and low-level ascent ($-w'\partial_z\overline{q}$, with the prime denoting the intraseasonal anomaly and the overbar denoting the seasonal mean) about 3° poleward of the convective center (Figure 3.5a,d), completed by horizontal advection resulting from the converging anomalous meridional wind in a seasonal background characterized by a poleward increase in low-level humidity ($-v'\partial_y\overline{q}$). This ABL convergence results, by continuity, from free-tropospheric divergence. In turn, free-tropospheric divergence results from a troposphere-deep

vorticity pattern 3-4° poleward of the convective center (Fig. 3.5b): the last term on the left-hand side of Equation (1.10) shows that the effect of planetary rotation creates a source of divergence $f\zeta$ proportional to the vorticity. Understanding the poleward propagation therefore boils down to explaining the development of the vorticity maximum poleward of the convective center. This point is where the proposed mechanisms diverge; this vorticity pattern is attributed to different terms of Equation (1.11), either:

- the tilting term, and more precisely the anomalous vertical advection of the seasonal-mean vertical shear of the zonal wind $\partial_z \overline{u} \partial_y w'$ (Jiang et al., 2004; Drbohlav & Wang, 2005; Li et al., 2021), on the basis of a simple analytical model on an f-plane.
- advection of the anomalous vorticity by the seasonal-mean flow, and more precisely the advection of anomalous baroclinic vorticity by the seasonal-mean, baroclinic, meridional wind in $-\overline{v}\partial_y \zeta'$. This is a mechanism identified in simulations of poleward-propagating intraseasonal disturbances by an intermediate-complexity model, illustrated in Figure 3.6 (Bellon & Sobel, 2008b,a).
- non-linear advection of the disturbance by itself $-\overline{v'\partial_y \zeta'}$, with the northward propagation resulting from the β-drift [3] of synoptic disturbances developing from the breakdown of the ITCZ (Boos & Kuang, 2010).

Some evidence of the two first mechanisms have been found in the observations (Chou & Hsueh, 2010; DeMott et al., 2013), with their relative importance varying geographically.

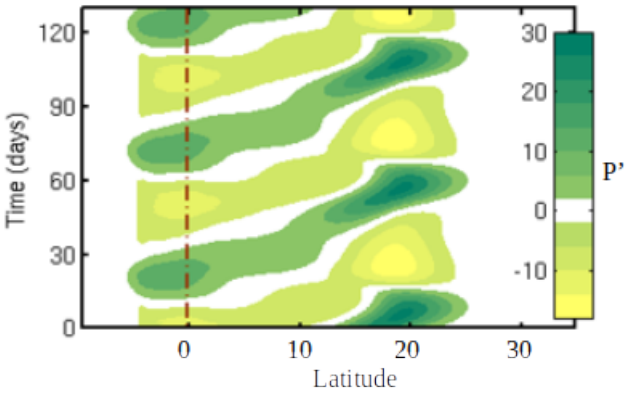

Figure 3.6: Northward propagation resulting from the anomalous vorticity advection by the seasonal mean flow in an intermediate-complexity model: Hovmöller of the simulated precipitation anomaly. Adapted from Bellon & Sobel (2008b).

3.2.3 Energetics

The active phase of a subseasonal convective disturbance is co-located with a maximum of the vertically integrated MSE, $[h]$ (conversely, a suppressed phase corresponds to a minimum of [h]). An intraseasonal disturbance can therefore be considered as an accumulation and a discharge of MSE. Budgets of [h] following Equation (1.13), shed light on the energetics of the MJO (Kiranmayi & Maloney, 2011; Sobel et al., 2014; Ren et al., 2021). Overall, the diabatic terms (surface and radiative fluxes) tend to sustain the convective disturbances. Indeed, the terrestrial radiative effect of moisture and clouds warm the atmospheric column during the active phase of intraseasonal disturbances (Bony & Emanuel, 2005). The effect of surface fluxes is more complex: the wind-induced contribution was initially thought to cause the eastward propagation of the MJO (Emanuel, 1987; Neelin et al., 1987), but it is now established that it contributes to developing and sustaining intraseasonal disturbances (Sobel et al., 2008, 2010) and it is included in most simple models supporting the theories presented in the previous section. The contribution of air-sea thermodynamic contrast, on the other hand, damps the disturbances.

As for the contribution of MSE transport, it is overall a damping, because vertical transport is dominant and the GMS is positive in the Indo-Pacific tropical regions (see Equation (1.17)). Not surprisingly,

[3] which is the mechanism involving the anomalous meridional advection of planetary vorticity $v'\partial_y f = v'\beta$, also responsible for the poleward migration of tropical cyclone.

the model average GMS has a strong impact on the amplitude of the MJO signal in models (Benedict et al., 2014). But MSE transport is also essential to the propagation of the convective disturbance: the GMS increases during the active phase of intraseasonal variability, which means that vertical advection exports less MSE from the atmospheric column during the transition from suppressed to active phases than during the opposite transition. This evolution of the GMS follows the evolution of the vertical motion from more shallow circulation to a top-heavy profile and the evolution of the cloud regime, from shallow and congestus convection to stratiform precipitating clouds. This asymmetry of vertical advection with respect to the convective disturbance favors propagation, but horizontal advection contributes at least as much to propagation, with a contribution of zonal advection by the low-level westerly jet but also a strong non-linear contribution of smaller-scale synoptic eddies to meridional advection (Kiranmayi & Maloney, 2011; Sobel et al., 2014).

3.2.4 Modeling

Another surprise is that none of the theories above except Theory 1 include processes that are not represented in GCMs, but most of the current models struggle to simulate the MJO (Le et al., 2021; Chen et al., 2022; Li et al., 2022) and MISO (Sabeerali et al., 2013), as in previous generations of models (Hung et al., 2013; Sabeerali et al., 2013; Duvel et al., 2013; Jiang et al., 2015). Modelers attributed the limited ability of GCMs to simulate tropical intraseasonal variability to either:

1. the models' incorrect simulation of the vertical profile of diabatic heating Q_1;
2. the models' inability to simulate the real-world spatial organization of convection, and therefore the horizontal pattern of diabatic heating Q_1.

The second hypothesis raises the question of the potential role of self-aggregation mechanisms in the simulation of the MJO and MISO. Models supporting Theory 1 above include a variable describing the synoptic-scale convective activity, whose tendency is controlled by humidity. It can be understood as an ad-hoc parameterization of the interaction between synoptic and large-scale convective disturbances and is probably instrumental in organizing convection on large scales in these models.

Simulations to investigate the first hypothesis were produced by an intercomparison project (Jiang et al., 2015). Overall, the profiles of diabatic heating simulated by GCMs are fairly similar, with only a small difference in shallow heating ahead of the active phase of MJO disturbances. Only the GCMs with the highest skill at simulating the MJO simulate such an early shallow heating (Jiang et al., 2015) which could be instrumental to the propagation of the disturbance via moistening and up-gradient MSE transport (since shallow circulations are associated with negative GMS). But reanalysis data does not seem to exhibit much shallow heating, so the importance of this mechanism might be inflated in such GCMs. The main difference between latent heating simulated by GCMs most skilled at simulating the MJO and GCMs least skilled is the larger horizontal size of the heating associated with intraseasonal disturbances (Jiang et al., 2015). Moreover, uncertainties in the estimates of diabatic-heating vertical profiles from satellite observations are as large as or even larger than inter-model differences (Bellon et al., 2017), which makes the diagnostic of this hypothesis inconclusive.

Examination of the second hypothesis is still ongoing. Some studies have advanced that the MJO results from self-aggregation mechanisms (Andersen & Kuang, 2012; Arnold & Randall, 2015; Khairoutdinov & Emanuel, 2018), but at times the disturbances obtained in these models are convectively coupled Kelvin waves (Shi & Bretherton, 2014). In the absence of rotation, self-aggregation organizes convection on planetary scales (4000 km in Andersen & Kuang, 2012), larger than the observed MJO heating (see Fig. 3.3). Rotation, and therefore dynamics, might play a role in the scale selection of the MJO. One key element in the observed MJO is the associated Gill convection: this is suggested by observations and confirmed by GCM *aquaplanet* [4] experiments in which MJO modes, when simulated, are systematically associated with such a circulation (Leroux et al., 2016), and no such circulation is associated with the simulated intraseasonal variability if the MJO is not simulated. This raises the question as to whether there are scales associated with the Gill circulation that could explain or contribute to the spatial scale selection of the MJO disturbances. As can be expected, the spatial scale of the Gill circulation increases with the spatial scale of the diabatic heating forcing this circulation. However, the intensity of the overturning circulation (i.e., the mass flux that ascends in the ascending region and subsides in the surrounding regions) decreases with increasing horizontal scales of the diabatic heating as illustrated in Figure 3.7a (Reboredo & Bellon, 2022; Bellon & Reboredo, 2022). Considering that the overturning

[4] aquaplanet configurations consider a planet with no continent.

circulation provides the moisture necessary to maintain diabatic heating via latent heat release and cloud radiative effect, this suggests that the spatial scale selection of the MJO could result from competition between aggregating mechanisms favoring large scales and circulation response favoring small scales.

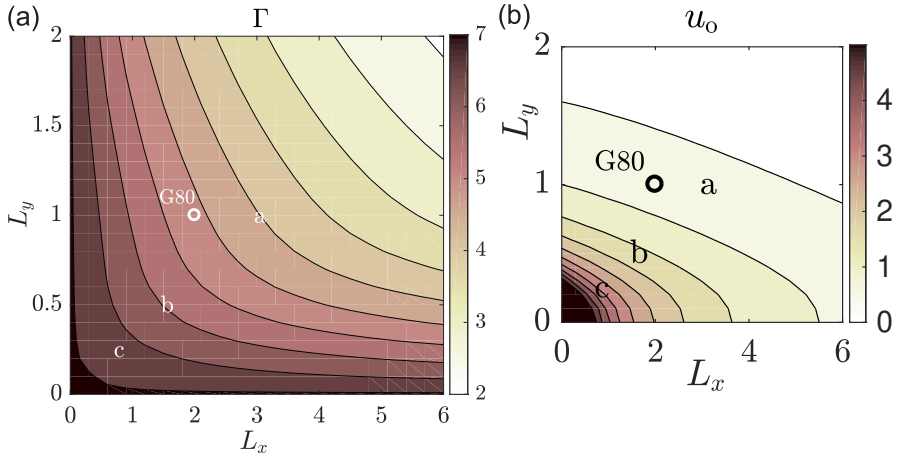

Figure 3.7: Sensitivity of the equatorial Gill circulation to the horizontal scales of the imposed diabatic heating: (a) normalized intensity Γ of the overturning circulation and (b) normalized velocity u_o of the low-level westerly wind at the center of the diabatic heating, as a function of the normalized zonal scale L_x and meridional scale L_y of the diabatic heating. For normalized spatial scales, $1 \sim 1000$ km; adapted from Reboredo & Bellon (2022).

3.2.5 Surface–atmosphere interaction at the intraseasonal scale

Although intraseasonal variability essentially results from atmospheric processes, it is enhanced by ocean-atmosphere coupled processes (see DeMott et al., 2015, for a review). The fundamental reason for this is that the time scales associated with heat storage in the upper ocean (i.e., in an oceanic mixed layer depth of a few tens of meters) are in the intraseasonal range (Sobel & Gildor, 2003; Maloney & Sobel, 2004) and this storage can interact with the intraseasonal modes of atmospheric variability. The optimal enhancement of the atmospheric variability occurs over regions of the oceanic mixed layer depth of 20 – 30 m (Bellenger & Duvel, 2007). During suppressed phases of intraseasonal variability, surface downward solar radiation is large and turbulent fluxes are small, yielding a warming of the upper ocean; on the contrary, downward solar radiation is reduced by the albedo of convective clouds and turbulent fluxes are increased by gustiness during active phases, yielding a cooling of the ocean. As a result, SST maxima lead the intraseasonal convective disturbances and SST minima lag convection (Woolnough et al., 2000; Vecchi & Harrison, 2002; Rajendran et al., 2004; Rajendran & Kitoh, 2006; Roxy & Tanimoto, 2007; Duvel & Vialard, 2007). In turn, this SST pattern modulate the surface fluxes: it increases them ahead of the convective disturbance and decreases them after it, therefore accelerating the propagation of the convective disturbance (Bellon et al., 2008). In addition, the oceanic mixed layer shoals during suppressed phases and deepens during active phases because of the co-localized turbulent surface fluxes, dominated by the wind-induced contribution, and wind stirring (Bellon et al., 2008, Keerthi et al., 2016). The associated modulation of vertical mixing enhances the SST pattern. These coupled ocean-atmosphere mechanisms enhance the intrasesonal variability in coupled ocean-atmosphere GCMs compared to their atmosphere-only counterpart (Rajendran & Kitoh, 2006; Wyant et al., 2007; Watterson & Syktus, 2007; Daleu et al., 2015; Jiang et al., 2015; Gao et al., 2020)

In some regions, the ocean is very stratified near the surface and the heat capacity of the surface layer has the same order of magnitude as over continental surfaces. In these regions, the time scales typical of the upper ocean heat storage are much shorter than intraseasonal scales and the SST can exhibit a strong diurnal cycle similar to the diurnal cycle of surface temperature over land, resulting in so-called *diurnal warm layers*. Over these regions, deep convection also exhibits a diurnal cycle similar to that over islands with a maximum of precipitation in the afternoon. Such strong stratification of the upper ocean occurs when surface winds, and therefore surface buoyancy flux and wind stirring, are weak, as is the case during the suppressed phase of intraseasonal variability. As a result, diurnal warm layers tend to occur during the suppressed phase of intraseasonal variability and the transition to the active phase

(Bellenger & Duvel, 2009; Bellenger et al., 2010). The associated convective free-tropospheric moistening favors the eastward propagation of the MJO.

Over the islands of the Maritime Continent, a similar pattern is observed: in austral summer, the precipitation over the islands starts intensifying 5 to 10 days before the active phase of the Madden Julian Oscillation, resulting from an amplified diurnal cycle (Peatman et al., 2014; Sakaeda et al., 2017, see Section 4.2 for details). It appears that, unlike the contribution of the diurnal warm layers, this diurnal cycle over the islands is at least one of the factors which explain why the Maritime Continent forms a barrier to the propagation of the MJO: the stationary convection over the islands disrupts and competes with the MJO convective disturbance (Hagos et al., 2016; Ajayamohan et al., 2021).

Another way for the surface to impact intraseasonal variability is through its impact on the seasonal mean; this appears to be a factor in the barrier effect of the Maritime Continent through the effect of island precipitation on the seasonal-mean moisture gradients which modify moisture and MSE transport at the intraseasonal scale (Ahn et al., 2020). The poleward extent of the monsoon, which is affected by land albedo, also appears to condition the development of MISO disturbances (Bellon, 2011). I won't expand on this topic here since the effect of the surface on the long-term or seasonal-mean convergence zones and circulation is among the topics of the next chapter.

3.3 Perspectives

3.3.1 Mechanisms of self-aggregation

I have an interest in investigating further the spontaneous organization of convection, with a particular focus on the link between self-aggregation and intraseasonal disturbances. I feel that a small gap remains in translating our understanding of self-aggregation into a simple physical model. Most current simple models present self-aggregation as a linear instability of the RCE (Emanuel et al., 2014; Beucler et al., 2018; Kuang, 2018). This contrasts with results from storm-resolving and general-circulation models that exhibit multiple stationary states (as in Figure 3.1; Muller & Held, 2012; Coppin & Bony, 2015; Bellon & Coppin, 2022). Linear models can explain the behavior of these models above the threshold for instability of the non-aggregated RCE, but not the existence of multiple equilibria or stationary states.

Furthermore, all linear simple models are essentially 1D in the vertical (Emanuel et al., 2014; Beucler et al., 2018; Kuang, 2018), focusing on thermodynamic column budgets with dynamics parameterized using WTG or DGW. One recent simple model of self-aggregation based on anelastic equations is non-linear (Yang, 2021), with the non-linearity resulting from inhibition and triggering of convection. It is 1D on the horizontal, focusing on a simple representation of ABL thermodynamics.

A couple non-linear models have been proposed that present self-aggregation as a coarsening phenomenon (Craig & Mack, 2013; Biagioli & Tompkins, 2023). These models are conceptually interesting and explain the spatial behavior of the aggregating process. They are based on a highly idealized moisture budget and it would be interesting to investigate whether such a coarsening mechanism occurs in a model based on anelastic or primitive equations, possibly with some tweaks.

In my opinion, a physical model describing how the diabatic processes can couple to the dynamics in a 3D or 2D horizontal-vertical geometry to cause self-aggregation would provide another level of understanding of the fundamentals of this phenomenon. The vertical dimension is important for analyzing the results in terms of MSE variance to validate that the mechanisms are the same as in the SRMs and GCMs. It would also be interesting to reproduce the hysteresis and explain the mechanisms responsible for this non-linear behavior. Improved simple models of atmospheric dynamics as envisioned in the Perspectives of Chapter 2 could be used in this endeavor, with a hierarchy of representations of thermodynamic processes.

3.3.2 Self-aggregation and large-scale organization

Another interest of mine is to try to understand whether there is a link between self-aggregation and intraseasonal variability. At this point in time, understanding and simulating the MJO and MISO are still challenges for our community. Investigating the link between intraseasonal variability and self-aggregation is a way to investigate whether, as suspected, it is the spatial organisation of convection that is fundamental to the development of intraseasonal disturbances and is challenging to simulate in GCMs.

The space and time scales of self-aggregation are consistent with those of the MJO and MISO, so one hypothesis would be that the self-aggregation mechanisms are instrumental in the development of intraseasonal disturbances. But the convective patches obtained in the aggregated states appear more

compact and continuous than the observed intraseasonal disturbances, which appear more as envelopes of convective systems rather than one large-scale convective system. And mesoscale convective organization varies with the MJO (Mapes et al., 2006; Sakaeda & Torri, 2022), so an antithesis is that self-aggregation mechanisms participate in mesoscale convective organization and the intraseasonal variability results from other mechanisms and only modulates self-aggregation; there is considerable interest in the community to investigate this modulation in observations of cloud systems. If so, how do these intraseasonally modulated MCSs influence the large-scale intraseasonal disturbance? This is still a very unclear.

One way to test the first hypothesis is to attempt to understand how the intraseasonal spatial scale is selected. On one hand, over a non-rotating domain, self-aggregation appears to have an upper limit of a few thousand kilometers for the horizontal scale of convective disturbances (Patrizio & Randall, 2019). On the other hand, the sensitivity of the Gill circulation shows that, in a rotating system, transport feedbacks are weaker than in the non-rotating system and favor small scales (Reboredo & Bellon, 2022; Bellon & Reboredo, 2022). The articulation of thermodynamic self-aggregation mechanisms and the circulation in the presence of rotation (on a β-plane) is certainly the key to the scale selection of the MJO and MISO. A first step will be to examine how well the observed/reanalyzed MJO and MISO circulations relate to the Gill circulation; i.e., determine whether the linear equations and the Rayleigh damping are reasonable approximations for intraseasonal disturbances. This requires an analysis of the momentum budget at intraseasonal scales using reanalysis data. Beyond this step, estimates of intraseasonal diabatic heating from reanalysis or satellite observations can be analyzed to document the evolution of diabatic heating and its horizontal scales throughout the life cycles of MJO and MISO disturbances. The relationship between scales of diabatic heating and circulation can then be evaluated and compared to theoretical predictions. These investigations might shed some light on the intensity, growth, and decay of intraseasonal convective disturbances.

The possibility that intraseasonal convective disturbances result from the combination of self-aggregation mechanisms and Gill circulation can be further evaluated using intermediate-complexity models, such as the Quasi-equilibrium Tropical Circulation Model (Neelin & Zeng, 2000; Lintner et al., 2012). The interest of using such a model is its relative simplicity and computational availability, which allow for easy modifications and multiple tests. The QTCM does not simulate self-aggregation or MJO in its current formulation. Modifications of the convective triggering can be implemented to try to obtain convective aggregation, such as modifying convective and radiative parameters, including a stochastic factor, possibly influenced by memory effects (deep convection is more likely to be triggered if it was triggered at the previous time step) and/or neighbor effects (deep convection is more likely to be triggered if it was triggered in a neighboring location at the previous time step). It would be interesting to investigate whether different types and scales of self-aggregation can be obtained by changing the parameters controlling these effects and whether these different regimes remain once rotation is included, so that a diversity of disturbances, including but not limited to tropical cyclones, can be obtained. The results would further investigate the link between self-aggregation in non-rotating and rotating configurations and would hopefully shed some light on the relevance of self-aggregation for intraseasonal disturbances. Possibly, this work could yield an intermediate-complexity model of the MJO and MISO to confront to existing theories.

Finally, an opportunity to document the link between convective self-aggregation and MJO simulation in GCMs is provided by the participation of many models to both CMIP6 and RCEMIP (Wing et al., 2018): convective self-aggregation in these models in RCE can be evaluated in relation with their skill at MJO simulation in more realistic settings (aquaplanet, atmosphere-only, or coupled ocean-atmosphere configurations). This might also help understanding the GCMs' limited skill at simulating intraseasonal disturbances in the tropics.

4 Organization due to surface conditions

In this chapter, we will present some of the ways the surface can cause spatial organization of deep convection. The most prominent surface forcing is the sea surface temperature (SST): surface heat fluxes increase with increasing SST, warm and moisten the ABL, and destabilize the atmospheric column. As a result, deep convection tends to occur over warm oceanic surfaces. There is also an influence of surface heterogeneity, of the contrast between continental and oceanic surfaces. At large scales, this contrast is responsible for most of the monsoons and at mesoscale this contrast creates the coastal breeze systems and the associated rains.

Large-scale convective regions are called tropical convergence zones (CZs) and they are coupled to large-scale circulations, the Hadley and Walker circulations. At the planetary scale, the main convergence zone is the *Intertropical Convergence Zone* (ITCZ), a longitudinal rain band that lies close to the equator, between 4 and 10 °N of the Equator in the Pacific and Atlantic oceans and that is co-located with the ascending branch of the Hadley circulation. Monsoons can be considered as a poleward migration of the ITCZ, or at least a change in the ITCZ regime. For example the West-African monsoon is a northward migration of the ITCZ, and the seasonal-mean Indian monsoon is characterized by two convergence zones, one near the equator and one in the subtropics (around 20°N).

4.1 ITCZ and monsoons

4.1.1 Hadley circulation theory

Our understanding of the ITCZ characteristics relies heavily on theories of the Hadley circulation. The earliest one was the *angular-momentum conserving* (AMC) theory (Held & Hou, 1980; Lindzen & Hou, 1988; Plumb & Hou, 1992) which described the response of an axisymmetric atmosphere to Newtonian temperature relaxation towards a latitude-varying reference temperature, assumed to encompass all diabatic processes. Held & Hou (1980) studied the case of a maximum reference temperature at the equator, which is known as the equinoctial Hadley circulation; Lindzen & Hou (1988) and Plumb & Hou (1992) extended the study to an off-equatorial maximum.

In these models, the temperature relaxation creates meridional pressure gradients that force the vertical-meridional overturning Hadley circulation. In the equinoctial case, two overturning cells form, one in each hemisphere, with ascent around the equator, poleward motion in the upper troposphere, subsidence in the subtropics, and equatorward flow in the lower troposphere. In the almost-inviscid free troposphere, angular momentum with respect to the Earth's axis of rotation is conserved, so a parcel of air with little zonal wind in the ascending branch accelerates eastward as it moves poleward in the upper troposphere because it gets closer to the Earth's axis. This explains the subtropical westerly jets. At the poleward boundary of the Hadley circulation, mixing by extratropical eddies reduces the angular momentum. In the return equatorward surface flow of the Hadley circulation, air parcels with smaller angular momentum move away from the Earth's axis and therefore accelerate westward with respect to the surface, forming the easterly trade winds.

In the case of maximum off-equatorial heating, the two Hadley cells are asymmetric with respect to the equator: a large winter cell extends from the region of ascent around the heating to the subtropics of the other hemisphere while a weak summer cell extends only poleward of the region of heating. Parcels can move equatorward in the upper troposphere from the location of ascent and accelerate westward and, for cases with heating poleward of about 10°, near-surface westerlies can develop between the equator and the region of ascent. This is typical of a monsoon circulation, and these westerlies are sometimes called the monsoon jet. The AMC theory predicts a latitudinal extent of the Hadley circulation similar to the observed circulation (30° north and south of the equator in the equinoctial case), but an intensity of the

overturning circulation weaker than observed, even if the seasonal cycle is taken into account (Lindzen & Hou, 1988).

In the AMC theory, the role of eddies is considered very limited, as an angular-momentum sink at the poleward boundaries of the Hadley cells. Subsequent studies investigating the role of eddies have shown that eddy momentum transport is very significant in the equinoctial case and cases with the maximum reference temperature close to the equator: it actually controls the strength of the Hadley circulation (Walker & Schneider, 2006; Bordoni & Schneider, 2010). This has bearing on the latitudinal extent of the Hadley circulation and the intensity of the circulation. In particular, the AMC theory predicts a much faster circulation in the off-equatorial case than in the equinoctial case (Lindzen & Hou, 1988); the seasonal cycle of heating therefore results in an overall more intense annual-mean circulation than the circulation forced by annual-mean heating. It is not the case in the eddy-driven circulation (Walker & Schneider, 2006), which is almost as intense in the equinoctial case as in the off-equatorial case. The influence of eddies decreases if the maximum reference temperature is located further from the equator and monsoon-like circulations with a maximum reference temperature poleward of 10° essentially conserve angular momentum (Walker & Schneider, 2006; Privé & Plumb, 2007b; Bordoni & Schneider, 2010) and the strength of the Hadley circulation roughly follows the predictions of the angular-momentum theory.

For obvious reasons of symmetry, both AMC and eddy-driven theories predict that maximum ascent and the boundary between the two Hadley cells are located at the equator in the equinoctial case. In off-equatorial cases, the AMC theory predicts that the boundary between winter and summer cells is located at the free-tropospheric temperature maximum and maximum ascent is located slightly equatorward of that boundary, in the winter cell (Privé & Plumb, 2007a).

The observed ITCZ and Hadley circulation are in the equinoctial eddy-driven regime except in monsoon regions where a transition from this regime to a monsoon, angular-momentum-conserving circulation is observed during spring and the reverse transition occurs in the fall. These transitions are abrupt (Plumb & Hou, 1992; Privé & Plumb, 2007a) and mediated by eddies (Bordoni & Schneider, 2010). Thermodynamic feedbacks such as wind-induced surface fluxes contribute to the abruptness of this transition (Boos & Emanuel, 2008b,a).

4.1.2 Coupling between moist thermodynamics and Hadley circulation

As noted in Section 1.7, convective quasi-equilibrium is verified over oceans and most of tropical continents (Brown & Bretherton, 1997; Nie et al., 2010). This means that, in convective regions, the free-tropospheric temperature is tied to the near-surface moist static energy, through the quasi-equilibrium vertical profile. Combining the AMC theory to CQE predicts the location of maximum ascent and the center of the ITCZ to be slightly equatorward of the maximum near-surface MSE for off-equatorial diabatic heating (Privé & Plumb, 2007a; Singh, 2019) and at the equator in the equinoctial case. The latent heating in the ITCZ also reduces the influence of eddies (Singh & Kuang, 2016) and accelerates the Hadley circulation (Fang & Tung, 1996).

This prediction bears out in the observations for Hadley circulations that are mostly troposphere-deep (i.e with poleward flow in the upper troposphere and return flow in the lower troposphere). But in monsoon regions neighboring a subtropical desert (as in West Africa and Australia), the monsoon circulations are characterized by a combination of a troposphere-deep circulation and a strong shallow circulation on the poleward side of the ascending branch (i.e. with poleward flow in the ABL and the equatorward flow in the lower to middle free troposphere). These shallow circulations result from the heat low that develops in summer over subtropical deserts. The associated moisture and energy transport influences the location of the ITCZ (Hall & Peyrillé, 2006; Peyrillé et al., 2007; Peyrillé & Lafore, 2007). They involve limited phase changes and therefore essentially verify a "dry" quasi-equilibrium (Nie et al., 2010). In these cases, determining the location of the ITCZ requires considering a combination of the dry and convective quasi-equilibria and associated circulations.

Even in most of the region where CQE is valid, determining the location of the maximum ABL MSE is not straightforward. One could think that this maximum is located over the warmest SST where surface heat fluxes are large. However, the observed location of the ITCZ departs from the latitude of warmest SST, which is particularly surprising if that maximum is at the equator (Waliser & Somerville, 1994). Transport has to be taken into account and ABL dynamics determine a large part of the response (Sobel & Neelin, 2006; Pauluis, 2004). As mentioned in the introduction, SST gradients control a large part of, but not all, ABL flow (Back & Bretherton, 2009). In particular, these gradients, where large, cause shallow circulations in the off-equatorial Hadley circulation even over oceans (Zhang et al., 2004, 2008). Transport may cause ascent to be away from the equator even it the SST is warmest at the equator

(Waliser & Somerville, 1994; Chao & Chen, 2004).

In aquaplanet GCMs, equinoctial conditions with a peaked equatorial SST maximum yield one equatorial ITCZ, but if the equatorial SST maximum is smooth, two off-equatorial ITCZs symmetric about the equator are simulated. The general behavior is common to all models but inter-model differences are significant in terms of threshold, ITCZ precipitation amplitude and off-equatorial latitude (Oueslati & Bellon, 2013b; Williamson et al., 2013). These differences result from the feedbacks between circulation and convection, which are dependent on the convective parameterization in these models. In particular, the contributions of different convective processes (overshoot, downdrafts, etc.) are not parameterized in the same fashion in different GCMs. As an example, Figure 4.1 shows, for two GCMs, the different feedback loops that control the ABL thermodynamics and modulate the transition from a double-ITCZ regime to a single-ITCZ regime if the SST latitudinal distribution is made more peaked at the equator. Both in ARPEGE and LMDz, enhancement of ABL advection closes a positive loop between ABL temperature and meridional winds. LMDz simulates additional negative feedback loops that are absent from ARPEGE: one via the off-equatorial decrease in downdraft cooling accompanying the decrease in deep convection, and another via the active upper-tropospheric/lower-stratospheric cooling known as *cold top* which is caused by upward adiabatic displacement at the top of convective regions (Holloway & Neelin, 2007). This high-altitude temperature perturbations are also density perturbations and can therefore impact the ABL pressure because of the hydrostatic approximation [1].

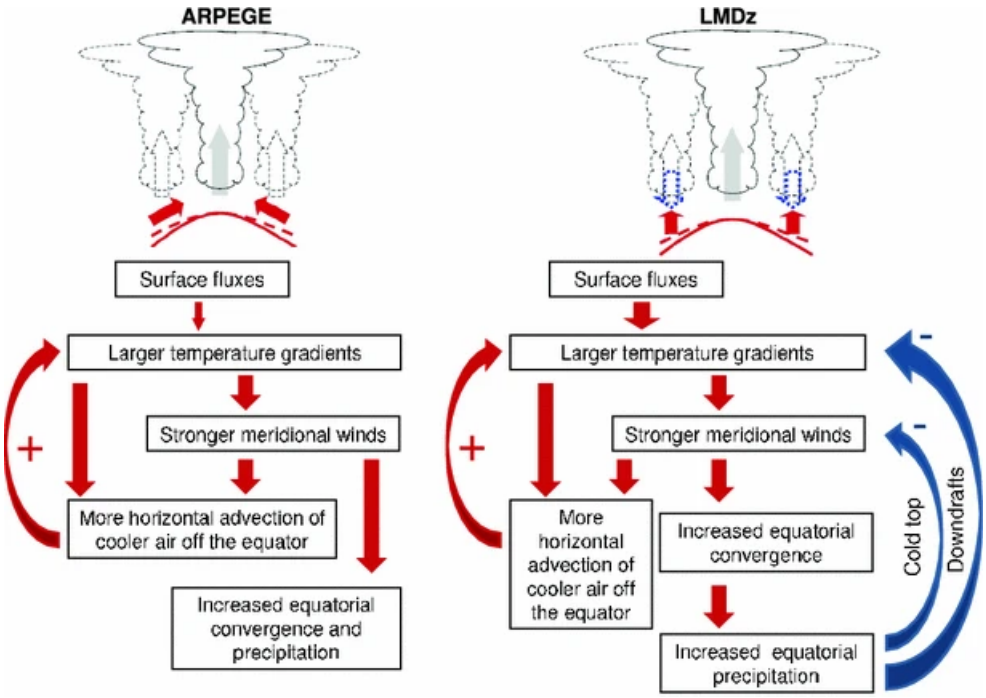

Figure 4.1: Feedback loops active in the transition from double-ITCZ to single-ITCZ regime in two aquaplanet GCMs: the CNRM-CM5 atmospheric component ARPEGE (left) and the IPSL-CM5 atmospheric component LMDz (right); from Oueslati & Bellon (2013b).

Feedbacks between ABL thermodynamics and circulation can even create symmetry-breaking mechanisms in intermediate-complexity models, which yield multiple equilibria of the convectively coupled Hadley circulation (Bellon & Sobel 2010). For an SST latitudinal distribution symmetric about the equator, one equilibrium is symmetric, with an equatorial ITCZ for a maximum SST at the equator, and one equilibrium is asymmetric, with an off-equatorial ITCZ, as illustrated in Figure 4.2. This non-linear behavior essentially results from the main non-linearity in tropical atmospheric physics: whether convection is triggered or inhibited in one of the dry subtropical regions (in the southern subtropics in Figure 4.2). This inhibiting/triggering bifurcation is reinforced by multiple radiative and dynamical feedbacks. Whether such symmetry-breaking mechanisms are robust to the presence of synoptic variability is yet to be established.

Finally, coupled ocean-atmosphere feedbacks can create an off-equatorial SST maximum and significantly impact the location of the ITCZ (Xie & Seki, 1997; Xie, 2005). Off-equatorial convection causes

[1] Hydrostatic balance means that pressure in the ABL equals the weight of the atmospheric column above

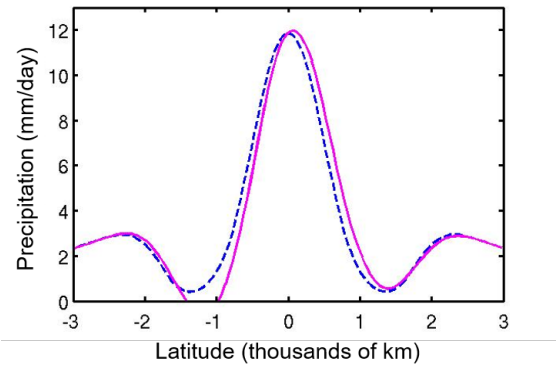

Figure 4.2: Precipitation latitudinal distribution in the two equilibria of an axisymmetric intermediate-complexity model for a latitudinally symmetric SST distribution: symmetric (blue) and asymmetric (purple) equilibria; adapted from Bellon & Sobel (2010).

additional subsidence on the other side of the equator, which enhances low-cloud albedo and reduces surface radiative heating, providing a coupled ocean-atmosphere symmetry-breaking mechanism. Continents shape and orography can also influence the position of the ITCZ. In particular, the along-wind direction of the South American Pacific coast creates a link between trade-wind intensity and coastal upwelling which favors off-equatorial convection in the northern tropics (Xie, 2005). Additionally, the Andes deflect part of the mid-latitude westerlies along isentropes towards the equator and the surface, creating subsidence, inhibiting convection, and enhancing the stratocumulus cover (Takahashi & Battisti, 2006). They also isolate the eastern Pacific from Amazonia, preventing moisture transport from the latter to the former region (Xu et al., 2004).

4.1.3 Energetic constraints on the Hadley circulation

At seasonal timescales, the Gross Moist Stability (GMS) associated with troposphere-deep circulations is positive. The Hadley circulation transports energy from its rising branch, the ITCZ, to the regions where it subsides. In average, it exports energy from equatorial regions to the subtropics. This poleward energy transport participates to the global redistribution of energy from the equator to the poles. If the rising branch is away from the equator, the Hadley circulation also performs an inter-hemispheric energy transport, from the hemisphere in which its ascending branch is located, to the other hemisphere where most of the subsidence occurs.

As it happens, both hemispheres are close to radiative balance at the top of the atmosphere (i.e., there is little net radiative flux), and the difference between the two hemispheres is small: the southern hemisphere receives in average about 1.5 W m^{-2}, or about 0.2 petawatts overall, more than the northern hemisphere (Stephens et al., 2016). On the other hand, the thermohaline circulation transports warm surface water from the southern hemisphere to the northern hemisphere and cold bottom water in the other direction, resulting in a transport of about 0.4 petawatts. At equilibrium, the hemispheric energy budget of the atmosphere therefore imposes a southward atmospheric energy transport of about 0.2 petawatts, hence an ITCZ located in the northern tropics (Frierson et al., 2013; Marshall et al., 2014).

The thermohaline circulation results from the continent spatial distribution (Ferreira et al., 2010), so the northward oceanic transport is a robust feature of the Earth's climate, at least on timescales shorter than those of continental drift. The hemispheric radiative near-balance and location of the ITCZ in the northern tropics are therefore related features of the Earth's atmosphere, but the causal chain between the two is still unclear: how inter-hemispheric asymmetry in surface net heat flux translates into temperature and pressure gradients that force tropical atmospheric circulations without affecting the top-of-the-atmosphere balance is still to be understood.

A similar energetic constraint applies regionally to monsoons: subtropical deserts limit the poleward migration of the ITCZ (Neelin & Chou, 2001; Bellon, 2011). This is because the high albedo of desertic surfaces reduces the net solar flux into the surface; since heat storage in land surfaces at the seasonal scale is negligible, this has to be compensated by a decrease of the other surface heat fluxes into the atmosphere. For a large decrease of these fluxes, the diabatic heating of the atmospheric column becomes negative, which is compensated by MSE transport. Some of this transport results from the shallow

circulation associated with the heat low, with ascent in the lower troposphere, associated with a negative GMS, but this is not sufficient. The residual is obtained by troposphere-deep subsidence, associated with a positive GMS. As a result, the rising branch of the troposphere-deep Hadley circulation is contained equatorward of the desert.

4.1.4 Double ITCZ bias

In terms of tropical precipitation, one major bias of climate models is the simulation of a second, spurious ITCZ south of the equator, creating a double-ITCZ pattern similar to the pattern obtained in aquaplanet GCMs for a smooth equatorial SST maximum. It is simulated by virtually all models in the Pacific ocean, with varying amplitudes, and in some in the Atlantic ocean as well (Tian & Dong, 2020; Si et al., 2021). Figure 1.4 illustrates this bias for the CNRM-CM6, which additionally simulates a double ITCZ in the Indian ocean as well. This systematic bias is among the most resilient to improvements of our climate models, a widespread "syndrome" affecting generations after generations of models (Mechoso et al., 1995; Dai, 2006; Li & Xie, 2014; Zhang et al., 2015). Although this precipitation pattern is observed in the Pacific ocean during boreal spring (Hubert et al., 1969; Zhang, 2001), climate models tend to simulate it year-round.

The inter-hemispheric energetic constraints described in the previous section apply to the double-ITCZ bias: a radiative bias in the southern extratropics is statistically correlated to the bias of inter-hemispheric contrast in tropical precipitation (Hwang & Frierson, 2013; Li & Xie, 2014): an underestimated albedo in the Southern ocean due to a deficit of low and supercooled clouds in midlatitude storms warms the southern hemisphere and this warming appears compensated by decreased southward cross-equatorial atmospheric transport, which is associated with a more symmetric Hadley circulation and tropical precipitation pattern. The causal chain between the midlatitude radiative bias and the tropical precipitation SST is unclear; since the precipitation responds to SST and circulation, this causal chain would have to explain the link between the midlatitude radiative bias and the tropical circulation and SST pattern. The latter results in large part from the tropical surface energy imbalance in the atmosphere-only GCM (Xiang et al., 2017). Besides, reducing the southern-ocean radiative bias is not sufficient to reduce the double-ITCZ bias (Kawai et al., 2021), because oceanic transport, rather than atmospheric transport, compensates the resulting cooling of the southern hemisphere; in some models reducing the southern-ocean radiative bias does not even seem to significantly influence tropical precipitation (Kay et al., 2016; Hawcroft et al., 2017).

The double ITCZ bias is linked to oceanic biases: a warm SST bias in the southern tropics and equatorial cold tongues that are too cold and extend too far westward from the eastern equatorial basins (Li & Xie, 2014), thermocline biases at the equator and southward (Samuels et al., 2021): cold equatorial waters create a southward SST gradient south of the equator which forces meridional convergence further south and creates a convergence zone there. The SST biases are mostly controlled by the biases of the surface heat budget already present in atmosphere-only simulations (Xiang et al., 2017). Coupled ocean-atmosphere mechanisms provide strong positive feedbacks to the double ITCZ and cold tongue bias (the same feedbacks that explain the observed location of the ITCZ, Xie, 2005). Additionally, biases in simulated coupled feedbacks add to the poor simulation of the tropical climate, particularly in the eastern Pacific (Lin, 2007). But this is not systematic: in some models, changes in the atmospheric parameterizations are enough to remediate the double-ITCZ bias (Song & Zhang, 2018).

In most cases, the double-ITCZ bias originates in the simulation of atmospheric processes (Schneider, 2002) and is visible in atmosphere-only simulations. All the coupled feedbacks described above amplify the amplitude of this bias. As a result, the amplitude of the bias in coupled ocean-atmosphere simulations is not systematically related to the amplitude of the double-ITCZ bias in atmosphere-only simulations with the same model (Oueslati & Bellon, 2015); rather, it is linked to the inter-hemispheric surface energy imbalance in the atmosphere-only simulations (Xiang et al., 2017). Despite model-dependent roles of the ocean and extratropical regions in amplifying the double-ITCZ bias, a significant contribution to the double-ITCZ bias can be statistically attributed to tropical atmospheric processes. Oueslati & Bellon (2015) shows that most of the double-ITCZ bias in coupled ocean-atmopshere GCMs in CMIP5 can be attributed to two factors. The first is the models' precipitation response to SST, as measured by a simple index relating SST in the double-ITCZ region and model SST threshold necessary for convection (Bellucci et al., 2010). The second factor is the error in the simulated relationship between circulation and precipitation, using a metrics based on the distribution of mid-tropospheric vertical motion regimes and precipitation associated to these regimes.

In terms of atmospheric processes, model changes that make deep convection more difficult inhibit

convection in moderately convective regions such as margins of CZs and the double-ITCZ region. For example, increasing convective entrainment (see Figure 1.9 for a schematic of a convective updraft and entrainment) reduces deep convection in isolated convective clouds and reduces the double-ITCZ bias in realistic configurations, while favoring the single-ITCZ regime in aquaplanet simulations, as shown in Figure 4.3 (Oueslati & Bellon, 2013a; Möbis & Stevens, 2012). On the other hand, increased convective entrainment intensifies large-scale convective perturbations and yields an overestimation of precipitation at the center of CZs (Oueslati & Bellon, 2013a; Hirota et al., 2014).

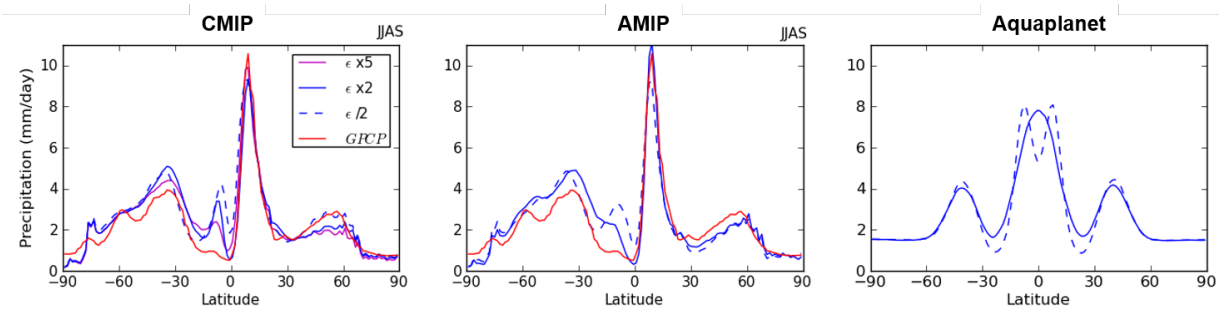

Figure 4.3: Latitudinal distribution of precipitation in the eastern Pacific in ocean-atmosphere coupled simulations (CMIP), atmosphere-only simulations (AMIP) and aquaplanet simulations using CNRM-CM5, for different values of the lateral entrainment into convective updraft, given as a multiple of the reference entrainment parameter ϵ (purple: $\epsilon \times 5$, solid blue: $\epsilon \times 2$, dashed blue: $\epsilon/2$, red: GPCP observations); from Oueslati & Bellon (2013a).

Removing the cloud radiative effect also favors a double-ITCZ regime because it makes convection easier: clouds interaction with terrestrial radiation heats the upper troposphere, making the troposphere more stable and less prone to deep convection (Harrop & Hartmann, 2016). The cloud radiative effect also has an energetic effect: more atmospheric heating in equatorial regions means faster Hadley circulation to compensate this heating by transport which means stronger ABL equatorward meridional wind and more cooling by ABL MSE meridional advection off the equator which moves the ABL MSE maximum and the ITCZ equatorward (Popp & Silvers, 2017). Cloud atmospheric heating can also decrease the GMS and narrow the ascending branch of the Hadley circulation (Dixit et al., 2018).

It now appears that the double-ITCZ syndrome is a multi-factor bias, with, at its core, tropical atmospheric processes, influenced by extratropical atmospheric biases, with coupled ocean-atmosphere processes as amplifiers of the double-ITCZ bias, possibly aggravated by a poor simulations of ocean-atmosphere coupled feedbacks. It is no wonder that it has been so difficult to reduce and has affected generations after generations of coupled ocean-atmosphere GCMs. This complex problem is illustrative of the remaining challenges to understand the number and position of the ITCZ in the different tropical sectors, both over ocean and in monsoon regions.

4.2 Island climate

At large scales, the contrast between land and ocean can cause, or at least trigger, a monsoon. As shown in the previous section, the interaction between surface forcing, moist atmospheric thermodynamics, and circulation is very complex over the ocean, and the presence of a continent adds a level of complexity. Despite progress in theoretical understanding at the global level (e.g., Geen et al., 2020) and in GCM simulations (Choudhury et al., 2022; Khadka et al., 2022), many aspects of monsoons are still poorly understood and their simulation remains a challenge for state-of-the-art climate models.

The contrast between land and ocean also causes atmospheric disturbances at the mesoscale and diurnal scale around coasts, associated with the breeze circulation. Coastal processes are significant for the large-scale climate: climatological tropical precipitation is maximum around coastlines, both inland and offshore (Ogino et al., 2016, 2017). Islands, with their extensive coastlines, contribute significantly to the spatial distribution of mean precipitation and therefore to tropical circulations.

But there is also a practical and opportunistic reason to investigate island climates: on one hand, simulating the regional climate of a tropical island or archipelago with a SRM is computationally affordable; on the other hand, some high-resolution satellite-based observational datasets (CMORPH, Joyce et al.,

2004; IMERG, Huffman et al., 2015) are available for analysis and model validation. Some islands are even equipped with a high-density surface observation network (e.g., New Caledonia: Specq et al., 2020; Dutheil et al., 2021). As a result, tropical islands offer a multitude of laboratories to understand the effect of land-sea contrast on convection, even if only on a limited range of scales. With some luck, some of this understanding might be upscaled to planetary scales, but in any case the expertise developed on islands will be useful to tackle problems at larger scales.

4.2.1 Coastal diurnal cycle

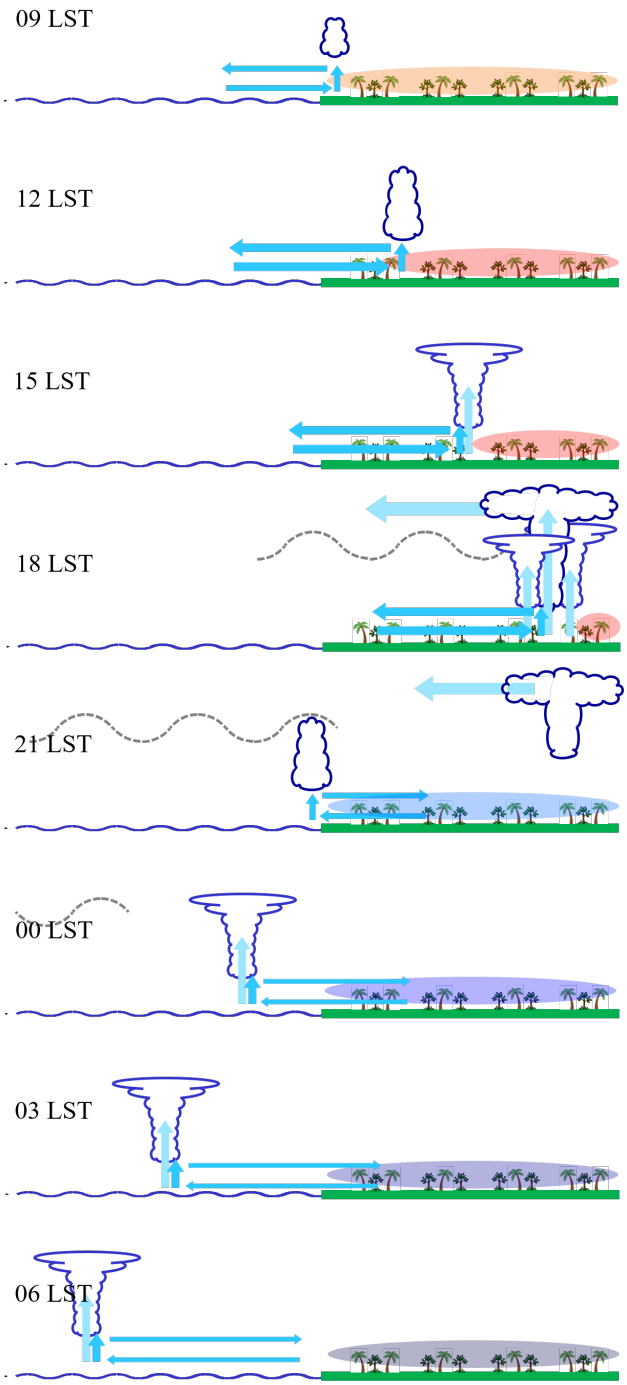

Figure 4.4: Schematic of a typical diurnal cycle around a tropical coast. Local Solar Time (LST) is indicated on the left, ABL temperatures are indicated by shadings (blue for cool and red for warm), circulations are indicated by blue arrows, and dashed lines indicate gravity waves.

Figure 4.4 illustrates the strong diurnal cycle observed over and around most tropical coasts (e.g., Mori et al., 2004; Zhou & Wang, 2006). Due to the small heat capacity of land compared to the ocean, morning sunlight warms the island surface faster than the surrounding ocean. This warming is communicated to the ABL by turbulent sensible heat fluxes and the ABL land-sea thermal contrast powers a surface sea breeze, with return flow at the top of the ABL (06-09LST). Advection of the oceanic ABL over the coast progressively displaces the thermal contrast inland. Together with the self-advection of the sea breeze, this thermal contrast progressively expands the sea breeze inland, with a propagation speed up to 6 m s^{-1} (Carbone et al., 2000; Fovell, 2005). Because of the initial abrupt contrast in temperature at the coast and the self-advection of the sea breeze, a front forms at the inland edge of the breeze, with concentrated convergence and upward motion (09-15LST).

Shallow convection starts at the sea-breeze front in mid-morning and propagates inland with the sea-breeze front, progressively deepening along the way (09-18LST). Deep convection and precipitation peak in the afternoon and starts cooling the ABL and the surface via downdrafts and suppressed sunlight (15-18LST). At the same time, a troposphere-deep circulation develops in response to the mid-tropospheric convective heating. The afternoon storm subsides in the evening or early night (18-21LST).

Meanwhile, the island surface starts cooling faster than the surrounding ocean after sunset and the resulting thermal contrast gives rise to a land breeze with a front on its offshore edge (18-21LST). Convergence and ascent in the land-breeze front favor the development of convection (21-00LST). The land-breeze front and the associated deep convection propagate offshore, at propagation speeds about 3 m s^{-1} (Coppin & Bellon, 2019a; Sakaeda et al., 2020), up to 400 km away from the coast (21LST-06LST). Over the open ocean, the precipitation is maximum at the end of the night as a result of the convective instability created by upper-tropospheric radiative cooling throughout the night, when no solar absorption occurs.

This typical diurnal cycle is modulated by many factors: islands' size and orography, prevailing winds, tropospheric moisture, etc.

4.2.2 Precipitation over tropical islands

Islands with an area larger than a threshold between 500 and 1000 km^2 receive more precipitation than the surrounding ocean (Gray & Jacobson Jr, 1977; Sobel et al., 2011; Ulrich & Bellon, 2019). This enhancement has been attributed to the so-called *rectification* of the diurnal cycle (Cronin et al., 2015; Qian, 2008): because the solar forcing is positive-only during the day, the daytime sea breeze and associated convection are stronger than the nighttime offshore convective propagation. This mechanism is modulated by geometrical factors: by and large, islands are convex and the surrounding ocean concave, so that for the same thermal forcing and wind speed, the convergence would be smaller over ocean than over the islands. Small islands do not exhibit rainfall enhancement compared to the surrounding ocean and exhibit a precipitation diurnal cycle similar to the open ocean (Gray & Jacobson Jr, 1977; Sobel et al., 2011).

Further investigation of the factors influencing rainfall over islands show that precipitation is larger at the center of the island than in the coastal regions for medium-to-large islands (between 2000 km^2 to 128 000 km^2, Ulrich & Bellon, 2019), as illustrated in Figure 4.5. This central *super-enhancement* is attributed to the convergence of sea-breeze fronts coming from different coasts at the center of the island (Zhu et al., 2017; Ulrich & Bellon, 2019). It is not statistically significant on very large islands because the sea breeze weakens in the evening before reaching the center of the islands. On small islands, there is neither precipitation enhancement nor super-enhancement because mean winds transport any ABL temperature anomaly away from the island faster than any breeze circulation can develop (Ulrich & Bellon, 2019).

Topography also strongly influences island precipitation. Mountains intensify evening convection at their top, often at the center of the islands, and slow its decay throughout the evening and into the night (Ulrich & Bellon, 2019; Coppin & Bellon, 2019b). In the presence of prevailing winds, mountain ranges also cause orographical uplift and associated convection on the windward slopes of mountain ranges, with little or no diurnal cycle (e.g., Smith et al., 2009; Kirshbaum & Smith, 2009). This effect does not occur if the wind is slow or if the mountain range is high (Liang & Wang, 2017), suggesting that the control parameter might be the Froude number (Phadtare et al., 2022), which measures the ability of the mean winds to go over the mountain range.

Prevailing winds also make the diurnal cycle weaker in general; more so on the windward side of the island than on the leeward (Wang & Sobel, 2017); this influence is enhanced in the presence of mountains, as can be seen in the sensitivity of the diurnal cycle to wind regimes (Ichikawa & Yasunari, 2006, 2008;

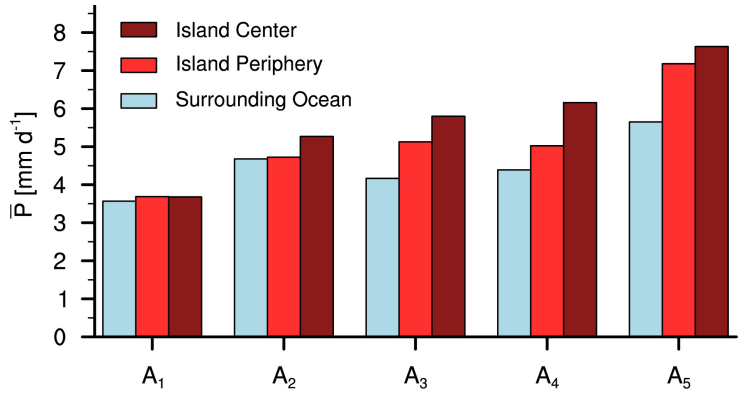

Figure 4.5: Mean precipitation (CMORPH satellite estimates) in the center (brown) and in the periphery (red) of tropical islands as well as over the surrounding ocean (blue), for different classes of island area: A1 for islands smaller than 2000 km^2, and A5 for islands larger than 128 000 km^2, and a geometric increase in between, for classes A2 to A4.

Qian et al., 2013; Yanase et al., 2017; Hopuare et al., 2019; Specq et al., 2020).

Elevated diurnal heating at the top of mountains ranges also creates up-slope winds that reinforce the sea breeze, and elevated cooling at night can enhance the land breeze with down-slope winds (Qian, 2008). On some large islands, the daytime up-slope winds can create enough convergence on the mountain ridge that deep convection starts there before the arrival of the sea-breeze front (Zhou & Wang, 2006), or another front and associated deep convection appear ahead of the sea-breeze front and propagate up-slope to the mountain ridge (Mori et al., 2004).

4.2.3 Precipitation around tropical islands

Many factors also influence the offshore propagating convective disturbances that occur in the evening and at night. These disturbances can propagate over 400 km away from the coast, and how far they propagate depends on the background meteorological conditions and the interaction between the land breeze and gravity waves emitted by convection over the island in the afternoon. A moist free troposphere, moisture convergence, significant CAPE and cool lower free troposphere favor off-shore propagation (Hassim et al., 2016; Coppin & Bellon, 2019a). Intense convection over the island in the afternoon emit gravity waves that can precondition the offshore troposphere for convection or reinforce convection offshore and therefore allow the land-breeze convective front to propagate further offshore (Yokoi et al., 2017; Hassim et al., 2016; Coppin & Bellon, 2019a). In some instances, gravity waves themselves further the propagation beyond 200 km from the coast, at a faster propagation speed than that of the land-breeze front (Love et al., 2011; Vincent & Lane, 2016; Short et al., 2019).

Idealized modeling suggests that the presence of mountains on the island dampens offshore propagation. Figure 4.6 shows the composite diurnal cycle for two simulations using Meso-NH in an idealized configuration, with an elongated rectangular "channel" domain (2048 km × 128 km) containing a square island (128 km × 128 km) spanning the whole domain in its smaller dimension. The island is flat in the first experiment and exhibit a ridge at the center of the island in the second experiment (Coppin & Bellon, 2019b). Offshore propagation is more intense and extends further away from the coast in the absence of orography. Persistent deep convection over the mountains at night and in the early morning smooths the diurnal cycle, weakens the land breeze, and reduces the emission of gravity waves which reduces the extent of the land-breeze front propagation. Also, in the case with a flat island, a shallow circulation episodically develops on one side of the island or the other and favors offshore propagation on that side. By anchoring convection at the top of the ridge, the mountain range ensures symmetry between the two sides of the island and prevents the development of that shallow circulation, which systematically weakens offshore propagation (Coppin & Bellon, 2019b).

4.2.4 Interaction with large-scale variability

The sensitivities of the diurnal cycle on and around islands to prevailing winds, to free-tropospheric moisture and moisture convergence are the main ways large-scale variability impacts the local climate. In particular, the convectively coupled equatorial gravity waves and the MJO influence the diurnal cycle

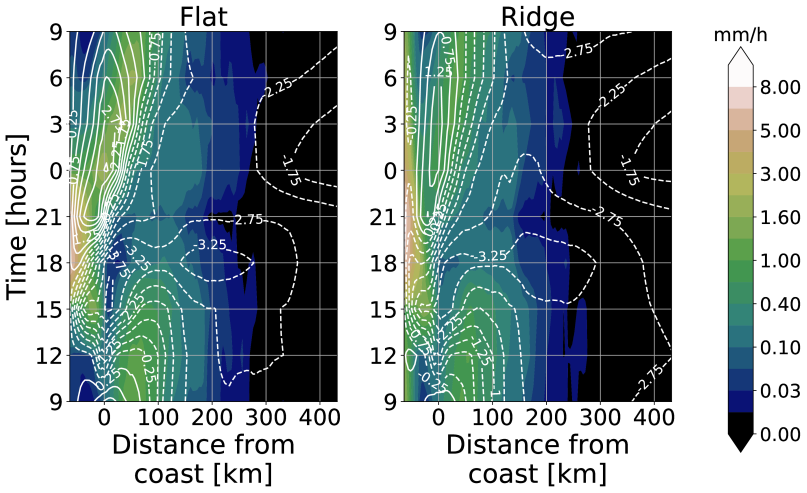

Figure 4.6: Composite diurnal cycle in idealized channel simulations with explicitly resolved deep convection: precipitation (shadings) and across-shore wind (contours) as a function of the distance from the coast and the time of day for a simulation without mountain range on the island ("Flat") and a simulation with an idealized mountain range ("Ridge"); adapted from Coppin & Bellon, 2019b.

on the islands. Their combined influence can be very significant since it can increase the likelihood of extreme precipitation events (Lubis & Respati, 2021; Peatman et al., 2021).

The intraseasonal variability of convection is smaller over most of the islands of the Maritime Continent that over the surrounding seas (Hidayat & Kizu, 2010), which could result in part from a scale selection involving energy storage in the upper ocean (Sobel et al., 2008, 2010) but for the most part from the competition between the large-scale processes and the modification of the local, diurnal processes by the large-scale variability (Rauniyar & Walsh, 2011). During the eastward propagation of the MJO convective disturbances over the Maritime Continent, the moist environment allows evening precipitation over islands to further develop into the night, with more stratiform rainfall, and the diurnal cycle peaks 2 to 3 hours later than usual (Rauniyar & Walsh, 2011; Sakaeda et al., 2017).

More surprisingly, convection develops over the islands 5 to 10 days before the arrival of the MJO convective envelope (Peatman et al., 2014; Sakaeda et al., 2017). This "vanguard" of the MJO can be attributed to enhanced coastal processes (Coppin et al., 2020), as shown in Figure 4.7. Overall convection starts over the islands of the Maritme Continent in MJO phase 3, one phase (about 5 days) before the large-scale convective envelope reaches the region (MJO phase 4), as seen in the top panel of Figure 4.7. This phase lead results from the contribution of coastal convective processes since the coastal precipitation anomaly is about two phases ahead of the convective envelope (as seen in the bottom panel of Figure 4.7).

This intraseasonal modulation of coastal convective processes is associated with a modulation of the diurnal cycle (Birch et al., 2016; Vincent & Lane, 2016): during MJO suppressed conditions, clear skies cause large surface insolation, and consequently large diurnal land-sea thermal contrasts and sea-breeze circulations (Birch et al., 2016); other factors, such as weak prevailing winds and an increasingly moist environment also enhance the diurnal cycle (Vincent & Lane, 2016). An object-oriented analysis of coastal precipitating cloud systems shows that these are larger and longer-lived during this vanguard than during other phases of the MJO (Coppin et al., 2020),

By creating convection out of phase with the convective envelope of the MJO, the Maritime Continent disturbs and can constitute a barrier to the MJO propagation, limiting the intraseasonal event to the Indian Ocean (Hagos et al., 2016). But, at the same time, the diurnal propagating disturbances over the ocean are enhanced during the active phase of the MJO and might participate to the fast eastward propagation across the Maritime Continent of the MJO disturbances that do propagate all the way to the Pacific ocean (Ichikawa & Yasunari, 2007).

Beyond the convective vanguard, the MJO influence over the islands of the Maritime Continent varies regionally depending on local factors. Over Sumatra, Java, Borneo, and New Guinea, the MJO influence differ from one side of the central mountain range to the other, as a result of the MJO influence on the prevailing winds (Ichikawa & Yasunari, 2006, 2008; Yanase et al., 2017; Sakaeda et al., 2020; Peatman et al., 2021): the diurnal cycle is more intense on the lee of the island than on the windward side, both

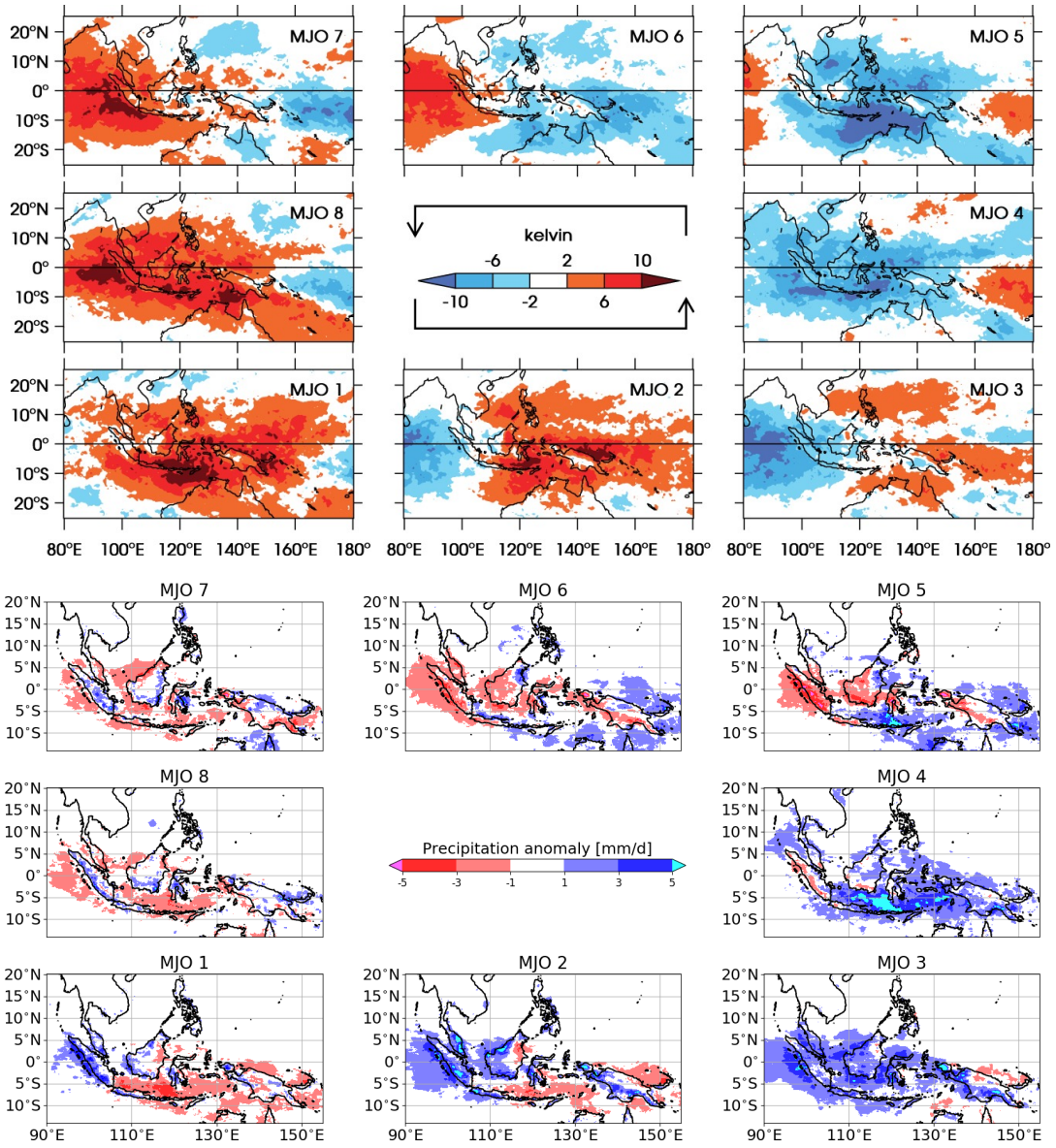

Figure 4.7: Maps of convective activity over the Maritime Continent during the different phases of the MJO (MJO 1 to MJO 8): (top) MJO anomaly of brightness temperature (from Peatman et al., 2014), (bottom) MJO coastal precipitation anomaly, which is quantified by an algorithm identifying and tracking precipitating systems and analyzing their origin, based on satellite estimates of precipitation CMORPH (from Coppin et al., 2020).

over land and over ocean. Further from the heart of the MJO convective signal, its influence on island precipitation can still be identified through its influence on wind regimes as in New Caledonia (Specq et al., 2020) or through its influence on both wind regime and free-tropospheric moisture in French Polynesia (Hopuare et al., 2019).

Vincent et al. (2016) suggests that Kelvin and Rossby waves influence precipitation on and around islands of the Maritime Continent similarly to the MJO, with maxima of normalized precipitation anomalies over islands ahead of the convective envelope that maximizes precipitation over the surrounding ocean. But considering the diversity of wind and humidity patterns in convectively coupled equatorial gravity waves, there is indeed a diversity of influence of these waves on the diurnal cycle over and around islands. The influence of prevailing winds appears important for Rossby waves similarly to the MJO, while the influence of moisture and low-level convergence is dominant for the other convectively coupled equatorial waves (Kelvin, Mixed Rossby Gravity, and inertio-gravity waves, Sakaeda et al., 2020).

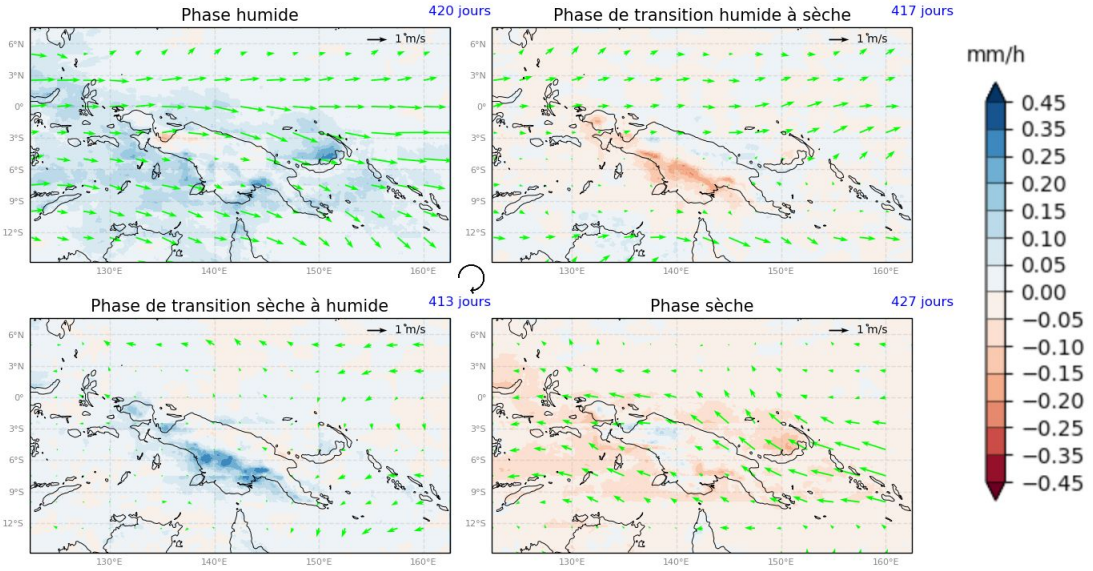

Figure 4.8: Anomaly of coastal precipitation (shadings) and low-level winds (green vectors) associated with convectively coupled Kelvin waves, divided in 4 phases; from Amarys Casnin's MSc thesis.

The example of New Guinea confirms this overall picture as illustrated in Figure 4.8: if a Kelvin wave is divided in four phases, we see increased precipitation in the moist phase and decreased precipitation in the dry phase over the ocean. During the transition phases, we see anomalous precipitation over the southern part of the island preceding anomalies of the same sign over the ocean, which is consistent with an island convective vanguard. But there is no such signal over the northern part of the island. These anomalies cannot be explained by the interaction of the prevailing winds since wind anomalies are very weak over the island in these transition phases. It suggests that some of the interaction between the mountain range and the atmospheric variability remains to be elucidated.

Although I will not cover it in detail, variability at interannual times scales (El Niño - Southern Oscillation) also impacts the diurnal cycle, via its impact on prevailing winds (Rauniyar & Walsh, 2013; Peatman et al., 2021)

4.3 Perspectives

4.3.1 ITCZ

As is obvious from the previous sections, many challenges remain in this general topic of the spatial organization of convection due to surface gradients or contrasts. A comprehensive theory of the position of the ITCZ that (i) would include the tropical thermodynamics and dynamics as well as the mechanisms of the influence of extratropical processes on the tropical circulation and (ii) would explain the regional convergence zone patterns is yet to be formulated. This is likely to remain a long-term challenge for our scientific community. Assuming that the convective quasi-equilibrium principle can be applied in convective regions, we can simplify the problem to:

- understanding the mechanisms controlling the thermodynamics in the dry regions: if a first-order energy balance between radiation and subsidence warming exists in the free troposphere of these regions, moisture balance and boundary-layer energetics are more complex and involve turbulent and large-scale transport contributions. These regions are also where interaction with the extratropics occurs since they include most of the subtropics, and therefore the momentum budget of these regions is to be considered as well.

- understanding what controls the location of the boundary between convective and dry regions, which requires unpacking how convective triggering translates into large-scale, slowly varying geographical convective patterns.

The second item is of particular interest because it essentially aims to reconcile CQE theory with activation control principle for large scales. It is also the more tractable item, because convective instability

at small scale is fairly well understood. In this regard, understanding convective entrainment is relevant: it impacts convective triggering as well as the reference thermodynamic profiles in CQE. Ad-hoc formulations of entrainment have shown very effective at improving tropical large-scale convective patterns (Bechtold et al., 2008; Chikira, 2010). Understanding convective entrainment will be my primary focus in this context. High-resolution observations and very-high resolution simulations of storm systems open new avenues to quantify entrainment and analyze the processes involved in the small-scale circulations that occur at the edge of convective clouds.

Note that, in fact, CQE is not valid everywhere in CZs, for example at the margins of some monsoon regions (Nie et al., 2010) and in the upper troposphere (Herman & Raymond, 2014). While Nie et al. (2010) proposes to treat marginal regions as a superposition of moist-adiabatic and dry-adiabatic circulations, we have no conceptual framework to describe the high-altitude regions where convection is not intense nor frequent enough to enforce CQE. Extending the existing framework(s) to the depth of a troposphere could be done by considering the boundary of CQE regions not as a vertical surface but as a 3D envelope, and potentially divide non-CQE regions into subregions with different dominant balances.

4.3.2 The special case of South Asian Monsoon

The South Asian monsoon, with its mean precipitation pattern with two CZs, one close to the equator and one in the monsoon trough around 20°N, is particularly intriguing. The existing theories of the Hadley circulation do not address this type of pattern. What regulates the momentum budget in this region is unclear: the Earth's highest mountain range is located at the poleward boundary of the region and further limits the interaction with the extratropical atmosphere, so the AMC theory should apply. But this regional Hadley circulation, with two ascending branches, requires rethinking the traditional AMC approach. This rethinking has to take into account the intraseasonal variability (MISO), which is very significant and might be crucial to the seasonal mean. As we saw in Section 3.2, the MISO itself arises from an instability of the seasonal-mean circulation; intraseasonal-seasonal scale interaction might be very fundamental in this regional pattern and has yet to be studied. Recent reanalysis (ERA5) provides better resolution in time and space, and might shed new light on budgets of energy, water and momentum at the seasonal and intraseasonal scales in the South Asian region. I intend to investigate the non-linear interaction between these time scales in this reanalysis and with the QTCM model.

4.3.3 Tropical islands

On a smaller scale, there is still much to understand about tropical island climates, and in particular about the role of orographic effects. Indeed, we can expect an effect of mountain range on the mean flow, with more or less blocking and orographic uplift depending on the speed of prevailing winds and the height of the mountain range. Diurnal elevated heating and cooling also play a role in creating diurnal circulations (valley and mountain breezes), which can interact constructively with the diurnal cycle; on some large islands, valley-mountain and land-sea breeze circulations appear juxtaposed rather than combined, and are therefore competing to some extent to form convergence fronts and precipitation. A finer understanding of what controls the constructive or competing relationship has yet to be developed. I intend to further investigate the island parameters and large-scale meteorological conditions which affect the precipitation patterns over the tropical islands, through the analysis of observations, idealized modeling, and modeling of test cases (such as over islands of French Polynesia within Amarys Casnin's ongoing PhD project). But there is also much to learn about the influence of the small-scale processes on the large-scale climate. If coastal regions receive more precipitation than the open ocean, the atmosphere above a region of archipelagos and peninsulas such as the Maritime Continent receives more diabatic heating, and this could have an influence on the large-scale circulation in long-term average; in particular on the Walker circulation. This type of upscale influence is yet to be investigated. Among other tools, the parameterizations of the large-scale dynamical response (WTG, DGW) to a regional climate could be used to investigate such an interaction.

5 Conclusion

What is striking in the tropical atmosphere is the ubiquity of deep-convective organization, on a range of scales spanning 6 orders of magnitude in space and about 4 orders of magnitude in time. On all scales, this organization results in the development of a convective cloud, cloud system or envelope surrounded by a dry region; this yields a bimodal distribution of humidity that was our starting point in the introduction. Of course, the characteristics of organized convective systems depend on their scale, but the fundamental fact of organizing does occur on this wide range of scales. There seems to be a fundamental tendency for convective features, either convective updrafts, clouds, or storms to occur next to each other. At large scales, this is specific to the tropical atmosphere. No extratropical mode of convective organization occurs on planetary scales. And synoptic extratropical storms result primarily from extratropical dynamical instabilities that do not involve phase changes, even if latent heating enhances these disturbances. In terms of the importance of convection in their fundamental mechanisms, these extratropical synoptic storms are akin to equatorial gravity waves: they would arise in a dry atmosphere with only slightly different features.

For tropical atmospheric variability, the basic question is: what is the commonality and what are differences in the mechanisms of spatial organization of convection at different scales in the tropics?

For example, large-scale atmospheric variability can be considered either as a mode of convective organization or as a modulation of mesoscale convective systems. In particular, the active phases of intraseasonal disturbances and convectively coupled equatorial gravity waves can be seen as convective envelopes that modulate mesoscale convective systems' life cycles (Mapes et al., 2006). So, to some extent, mesoscale convective organization is nested into the large-scale convective organization, and the large-scale interacts with the mesoscale. The convective cloud-scale processes also interact with the mesoscale and sometimes directly with the large-scale organization. So there is not only a similarity and differences between scales but also scale interaction.

This scale interaction adds a level of complexity to the system and hinders the progress in our understanding of tropical climate, and particularly of its large-scale features. So far, most modeling research on large-scale patterns, mine included, has used either simple, intermediate-complexity, or general-circulation models, in which convection is parameterized. Parameterizing convection has been a challenge for decades and, despite multiple initiatives and significant progress (Rio et al., 2019), remains challenging. The challenge stems from representing the effect of all convective-scale and mesoscale processes on the large scale, including scale interaction and subgrid-scale organization. It is a daunting task.

What alternatives do we have? Observation analysis faces challenges in documenting all scales involved in the large-scale climate feature. Existing observation systems (sondes, planes, surface-based observations, satellite-based passive and active sensors) provide information with either large-scale coverage or high resolution, but not both. And it is currently computationally impossible to perform global simulations with the resolution necessary to simulate all convective clouds. Kilometer-scale global models or storm-resolving models (SRMs) have been developed over the past decade, and this is a major step in representing convective structures in global models. These models are already very promising to better simulate the global climate and improve the reliability of climate projections, in particular in terms of precipitation. There is a caveat: low clouds, which currently contribute to a large part of the spread in climate projections, are not explicitly simulated in such models and are instead parameterized, with the same challenges as in current GCMs. Another, more practical issue is that computing and data storage resources needed to use such models are not widely available. Further, fine physical analysis of the simulations performed with such models must overcome technical challenges stemming from the shear volume of data. Nevertheless, SRM simulations are starting to be affordable to study regional climates.

Finally, perfectly documenting or simulating a phenomenon does not guaranty understanding it. The canonical approach to validate our understanding of a phenomenon is to develop a hierarchy of models of decreasing complexity down to a simple model that simulates an analog to the phenomenon of interest

with matching key characteristics. Such a hierarchy does exist for the main mode of interannual tropical variability, the El Niño - Southern Oscillation, even if it is an evolving hierarchy in which models are regularly being replaced by superseding ones (e.g., Guilyardi et al., 2020). Still, for all the modes of atmospheric variability described in this thesis, such model hierarchies are quite incomplete. A more complete and accurate depiction of these phenomena via SRM simulations might inspire new simple models; we will otherwise have to rely on educated guesses. Going back to the example of El Niño - Southern Oscillation, the latter approach was actually quite successful: the seminal models in this hierarchy of models (e.g., Cane & Zebiak, 1985) preceded comprehensive observation systems and the simulation of El Niño - Southern Oscillation in GCMs.

Acknowledgements

My PhD supervisors, Hervé Le Treut et Mickael Ghil, already proposed a PhD topic that treated the tropical climate system in a two-column framework. It was the turn of the millennium, but they already felt that there was something interesting in this direction. I still find that this topic is fascinating and I am grateful that they sent me on this journey. I also thank them for their support extending long after the completion of my PhD.

Jean-Philippe Duvel was on my PhD committee and has accompanied me in obtaining this new degree. I thank Jean-Philippe for his help and the many scientific discussions, lunches, and beers I have enjoyed with him over the decades.

A few scientists supported me in many different ways in my early career, I sure needed it and I thank them for it: Jean-Luc Redelsperger, Serge Planton, Jun-Ichi Yano. I had the chance to meet Bjorn Stevens almost by chance; our collaboration taught me a lot about tropical boundary layers and none of it appears in this manuscript so I must apologize to him as well as thank him for the time and resources he dedicated to help me, a young student he was not responsible for.

Many thanks to J. Srinivasan for his kindness, for introducing me to the mechanics of monsoon intraseasonal variability, and for allowing me to discover India. I extend special thanks to Adam Sobel, the apostle of the weak temperature gradient approximation who convinced me of its potential. He was also a great post-doc mentor, giving me expert feedback and lots of freedom.

I would also like to take the opportunity thank a few persons who, when in a position of power, made decisions that allowed me to overcome some knotty situations: thank you to Eric Brun, who supported my application to join the CNRM, to Philippe Bougeaud, who supported my application to leave the CNRM, and to Richard Easther, who led the Department of Physics at the University of Auckland during my secondment there and was always supportive.

I thank all the colleagues at LMD, UCLA, IISc, Columbia, University of Auckland, and CNRM with whom I have had the luck and pleasure to discuss and collaborate with. The list is too long for this page. I will just particularly salute the ones who have spent time with me in front of whiteboards; these are the good times.

Most importantly, I would like to thank the young scientists who trusted me to supervise or mentor them, brought fresh outlooks and energy to my projects, and allowed me to reap the benefits of their hard work and put it in this manuscript: Boutheina, Stéphanie, Beatriz, Max, David, Hamish, and Amarys. I will add a special shout-out to two younger students whom I have had the pleasure to torture from basic physics to geophysical fluid dynamics: Neelesh and Andrew.

Finally, I thank Caroline, Cathy, and Fabio who have agreed to review this manuscript. I hope they will forgive me and allow me to exploit more students.

Bibliography

Ackerman, A. S., Stevens, B., Savic-Jovcic, V., Bretherton, C. S., Chlond, A., Golaz, J.-C., Jiang, H., Khairoutdinov, M., Krueger, S. K., Zulauf, M., Lewellen, D. C., C.-H., M., K., N., R., S. J., & Weinbrecht, S. (2009). Large-Eddy Simulations of a drizzling, stratocumulus-topped marine boundary layer. *Monthly Weather Review*, *137*(3), 1083–1110.

Adam, O. (2018). Zonally Varying ITCZs in a Matsuno-Gill-Type Model With an Idealized Bjerknes Feedback. *Journal of Advances in Modeling Earth Systems*, *10*(6), 1304–1318.

Adames, Á. F. (2022). The basic equations underweak temperature gradient balance: Formulation, scaling, and types of convectively-coupled motions. *Journal of the Atmospheric Sciences*, (p. in press).

Adames, Á. F., & Kim, D. (2016). The MJO as a dispersive, convectively coupled moisture wave: Theory and observations. *Journal of the Atmospheric Sciences*, *73*(3), 913–941.

Ahmed, F. (2021). The MJO on the equatorial beta plane: An eastward-propagating rossby wave induced by meridional moisture advection. *Journal of the Atmospheric Sciences*, *78*(10), 3115 – 3135.

Ahmed, F., Neelin, J. D., & Adames, A. F. (2021). Quasi-equilibrium and weak temperature gradient balances in an equatorial beta-plane model. *Journal of the Atmospheric Sciences*, *78*(1), 209 – 227.

Ahn, M.-S., Kim, D., Ham, Y.-G., & Park, S. (2020). Role of maritime continent land convection on the mean state and MJO propagation. *Journal of Climate*, *33*(5), 1659 – 1675.

Ajayamohan, R. S., Khouider, B., Praveen, V., & Majda, A. J. (2021). Role of diurnal cycle in the maritime continent barrier effect on MJO propagation in an AGCM. *Journal of the Atmospheric Sciences*, *78*(5), 1545 – 1565.

Anber, U. M., Wang, S., Gentine, P., & Jensen, M. P. (2019). Probing the response of tropical deep convection to aerosol perturbations using idealized cloud-resolving simulations with parameterized large-scale dynamics. *Journal of the Atmospheric Sciences*, *76*(9), 2885 – 2897.

Andersen, J. A., & Kuang, Z. (2012). Moist static energy budget of MJO-like disturbances in the atmosphere of a zonally symmetric aquaplanet. *Journal of Climate*, *25*(8), 2782 – 2804.

Arakawa, A., & Schubert, W. H. (1974). Interaction of a cumulus cloud ensemble with the large-scale environment, Part I. *Journal of the Atmospheric Sciences*, *31*, 674–701.

Arnold, N. P., & Randall, D. A. (2015). Global-scale convective aggregation: Implications for the madden-julian oscillation. *Journal of Advances in Modeling Earth Systems*, *7*(4), 1499–1518.

Back, L. E., & Bretherton, C. S. (2009). On the relationship between sst gradients, boundary layer winds, and convergence over the tropical oceans. *Journal of Climate*, *22*(15), 4182–4196.

Battisti, D. S., Sarachik, E. S., & Hirst, A. C. (1999). A Consistent Model for the Large-Scale Steady Surface Atmospheric Circulation in the Tropics*. *Journal of Climate*, *12*(10), 2956–2964.

Beare, R. J., & Cullen, M. J. P. (2019). A simple model of a balanced boundary layer coupled to a large-scale convective circulation. *Journal of the Atmospheric Sciences*, *76*(3), 837 – 849.

Bechtold, P., Köhler, M., Jung, T., Doblas-Reyes, F., Leutbecher, M., Rodwell, M. J., Vitart, F., & Balsamo, G. (2008). Advances in simulating atmospheric variability with the ecmwf model: From synoptic to decadal time-scales. *Quarterly Journal of the Royal Meteorological Society*, *134*(634), 1337–1351.

Becker, T., Stevens, B., & Hohenegger, C. (2017). Imprint of the convective parameterization and sea-surface temperature on large-scale convective self-aggregation. *Journal of Advances in Modeling Earth Systems*, *9*(2), 1488–1505.

Bellenger, H., & Duvel, J.-P. (2007). Intraseasonal convective perturbations related to the seasonal march of the Indo-Pacific monsoons. *Journal of Climate*, *20*, 2853–2863.

Bellenger, H., & Duvel, J.-P. (2009). An analysis of tropical ocean diurnal warm layers. *Journal of Climate*, *22*(13), 3629–3646.

Bellenger, H., Takayabu, Y. N., Ushiyama, T., & Yoneyama, K. (2010). Role of diurnal warm layers in the diurnal cycle of convection over the tropical Indian Ocean during MISMO. *Monthly Weather Review*, *138*(6), 2426 – 2433.

Bellon, G. (2011). Monsoon intraseasonal oscillation and land-atmosphere interaction in an idealized model. *Climate Dynamics*.

Bellon, G., & Bony, S. (2020). Tropical and subtropical cloud systems. *Clouds and Climate: Climate Science's Greatest Challenge*, (p. 251).

Bellon, G., & Coppin, D. (2022). Sensitivity of convective self-aggregation to subsidence. *Journal of Advances in Modeling Earth Systems*, *14*(12), e2021MS002830.

Bellon, G., Ghil, M., & Le Treut, H. (2006). Scale separation for moisture-laden regions in the tropical atmosphere. *Geophysical Research Letters*, *33*(1).

Bellon, G., Le Treut, H., & Ghil, M. (2003). Large-scale and evaporation-wind feedbacks in a box model of the tropical climate. *Geophysical Research Letters*, *30*, 2145.

Bellon, G., & Reboredo, B. (2022). Scale sensitivity of the Gill circulation, Part II: off-equatorial case. *Journal of the Atmospheric Sciences*, *79*, 19–30.

Bellon, G., Reitebuch, O., & Naumann, A. K. (2017). Shallow circulations: Relevance and strategies for satellite observation. In *Shallow Clouds, Water Vapor, Circulation, and Climate Sensitivity*, (pp. 337–356). Springer.

Bellon, G., & Sobel, A. H. (2008a). Instability of the axisymmetric monsoon flow and intraseasonal oscillation. *Journal of Geophysical Research - Atmospheres*, *113*, D07108.

Bellon, G., & Sobel, A. H. (2008b). Poleward-propagating intraseasonal monsoon disturbances in an intermediate-complexity axisymmetric model. *Journal of the Atmospheric Sciences*, *65*, 470–489.

Bellon, G., & Sobel, A. H. (2010). Multiple equilibria of the hadley circulation in an intermediate-complexity axisymmetric model. *Journal of Climate*, *23*, 1760–1778.

Bellon, G., Sobel, A. H., & Vialard, J. (2008). Ocean-atmosphere coupling in the monsoon intraseasonal oscillation: a simple model study. *Journal of Climate*, *21*, 5254–5270.

Bellucci, A., Gualdi, S., & Navarra, A. (2010). The double-ITCZ syndrome in coupled general circulation models: the role of large-scale vertical circulation regimes. *Journal of Climate*, *5*, 1127–1145.

Benedict, J. J., Maloney, E. D., Sobel, A. H., & Frierson, D. M. W. (2014). Gross moist stability and mjo simulation skill in three full-physics gcms. *Journal of the Atmospheric Sciences*, *71*(9), 3327 – 3349.

Bergman, J. W., & Sardeshmukh, P. D. (2004). Dynamic stabilization of atmospheric single column models. *Journal of Climate*, *17*(5), 1004 – 1021.

Betts, A. K. (1986). A new convective adjustment scheme. Part I: Observational and theoretical basis. *Quarterly Journal of the Royal Meteorological Society*, *112*, 677–691.

Betts, A. K., & Miller, M. J. (1986). A new convective adjustment scheme. Part II: Single column tests using GATE wave, BOMEX, ATEX and arctic air-mass data sets. *Quarterly Journal of the Royal Meteorological Society*, *112*, 693–709.

Beucler, T., & Cronin, T. (2019). A budget for the size of convective self-aggregation. *Quarterly Journal of the Royal Meteorological Society*, *145*(720), 947–966.

Beucler, T., Cronin, T., & Emanuel, K. (2018). A linear response framework for radiative-convective instability. *Journal of Advances in Modeling Earth Systems*, *10*(8), 1924–1951.

Beucler, T., & Cronin, T. W. (2016). Moisture-radiative cooling instability. *Journal of Advances in Modeling Earth Systems*, *8*(4), 1620–1640.

Biagioli, G., & Tompkins, A. M. (2023). A dimensionless parameter for predicting convective self-aggregation onset in a stochastic reaction-diffusion model of tropical radiative-convective equilibrium. *Journal of Advances in Modeling Earth Systems*, (p. submitted).

Birch, C. E., Webster, S., Peatman, S. C., Parker, D. J., Matthews, A. J., Li, Y., & Hassim, M. E. E. (2016). Scale interactions between the mjo and the western maritime continent. *Journal of Climate*, *29*(7), 2471 – 2492.

Blossey, P. N., Bretherton, C. S., & Wyant, M. C. (2009). Subtropical low cloud response to a warmer climate in a superparameterized climate model. part ii: Column modeling with a cloud resolving model. *Journal of Advances in Modeling Earth Systems*, *1*(3).

Bony, S., Bellon, G., Klocke, D., Sherwood, S., Fermepin, S., & Denvil, S. (2013). Robust direct effect of carbon dioxide on tropical circulation and regional precipitation. *Nature Geoscience*, *6*(6), 447–451.

Bony, S., & Emanuel, K. A. (2005). On the role of moist processes in tropical intraseasonal variability: Cloud–radiation and moisture–convection feedbacks. *Journal of the atmospheric sciences*, *62*(8), 2770–2789.

Boos, W. R., & Emanuel, K. A. (2008a). Wind–evaporation feedback and abrupt seasonal transitions of weak, axisymmetric hadley circulations. *Journal of the Atmospheric Sciences*, *65*(7), 2194 – 2214.

Boos, W. R., & Emanuel, K. A. (2008b). Wind–evaporation feedback and the axisymmetric transition to angular momentum–conserving hadley flow. *Journal of the Atmospheric Sciences*, *65*(12), 3758 – 3778.

Boos, W. R., & Kuang, Z. (2010). Mechanisms of poleward propagating, intraseasonal convective anomalies in cloud system–resolving models. *Journal of the Atmospheric Sciences*, *67*(11), 3673–3691.

Bordoni, S., & Schneider, T. (2010). Regime transitions of steady and time-dependent hadley circulations: Comparison of axisymmetric and eddy-permitting simulations. *Journal of the Atmospheric Sciences*, *67*(5), 1643 – 1654.

Bretherton, C. S., Blossey, P. N., & Khairoutdinov, M. (2005). An energy-balance analysis of deep convective self-aggregation above uniform sst. *Journal of the Atmospheric Sciences*, *62*(12), 4273–4292.

Bretherton, C. S., Peters, M. E., & Back, L. E. (2004). Relationships between water vapor path and precipitation over the tropical oceans. *Journal of Climate*, *17*, 1517–1528.

Bretherton, C. S., & Smolarkiewicz, P. K. (1989). Gravity waves, compensating subsidence and detrainment around cumulus clouds. *Journal of Atmospheric Sciences*, *46*(6), 740 – 759.

Bretherton, C. S., & Sobel, A. H. (2002). A simple model of a convectively coupled walker circulation using the weak temperature gradient approximation. *Journal of climate*, *15*(20), 2907–2920.

Bretherton, C. S., & Sobel, A. H. (2003). The gill model and the weak temperature gradient approximation. *Journal of the atmospheric sciences*, *60*(2), 451–460.

Brown, R. G., & Bretherton, C. S. (1997). A test of the strict quasi-equilibrium theory on long time and space scales. *Journal of the Atmospheric Sciences*, *54*(5), 624 – 638.

Cane, M. A., & Zebiak, S. E. (1985). A Theory for El Nino and the Southern Oscillation. *Science*, *228*(4703), 1085–1087.

Carbone, R., Wilson, J., Keenan, T., & Hacker, J. (2000). Tropical island convection in the absence of significant topography. part i: Life cycle of diurnally forced convection. *Monthly weather review*, *128*(10), 3459–3480.

Chao, W. C. (1987). On the Origin of the Tropical Intraseasonal Oscillation. *Journal of the Atmospheric Sciences*, *44*(15), 1940–1949.

Chao, W. C., & Chen, B. (2004). Single and double ITCZ in an aqua-planet model with constant sea surface temperature and solar angle. *Climate Dynamics*, *22*, 447–459.

Charney, J. G., & Eliassen, A. (1964). On the growth of the hurricane depression. *Journal of Atmospheric Sciences*, *21*(1), 68–75.

Chen, G., Ling, J., Zhang, R., Xiao, Z., & Li, C. (2022). The MJO from CMIP5 to CMIP6: Perspectives from tracking MJO precipitation. *Geophysical Research Letters*, (p. e2021GL095241).

Chiang, J. C. H., Zebiak, S. E., & Cane, M. A. (2001). Relative roles of elevated heating and surface temperature gradients in driving anomalous surface winds in over tropical oceans. *Journal of the Atmospheric Sciences*, *58*, 1371–1394.

Chikira, M. (2010). A cumulus parameterization with state-dependent entrainment rate. part ii: Impact on climatology in a general circulation model. *Journal of the Atmospheric Sciences*, *67*, 2194–2211.

Chou, C., & Hsueh, Y.-C. (2010). Mechanisms of northward-propagating intraseasonal oscillation—a comparison between the Indian Ocean and the Western North Pacific. *Journal of Climate*, *23*(24), 6624 – 6640.

Choudhury, B. A., Rajesh, P., Zahan, Y., & Goswami, B. (2022). Evolution of the indian summer monsoon rainfall simulations from cmip3 to cmip6 models. *Climate Dynamics*, *58*(9), 2637–2662.

Clement, A. C., & Seager, R. (1999). Climate and the tropical oceans. *Journal of Climate*, *12*, 3383–3401.

Coppin, D., & Bellon, G. (2019a). Physical mechanisms controlling the offshore propagation of convection in the tropics: 1. flat island. *Journal of Advances in Modeling Earth Systems*, *11*(9), 3042–3056.

Coppin, D., & Bellon, G. (2019b). Physical mechanisms controlling the offshore propagation of convection in the tropics: 2. influence of topography. *Journal of Advances in Modeling Earth Systems*, *11*(10), 3251–3264.

Coppin, D., Bellon, G., Pletzer, A., & Scott, C. (2020). Detecting and tracking coastal precipitation in the tropics: Methods and insights into multiscale variability of tropical precipitation. *Journal of Climate*, *33*(15), 6689–6705.

Coppin, D., & Bony, S. (2015). Physical mechanisms controlling the initiation of convective self-aggregation in a general circulation model. *Journal of Advances in Modeling Earth Systems*, *7*(4), 2060–2078.

Coppin, D., & Bony, S. (2017). Internal variability in a coupled general circulation model in radiative-convective equilibrium. *Geophysical Research Letters*, *44*(10), 5142–5149.

Coppin, D., & Roehrig, R. (2022). Convection self-aggregation in cnrm-cm6-1: Equilibrium and transition sensitivity to surface temperature. *Journal of Advances in Modeling Earth Systems*, *14*(12), e2022MS003064. E2022MS003064 2022MS003064.

Craig, G. C., & Mack, J. M. (2013). A coarsening model for self-organization of tropical convection. *Journal of Geophysical Research: Atmospheres*, *118*(16), 8761–8769.

Cronin, T. W., Emanuel, K. A., & Molnar, P. (2015). Island precipitation enhancement and the diurnal cycle in radiative-convective equilibrium. *Quarterly Journal of the Royal Meteorological Society*, *141*(689), 1017–1034.

Dai, A. G. (2006). Precipitation characteristics in eighteen coupled climate models. *Journal of Climate*, *19*, 4605–4630.

Daleu, C. L., Plant, R. S., Woolnough, S. J., Sessions, S., Herman, M. J., Sobel, A., Wang, S., Kim, D., Cheng, A., Bellon, G., et al. (2015). Intercomparison of methods of coupling between convection and large-scale circulation: 1. comparison over uniform surface conditions. *Journal of Advances in Modeling Earth Systems*, *7*(4), 1576–1601.

Daleu, C. L., Plant, R. S., Woolnough, S. J., Sessions, S., Herman, M. J., Sobel, A., Wang, S., Kim, D., Cheng, A., Bellon, G., et al. (2016). Intercomparison of methods of coupling between convection and large-scale circulation: 2. comparison over nonuniform surface conditions. *Journal of advances in modeling earth systems*, *8*(1), 387–405.

Daleu, C. L., Woolnough, S. J., & Plant, R. S. (2012). Cloud-resolving model simulations with one- and two-way couplings via the weak temperature gradient approximation. *Journal of the Atmospheric Sciences*, *69*(12), 3683 – 3699.

DeMott, C. A., Klingaman, N. P., & Woolnough, S. J. (2015). Atmosphere-ocean coupled processes in the Madden-Julian oscillation. *Reviews of Geophysics*, *53*(4), 1099–1154.

DeMott, C. A., Stan, C., & Randall, D. A. (2013). Northward propagation mechanisms of the boreal summer intraseasonal oscillation in the ERA-Interim and SP-CCSM. *Journal of Climate*, *26*(6), 1973 – 1992.

Derbyshire, S. H., Beau, I., Bechtold, P., Grandpeix, J.-Y., Piriou, J.-M., Redelsperger, J.-L., & Soares, P. M. M. (2004). Sensitivity of moist convection to environmental humidity. *Quarterly Journal of the Royal Meteorological Society*, *130*, 3055–3079.

Dixit, V., Geoffroy, O., & Sherwood, S. C. (2018). Control of itcz width by low-level radiative heating from upper-level clouds in aquaplanet simulations. *Geophysical Research Letters*, *45*(11), 5788–5797.

Drbohlav, H.-K., & Wang, B. (2005). Mechanism of the northward-propagating intraseasonal oscillation: Insights from a zonally symmetric model. *Journal of Climate*, *18*, 952–972.

Dunkerton, T. J., Montgomery, M. T., & Wang, Z. (2009). Tropical cyclogenesis in a tropical wave critical layer: Easterly waves. *Atmos. Chem. Phys.*, *9*, 5587–5646.

Durran, D. R. (1989). Improving the anelastic approximation. *Journal of Atmospheric Sciences*, *46*(11), 1453–1461.

Dutheil, C., Menkès, C., Lengaigne, M., Vialard, J., Peltier, A., Bador, M., & Petit, X. (2021). Fine-scale rainfall over new caledonia under climate change. *Climate Dynamics*, *56*(1), 87–108.

Duvel, J. P., Bellenger, H., Bellon, G., & Remaud, M. (2013). An event-by-event assessment of tropical intraseasonal perturbations for general circulation models. *Climate dynamics*, *40*(3), 857–873.

Duvel, J.-P., & Vialard, J. (2007). Indo-Pacific sea surface temperature perturbations associated with intraseasonal oscillations of tropical convection. *Journal of Climate*, *20*, 3056–3082.

Edman, J. P., & Romps, D. M. (2014). An improved weak pressure gradient scheme for single-column modeling. *Journal of the Atmospheric Sciences*, *71*(7), 2415 – 2429.

Emanuel, K., Wing, A. A., & Vincent, E. M. (2014). Radiative-convective instability. *Journal of Advances in Modeling Earth Systems*, *6*(1), 75–90.

Emanuel, K., et al. (2003). Tropical cyclones. *Annual review of earth and planetary sciences*, *31*(1), 75–104.

Emanuel, K. A. (1987). An air-sea interaction model of intraseasonal oscillations in the tropics. *Journal of the Atmospheric Sciences*, *44*, 2324–2340.

Emanuel, K. A., Neelin, J. D., & Bretherton, C. S. (1994a). On large-scale circulations in convecting atmospheres. *Quarterly Journal of the Royal Meteorological Society*, *120*, 1111–1143.

Emanuel, K. A., et al. (1994b). *Atmospheric convection*. Oxford University Press on Demand.

Fang, M., & Tung, K. K. (1996). A simple model of nonlinear hadley circulation with an itcz: Analytic and numerical solutions. *Journal of Atmospheric Sciences*, *53*(9), 1241 – 1261.

Ferreira, D., Marshall, J., & Campin, J.-M. (2010). Localization of deep water formation: Role of atmospheric moisture transport and geometrical constraints on ocean circulation. *Journal of Climate*, *23*(6), 1456–1476.

Fovell, R. G. (2005). Convective initiation ahead of the sea-breeze front. *Monthly Weather Review*, *133*(1), 264–278.

Frierson, D. M., Hwang, Y.-T., Fučkar, N. S., Seager, R., Kang, S. M., Donohoe, A., Maroon, E. A., Liu, X., & Battisti, D. S. (2013). Contribution of ocean overturning circulation to tropical rainfall peak in the northern hemisphere. *Nature Geoscience*, *6*(11), 940–944.

Gao, Y., Klingaman, N. P., DeMott, C. A., & Hsu, P.-C. (2020). Boreal summer intraseasonal oscillation in a superparameterized general circulation model: effects of air–sea coupling and ocean mean state. *Geoscientific Model Development*, *13*(11), 5191–5209.

Geen, R., Bordoni, S., Battisti, D. S., & Hui, K. (2020). Monsoons, itczs, and the concept of the global monsoon. *Reviews of Geophysics*, *58*(4), e2020RG000700.

Gill, A. E. (1980). Some simple solutions for heat-induced tropical circulation. *Quarterly Journal of the Royal Meteorological Society*, *106*, 447–462.

Giordani, H., & Peyrillé, P. (2022). Dynamics of the atlantic marine intertropical convergence zone. *Journal of Geophysical Research: Atmospheres*, *127*(16), e2021JD036392.

Gray, W. M., & Jacobson Jr, R. W. (1977). Diurnal variation of deep cumulus convection. *Monthly Weather Review*, *105*(9), 1171–1188.

Guilyardi, E., Capotondi, A., Lengaigne, M., Thual, S., & Wittenberg, A. T. (2020). Enso modeling: History, progress, and challenges. In W. C. Michael J. McPhaden, Agus Santoso (Ed.) *El Niño Southern Oscillation in a Changing Climate*, (pp. 199–226). Wiley Online Library.

Haerter, J. O. (2019). Convective self-aggregation as a cold pool-driven critical phenomenon. *Geophysical Research Letters*, *46*(7), 4017–4028.

Haerter, J. O., Meyer, B., & Nissen, S. B. (2020). Diurnal self-aggregation. *npj Climate and Atmospheric Science*, *3*(1), 1–11.

Hagos, S. M., Zhang, C., Feng, Z., Burleyson, C. D., De Mott, C., Kerns, B., Benedict, J. J., & Martini, M. N. (2016). The impact of the diurnal cycle on the propagation of madden-julian oscillation convection across the maritime continent. *Journal of Advances in Modeling Earth Systems*, *8*(4), 1552–1564.

Hall, N. M., & Peyrillé, P. (2006). Dynamics of the west african monsoon. In *Journal de Physique IV (Proceedings)*, vol. 139, (pp. 81–99). EDP sciences.

Harrop, B. E., & Hartmann, D. L. (2016). The role of cloud radiative heating in determining the location of the itcz in aquaplanet simulations. *Journal of Climate*, *29*(8), 2741 – 2763.

Hassim, M. E. E., Lane, T. P., & Grabowski, W. W. (2016). The diurnal cycle of rainfall over new guinea in convection-permitting wrf simulations. *Atmospheric Chemistry and Physics*, *16*(1), 161–175.

Hawcroft, M., Haywood, J. M., Collins, M., Jones, A., Jones, A. C., & Stephens, G. (2017). Southern ocean albedo, inter-hemispheric energy transports and the double ITCZ: Global impacts of biases in a coupled model. *Climate Dynamics*, *48*(7), 2279–2295.

Held, I. M., & Hou, A. Y. (1980). Nonlinear axially symmetric circulations in a nearly inviscid atmosphere. *Journal of the Atmospheric Sciences*, *37*, 515–533.

Hendon, H. H., & Salby, M. L. (1994). The Life Cycle of the Madden–Julian Oscillation. *Journal of the Atmospheric Sciences*, *51*(15), 2225–2237.

Herman, M. J., & Raymond, D. J. (2014). Wtg cloud modeling with spectral decomposition of heating. *Journal of Advances in Modeling Earth Systems*, *6*(4), 1121–1140.

Hess, P. G., Battisti, D. S., & Rasch, P. J. (1993). Maintenance of the inter-tropical convergence zones and the tropical circulation on a water-covered earth. *Journal of the Atmospheric Sciences*, *50*, 691–713.

Hidayat, R., & Kizu, S. (2010). Influence of the madden–julian oscillation on indonesian rainfall variability in austral summer. *International Journal of Climatology*, *30*(12), 1816–1825.

Hirota, N., Takayabu, Y. N., Watanabe, M., Kimoto, M., & Chikira, M. (2014). Role of convective entrainment in spatial distributions of and temporal variations in precipitation over tropical oceans. *Journal of Climate*, *27*(23), 8707–8723.

Hohenegger, C., & Stevens, B. (2016). Coupled radiative convective equilibrium simulations with explicit and parameterized convection. *Journal of Advances in Modeling Earth Systems*, *8*(3), 1468–1482.

Holloway, C. E., & Neelin, J. D. (2009). Moisture vertical structure, column water vapor, and tropical deep convection. *Journal of the Atmospheric Sciences*, *66*(6), 1665 – 1683.

Holloway, C. E., Wing, A. A., Bony, S., Muller, C., Masunaga, H., L'Ecuyer, T. S., Turner, D. D., & Zuidema, P. (2018). Observing convective aggregation. In R. Pincus, D. Winker, S. Bony, & B. Stevens (Eds.) *Shallow Clouds, Water Vapor, Circulation, and Climate Sensitivity*, (pp. 26–62). Cham: Springer International Publishing.

Holloway, C. E., & Woolnough, S. J. (2016). The sensitivity of convective aggregation to diabatic processes in idealized radiative-convective equilibrium simulations. *Journal of Advances in Modeling Earth Systems*, *8*(1), 166–195.

Holloway, C. R., & Neelin, J. D. (2007). The convective cold top and quasi-equilibrium. *Journal of the Atmospheric Sciences*, *64*, 1467–1487.

Hopuare, M., Guglielmino, M., & Ortega, P. (2019). Interactions between intraseasonal and diurnal variability of precipitation in the south central pacific: The case of a small high island, tahiti, french polynesia. *International Journal of Climatology*, *39*(2), 670–686.

Houze, R. A. J. (2004). Mesoscale convective systems. *Reviews of Geophysics*, *42*(4).

Hu, Y., & Fu, Q. (2007). Observed poleward expansion of the hadley circulation since 1979. *Atmospheric Chemistry and Physics*, *7*(19), 5229–5236.

Hubert, L. F., Krueger, A. F., & Winston, J. S. (1969). The double intertropical convergence zone-fact or fiction? *Journal of atmospheric sciences*, *26*, 771–773.

Huffman, G. J., Bolvin, D. T., Braithwaite, D., Hsu, K., Joyce, R., Xie, P., & Yoo, S.-H. (2015). Nasa global precipitation measurement (gpm) integrated multi-satellite retrievals for gpm (imerg). *Algorithm Theoretical Basis Document (ATBD) Version*, *4*(26).

Hung, M.-P., Lin, J.-L., Wang, W., Kim, D., Shinoda, T., & Weaver, S. J. (2013). MJO and convectively coupled equatorial waves simulated by CMIP5 climate models. *Journal of Climate*, *26*(17), 6185–6214.

Hwang, Y.-T., & Frierson, D. M. W. (2013). Link between the double-intertropical convergence zone problem and cloud biases over the southern ocean. *Proceedings of the National Academy of Sciences*, *110*(13), 4935–4940.

Ichikawa, H., & Yasunari, T. (2006). Time–space characteristics of diurnal rainfall over borneo and surrounding oceans as observed by trmm-pr. *Journal of Climate*, *19*(7), 1238 – 1260.

Ichikawa, H., & Yasunari, T. (2007). Propagating diurnal disturbances embedded in the madden-julian oscillation. *Geophysical Research Letters*, *34*(18), L18811.

Ichikawa, H., & Yasunari, T. (2008). Intraseasonal variability in diurnal rainfall over new guinea and the surrounding oceans during austral summer. *Journal of Climate*, *21*(12), 2852 – 2868.

Inoue, K., & Back, L. E. (2017). Gross moist stability analysis: Assessment of satellite-based products in the gms plane. *Journal of the Atmospheric Sciences*, *74*(6), 1819 – 1837.

Jeevanjee, N., & Romps, D. M. (2013). Convective self-aggregation, cold pools, and domain size. *Geophysical Research Letters*, *40*(5), 994–998.

Jiang, X., Li, T., & Wang, B. (2004). Structures and mechanisms of the northward propagating boreal summer intraseasonal oscillation. *Journal of Climate*, *17*, 1022–1039.

Jiang, X., Waliser, D. E., Xavier, P. K., Petch, J., Klingaman, N. P., Woolnough, S. J., Guan, B., Bellon, G., Crueger, T., DeMott, C., Hannay, C., Lin, H., Hu, W., Kim, D., Lappen, C.-L., Lu, M.-M., Ma, H.-Y., Miyakawa, T., Ridout, J. A., Schubert, S. D., Scinocca, J., Seo, K.-H., Shindo, E., Song, X., Stan, C., Tseng, W.-L., Wang, W., Wu, T., Wu, X., Wyser, K., Zhang, G. J., & Zhu, H. (2015). Vertical structure and physical processes of the madden-julian oscillation: Exploring key model physics in climate simulations. *Journal of Geophysical Research: Atmospheres*, *120*(10), 4718–4748.

Johnson, R. H., Rickenbach, T. M., Rutledge, S. A., Ciesielski, P. E., & Schubert, W. H. (1999). Trimodal characteristics of Tropical convection. *Journal of Climate*, *12*(8 PART 1), 2397–2418.

Joyce, R. J., Janowiak, J. E., Arkin, P. A., & Xie, P. (2004). CMORPH : A Method that Produces Global Precipitation Estimates from Passive Microwave and Infrared Data at High Spatial and Temporal Resolution. *Journal of Hydrometeorology*, *5*, 487–503.

Kawai, H., Koshiro, T., & Yukimoto, S. (2021). Relationship between shortwave radiation bias over the southern ocean and the double-intertropical convergence zone problem in mri-esm2. *Atmospheric Science Letters*, *22*(12), e1064.

Kay, J. E., Wall, C., Yettella, V., Medeiros, B., Hannay, C., Caldwell, P., & Bitz, C. (2016). Global climate impacts of fixing the southern ocean shortwave radiation bias in the community earth system model (CESM). *Journal of Climate*, *29*(12), 4617 – 4636.

Keerthi, M. G., Lengaigne, M., Drushka, K., Vialard, J., de Boyer Montegut, C., Pous, S., Levy, M., & Muraleedharan, P. M. (2016). Intraseasonal variability of mixed layer depth in the tropical Indian Ocean. *Climate Dynamics*, *46*(7), 2633–2655.

Khadka, D., Babel, M. S., Abatan, A. A., & Collins, M. (2022). An evaluation of cmip5 and cmip6 climate models in simulating summer rainfall in the southeast asian monsoon domain. *International Journal of Climatology*, *42*(2), 1181–1202.

Khairoutdinov, M., & Emanuel, K. (2013). Rotating radiative-convective equilibrium simulated by a cloud-resolving model. *Journal of Advances in Modeling Earth Systems*, *5*(4), 816–825.

Khairoutdinov, M. F., & Emanuel, K. (2018). Intraseasonal variability in a cloud-permitting near-global equatorial aquaplanet model. *Journal of the Atmospheric Sciences*, *75*(12), 4337 – 4355.

Kikuchi, K. (2021). The boreal summer intraseasonal oscillation (bsiso): A review. *Journal of the Meteorological Society of Japan*, *99*(4), 933–972.

Kiladis, G. N., Straub, K. H., & Haertel, P. T. (2005). Zonal and vertical structure of the madden–julian oscillation. *Journal of the atmospheric sciences*, *62*(8), 2790–2809.

Kiladis, G. N., Wheeler, M. C., Haertel, P. T., Straub, K. H., & Roundy, P. E. (2009). Convectively coupled equatorial waves. *Reviews of Geophysics*, *47*(2).

Kim, J.-E., & Zhang, C. (2021). Core dynamics of the MJO. *Journal of the Atmospheric Sciences*, *78*(1), 229 – 248.

Kiranmayi, L., & Maloney, E. D. (2011). Intraseasonal moist static energy budget in reanalysis data. *Journal of Geophysical Research: Atmospheres*, *116*(D21).

Kirshbaum, D. J., & Smith, R. B. (2009). Orographic precipitation in the tropics: Large-eddy simulations and theory. *Journal of the Atmospheric Sciences*, *66*(9), 2559–2578.

Kuang, Z. (2008). Modeling the interaction between cumulus convection and linear gravity waves using a limited-domain cloud system–resolving model. *Journal of the Atmospheric Sciences*, *65*(2), 576–591.

Kuang, Z. (2018). Linear stability of moist convecting atmospheres. part i: From linear response functions to a simple model and applications to convectively coupled waves. *Journal of the Atmospheric Sciences*, *75*(9), 2889 – 2907.

Kuo, H. L. (1974). Further studies of parameterization of influence of cumulus convection on large-scale flow. *Journal of the Atmospheric Sciences*, *31*, 1232–1240.

Le, P. V. V., Guilloteau, C., Mamalakis, A., & Foufoula-Georgiou, E. (2021). Underestimated MJO variability in CMIP6 models. *Geophysical research letters*, *48*(12), e2020GL092244.

Leroux, S., Bellon, G., Roehrig, R., Caian, M., Klingaman, N. P., Lafore, J.-P., Musat, I., Rio, C., & Tyteca, S. (2016). Inter-model comparison of subseasonal tropical variability in aquaplanet experiments: Effect of a warm pool. *Journal of Advances in Modeling Earth Systems*, *8*(4), 1526–1551.

Li, B., Zhou, L., Qin, J., & Murtugudde, R. (2021). The role of vorticity tilting in northward-propagating monsoon intraseasonal oscillation. *Geophysical Research Letters*, *48*(13), e2021GL093304.

Li, G., & Xie, S.-P. (2014). Tropical biases in CMIP5 multimodel ensemble: The excessive equatorial pacific cold tongue and double ITCZ problems. *Journal of Climate*, *27*(4), 1765–1780.

Li, Y., Wu, J., Luo, J.-J., & Yang, Y. M. (2022). Evaluating the eastward propagation of the MJO in CMIP5 and CMIP6 models based on a variety of diagnostics. *Journal of Climate*, *35*(6), 1719–1743.

Liang, Z., & Wang, D. (2017). Sea breeze and precipitation over hainan island. *Quarterly Journal of the Royal Meteorological Society*, *143*(702), 137–151.

Lin, J. L. (2007). The double-ITCZ problem in IPCC AR4 coupled GCMs: Ocean-atmosphere feedback analysis. *Journal of Climate*, *18*, 4497–4525.

Lin, J. L., Qian, T., Shinoda, T., & Li, S. (2015). Is the Tropical Atmosphere in Convective Quasi-Equilibrium? *Journal of Climate*, *28*(11), 4357–4372.

Lindzen, R. S. (1974). Wave-CISK in the tropics. *Journal of the Atmospheric Sciences*, *31*, 156–179.

Lindzen, R. S., & Hou, A. Y. (1988). Hadley circulations for zonally averaged heating centered off the equator. *Journal of the Atmospheric Sciences*, *45*, 2416–2427.

Lindzen, R. S., & Nigam, S. (1987). On the role of the sea surface temperature gradients in forcing the low-level winds and convergence in the tropics. *Journal of the Atmospheric Sciences*, *44*, 2418–2436.

Lintner, B. R., Bellon, G., Sobel, A. H., Kim, D., & Neelin, J. D. (2012). Implementation of the quasi-equilibrium tropical circulation model 2 (qtcm2): Global simulations and convection sensitivity to free tropospheric moisture. *Journal of Advances in Modeling Earth Systems*, *4*(4).

Love, B. S., Matthews, A. J., & Lister, G. M. S. (2011). The diurnal cycle of precipitation over the maritime continent in a high-resolution atmospheric model. *Quarterly Journal of the Royal Meteorological Society*, *137*(657), 934–947.

Lubis, S. W., & Respati, M. R. (2021). Impacts of convectively coupled equatorial waves on rainfall extremes in java, indonesia. *International Journal of Climatology*, *41*(4), 2418–2440.

Madden, R. A., & Julian, P. R. (1971). Detection of a 40–50 Day Oscillation in the Zonal Wind in the Tropical Pacific. *Journal of the Atmospheric Sciences*, *28*(5), 702–708.

Majda, A. J., & Stechmann, S. N. (2009). The skeleton of tropical intraseasonal oscillations. *Proceedings of the National Academy of Sciences*, *106*(21), 8417–8422.

Majda, A. J., & Stechmann, S. N. (2011). Nonlinear dynamics and regional variations in the MJO skeleton. *Journal of the Atmospheric Sciences*, *68*(12), 3053 – 3071.

Maloney, E., & Sobel, A. H. (2004). Surface fluxes and ocean coupling in the tropical intraseasonal oscillation. *Journal of Climate*, *17*, 4368–4386.

Mapes, B. (1997). Equilibrium Vs. Activation Control of Large-Scale Variations of Tropical Deep Convection. In *The Physics and Parameterization of Moist Atmospheric Convection*, (pp. 321–358). Springer, Dordrecht.

Mapes, B., Tulich, S., Lin, J., & Zuidema, P. (2006). The mesoscale convection life cycle: Building block or prototype for large-scale tropical waves? *Dynamics of atmospheres and oceans*, *42*(1-4), 3–29.

Mapes, B. E. (1998). The large-scale part of tropical mesoscale convective system circulations. *Journal of the Meteorological Society of Japan. Ser. II*, *76*(1), 29–55.

Mapes, B. E. (2000). Convective inhibition, subgrid-scale triggering energy, and stratiform instability in a toy tropical wave model. *Journal of the Atmospheric Sciences*, *57*(10), 1515–1535.

Marshall, J., Donohoe, A., Ferreira, D., & McGee, D. (2014). The ocean's role in setting the mean position of the inter-tropical convergence zone. *Climate Dynamics*, *42*(7), 1967–1979.

Matsuno, T. (1966). Quasi-geostrophic motions in the equatorial area. *Journal of the Meteorological Society of Japan*, *44*(February), 25–43.

Mechoso, C. R., Robertson, A. W., Barth, N., Davey, M. K., Delecluse, P., Gent, P. R., Ineson, S., Kirtman, B., Latif, M., Le Treut, H., Nagai, T., Neelin, J. D., Philander, S. G. H., Polcher, J., Schopf, P. S., Stockdale, T., Suarez, M. J., Terray, L., Thual, O., & Tribbia, J. J. (1995). The seasonal cycle over the tropical Pacific in coupled ocean-atmosphere general circulation models. *Monthly Weather Review*, *123*, 2825–2838.

Merlis, T. M., Zhou, W., Held, I. M., & Zhao, M. (2016). Surface temperature dependence of tropical cyclone-permitting simulations in a spherical model with uniform thermal forcing. *Geophysical Research Letters*, *43*(6), 2859–2865.

Miller, R. L. (1997). Tropical thermostats and low cloud cover. *Journal of Climate*, *10*, 409–440.

Moorthi, S., & Suarez, M. J. (1992). Relaxed Arakawa-Schubert: a parametrization of moist convection for general circulation models. *Monthly Weather Review*, *120*, 978–1002.

Mori, S., Jun-Ichi, H., Tauhid, Y. I., Yamanaka, M. D., Okamoto, N., Murata, F., Sakurai, N., Hashiguchi, H., & Sribimawati, T. (2004). Diurnal land–sea rainfall peak migration over sumatera island, indonesian maritime continent, observed by trmm satellite and intensive rawinsonde soundings. *Monthly Weather Review*, *132*(8), 2021 – 2039.

Muller, C., & Bony, S. (2015). What favors convective aggregation and why? *Geophysical Research Letters*, *42*(13), 5626–5634.

Muller, C., & Held, I. M. (2012). Detailed investigation of the self-aggregation of convection in cloud-resolving simulations. *Journal of the Atmospheric Sciences*, *69*(8), 2551–2565.

Muller, C. J., Back, L. E., O'Gorman, P. A., & Emanuel, K. A. (2009). A model for the relationship between tropical precipitation and column water vapor. *Geophysical Research Letters*, *36*(16).

Muller, C. J., & Romps, D. M. (2018). Acceleration of tropical cyclogenesis by self-aggregation feedbacks. *Proceedings of the National Academy of Sciences*, *115*(12), 2930–2935.

Möbis, B., & Stevens, B. (2012). Factors controlling the position of the intertropical convergence zone on an aquaplanet. *Journal of Advances in Modeling Earth Systems*, *4*(4), M00A04.

Müller, S. K., & Hohenegger, C. (2020). Self-aggregation of convection in spatially varying sea surface temperatures. *Journal of Advances in Modeling Earth Systems*, *12*(1), e2019MS001698.

Neelin, J. D. (1989). On the interpretation of the gill model. *Journal of the Atmospheric Sciences*, *46*, 2466–2468.

Neelin, J. D., & Chou, C. (2001). Mechanisms limiting the southward extent of the South American monsoon. *Geophysical Research Letters*, *28*, 2433–2436.

Neelin, J. D., & Held, I. M. (1987). Modeling Tropical Convergence Based on the Moist Static Energy Budget. *Monthly Weather Review*, *115*(1), 3–12.

Neelin, J. D., Held, I. M., & Cook, K. H. (1987). Evaporation-wind feedback and low frequency variability in the tropical atmosphere. *Journal of the Atmospheric Sciences*, *44*, 2341–2348.

Neelin, J. D., Peters, O., & Hales, K. (2009). The transition to strong convection. *Journal of the Atmospheric Sciences*, *66*(8), 2367 – 2384.

Neelin, J. D., & Yu, J.-Y. (1994). Modes of tropical variability under convective adjustment and the madden–julian oscillation. part i: Analytical theory. *Journal of Atmospheric Sciences*, *51*(13), 1876–1894.

Neelin, J. D., & Zeng, N. (2000). A quasi-equilibrium tropical circulation model - formulation. *Journal of the Atmospheric Sciences*, *57*, 1741–1766.

Nie, J., Boos, W. R., & Kuang, Z. (2010). Observational evaluation of a convective quasi-equilibrium view of monsoons. *Journal of Climate*, *23*(16), 4416 – 4428.

Ogino, S.-Y., Yamanaka, M. D., Mori, S., & Matsumoto, J. (2016). How Much is the Precipitation Amount over the Tropical Coastal Region ? *Journal of Climate*, *29*, 1231–1236.

Ogino, S.-Y., Yamanaka, M. D., Mori, S., & Matsumoto, J. (2017). Tropical Coastal Dehydrator in Global Atmospheric Water Circulation. *Geophysical Research Letters*, *44*(11), 636–643.

Ooyama, K. (1964). A dynamical model for the study of tropical cyclone development. *Geofisica Internacional (Mexico)*, *4*, 187–198.

Oueslati, B., & Bellon, G. (2013a). Convective entrainment and large-scale organization of tropical precipitation: Sensitivity of the CNRM-CM5 hierarchy of models. *Journal of Climate*, *26*(9), 2931–2946.

Oueslati, B., & Bellon, G. (2013b). Tropical precipitation regimes and mechanisms of regime transitions: contrasting two aquaplanet general circulation models. *Climate Dynamics*, *40*(9), 2345–2358.

Oueslati, B., & Bellon, G. (2015). The double ITCZ bias in CMIP5 models: Interaction between sst, large-scale circulation and precipitation. *Climate dynamics*, *44*(3), 585–607.

Patrizio, C. R., & Randall, D. A. (2019). Sensitivity of convective self-aggregation to domain size. *Journal of Advances in Modeling Earth Systems*, *11*(7), 1995–2019.

Pauluis, O. (2004). Boundary layer dynamics and cross-equatorial Hadley circulation. *Journal of the Atmospheric Sciences*, *61*, 1161–1173.

Pazan, S. E., & Meyers, G. (1982). Interannual Fluctuations of the Tropical Pacific Wind Field and the Southern Oscillation. *Monthly Weather Review*, *110*(6), 587–600.

Peatman, S. C., Matthews, A. J., & Stevens, D. P. (2014). Propagation of the madden–julian oscillation through the maritime continent and scale interaction with the diurnal cycle of precipitation. *Quarterly Journal of the Royal Meteorological Society*, *140*(680), 814–825.

Peatman, S. C., Schwendike, J., Birch, C. E., Marsham, J. H., Matthews, A. J., & Yang, G.-Y. (2021). A local-to-large scale view of maritime continent rainfall: Control by enso, mjo, and equatorial waves. *Journal of Climate*, *34*(22), 8933 – 8953.

Peters, O., & Neelin, J. D. (2006). Critical phenomena in atmospheric precipitation. *Nature physics*, *2*(6), 393–396.

Peyrillé, P., & Lafore, J.-P. (2007). An idealized two-dimensional framework to study the west african monsoon. part ii: Large-scale advection and the diurnal cycle. *Journal of the atmospheric sciences*, *64*(8), 2783–2803.

Peyrillé, P., Lafore, J.-P., & Redelsperger, J.-L. (2007). An idealized two-dimensional framework to study the west african monsoon. part i: Validation and key controlling factors. *Journal of the atmospheric sciences*, *64*(8), 2765–2782.

Phadtare, J. A., Fletcher, J. K., Ross, A. N., Turner, A. G., & Schiemann, R. K. H. (2022). Froude-number-based rainfall regimes over the western ghats mountains of india. *Quarterly Journal of the Royal Meteorological Society*, *n/a*(n/a), in press.

Philander, S. G. H. (1983). El Niño Southern Oscillation phenomena. *Nature*, *302*(5906), 295–301.

Pierrehumbert, R. T. (1995). Thermostats, radiator fins, and the local runaway greenhouse. *Journal of the Atmospheric Sciences*, *52*, 1784–1806.

Pierrehumbert, R. T., & Hammond, M. (2019). Atmospheric circulation of tide-locked exoplanets. *Annual Review of Fluid Mechanics*, *51*, 275–303.

Plumb, R. A., & Hou, A. Y. (1992). The response of a zonally symmetric atmosphere to subtropical thermal forcing: Threshold behavior. *Journal of Atmospheric Sciences*, *49*(19), 1790 – 1799.

Polvani, L. M., & Sobel, A. H. (2002). The Hadley Circulation and the Weak Temperature Gradient Approximation. *Journal of the Atmospheric Sciences*, *59*(10), 1744–1752.

Popp, M., & Silvers, L. G. (2017). Double and single itczs with and without clouds. *Journal of Climate*, *30*(22), 9147 – 9166.

Privé, N., & Plumb, R. (2007a). Monsoon dynamics with interactive forcing. Part I: Axisymmetric studies. *Journal of the Atmospheric Sciences*, *64*(5), 1417–1430.

Privé, N., & Plumb, R. (2007b). Monsoon dynamics with interactive forcing. Part II: Impact of eddies and asymmetric geometries. *Journal of the Atmospheric Sciences*, *64*(5), 1431–1442.

Qian, J.-H. (2008). Why precipitation is mostly concentrated over islands in the maritime continent. *Journal of the Atmospheric Sciences*, *65*(4), 1428–1441.

Qian, J.-H., Robertson, A. W., & Moron, V. (2013). Diurnal cycle in different weather regimes and rainfall variability over borneo associated with enso. *Journal of Climate*, *26*(5), 1772 – 1790.

Rajendran, K., & Kitoh, A. (2006). Modulation of tropical intraseasonal oscillations by ocean-atmosphere coupling. *Journal of Climate*, *19(3)*, 366–391.

Rajendran, K., Kitoh, A., & Arakawa, O. (2004). Monsoon low-frequency intraseasonal oscillation and ocean-atmosphere coupling over the Indian Ocean. *Geophysical Research Letters*, *31(2)*, L02210.

Rauniyar, S. P., & Walsh, K. J. (2013). Influence of enso on the diurnal cycle of rainfall over the maritime continent and australia. *Journal of Climate*, *26*(4), 1304–1321.

Rauniyar, S. P., & Walsh, K. J. E. (2011). Scale interaction of the diurnal cycle of rainfall over the maritime continent and australia: Influence of the mjo. *Journal of Climate*, *24*(2), 325 – 348.

Raymond, D. J. (2007). Testing a cumulus parametrization with a cumulus ensemble model in weak-temperature-gradient mode. *Quarterly Journal of the Royal Meteorological Society*, *133*(626), 1073–1085.

Raymond, D. J., & Fuchs-Stone, Ž. (2021). Weak temperature gradient modeling of convection in otrec. *Journal of Advances in Modeling Earth Systems*, *13*(10), e2021MS002557.

Raymond, D. J., & Herman, M. J. (2011). Convective quasi-equilibrium reconsidered. *Journal of Advances in Modeling Earth Systems*, *3*(3).

Raymond, D. J., Sessions, S. L., Sobel, A. H., & Fuchs, Ž. (2009). The mechanics of gross moist stability. *Journal of Advances in Modeling Earth Systems*, *1*(3).

Raymond, D. J., & Zeng, X. (2005). Modelling tropical atmospheric convection in the context of the weak temperature gradient approximation. *Quarterly Journal of the Royal Meteorological Society*, *126*, 1301–1320.

Reboredo, B., & Bellon, G. (2022). Scale sensitivity of the Gill circulation, Part I: equatorial case. *Journal of the Atmospheric Sciences*, *79*, 1–17.

Redelsperger, J.-L., Brown, P., Guichard, F., How, C., Kawasima, M., Lang, S., Montmerle, T., Nakamura, K., Saito, K., Seman, C., et al. (2000). A gcss model intercomparison for a tropical squall line observed during toga-coare. i: Cloud-resolving models. *Quarterly Journal of the Royal Meteorological Society*, *126*(564), 823–863.

Ren, P., Kim, D., Ahn, M.-S., Kang, D., & Ren, H.-L. (2021). Intercomparison of mjo column moist static energy and water vapor budget among six modern reanalysis products. *Journal of Climate*, *34*(8), 2977 – 3001.

Rio, C., Del Genio, A. D., & Hourdin, F. (2019). Ongoing breakthroughs in convective parameterization. *Current Climate Change Reports*, *5*, 95–111.

Romps, D. M. (2012a). Numerical tests of the weak pressure gradient approximation. *Journal of the atmospheric sciences*, *69*(9), 2846–2856.

Romps, D. M. (2012b). Weak pressure gradient approximation and its analytical solutions. *Journal of the atmospheric sciences*, *69*(9), 2835–2845.

Romps, D. M. (2014). Rayleigh damping in the free troposphere. *Journal of the Atmospheric Sciences*, *71*(2), 553 – 565.

Romps, D. M. (2021). Ascending columns, wtg, and convective aggregation. *Journal of the Atmospheric Sciences*, *78*(2), 497 – 508.

Rostami, M., & Zeitlin, V. (2019). Eastward-moving convection-enhanced modons in shallow water in the equatorial tangent plane. *Physics of Fluids*, *31*(2), 021701.

Roxy, M., & Tanimoto, Y. (2007). Role of SST over the Indian ocean in influencing the intraseasonal variability of the Indian summer monsoon. *Journal of the Meteorological Society of Japan*, *85(3)*, 349–358.

Ruppert, J. H. J. (2016). Diurnal timescale feedbacks in the tropical cumulus regime. *Journal of Advances in Modeling Earth Systems*, *8*(3), 1483–1500.

Ruppert, J. H. J., & Johnson, R. H. (2016). On the cumulus diurnal cycle over the tropical warm pool. *Journal of Advances in Modeling Earth Systems*, *8*(2), 669–690.

Sabeerali, C., Ramu Dandi, A., Dhakate, A., Salunke, K., Mahapatra, S., & Rao, S. A. (2013). Simulation of boreal summer intraseasonal oscillations in the latest CMIP5 coupled GCMs. *Journal of Geophysical Research: Atmospheres*, *118*(10), 4401–4420.

Sakaeda, N., Kiladis, G., & Dias, J. (2017). The diurnal cycle of tropical cloudiness and rainfall associated with the madden–julian oscillation. *Journal of Climate*, *30*(11), 3999 – 4020.

Sakaeda, N., Kiladis, G., & Dias, J. (2020). The diurnal cycle of rainfall and the convectively coupled equatorial waves over the maritime continent. *Journal of Climate*, *33*(8), 3307 – 3331.

Sakaeda, N., & Torri, G. (2022). The behaviors of intraseasonal cloud organization during dynamo/amie. *Journal of Geophysical Research: Atmospheres*, *127*(7), e2021JD035749.

Samuels, M., Adam, O., & Gildor, H. (2021). A shallow thermocline bias in the southern tropical pacific in CMIP5/6 models linked to double-ITCZ bias. *Geophysical Research Letters*, *48*(15), e2021GL093818.

Satoh, M., Noda, A. T., Seiki, T., Chen, Y.-W., Kodama, C., Yamada, Y., Kuba, N., & Sato, Y. (2018). Toward reduction of the uncertainties in climate sensitivity due to cloud processes using a global non-hydrostatic atmospheric model. *Progress in Earth and Planetary Science*, *5*(1), 1–29.

Schneider, E. K. (2002). Understanding differences between the equatorial pacific as simulated by two coupled gcms. *Journal of Climate*, *15*(5), 449 – 469.

Schumacher, R. S., & Rasmussen, K. L. (2020). The formation, character and changing nature of mesoscale convective systems. *Nature Reviews Earth & Environment*, *1*(6), 300–314.

Sessions, S. L., Herman, M. J., & Sentić, S. (2015). Convective response to changes in the thermodynamic environment in idealized weak temperature gradient simulations. *Journal of Advances in Modeling Earth Systems*, *7*(2), 712–738.

Sessions, S. L., Sugaya, S., Raymond, D. J., & Sobel, A. H. (2010). Multiple equilibria in a cloud resolving model. *Journal of Geophysical Research - Atmospheres*, *115*(D12).

Shamekh, S., Muller, C., Duvel, J.-P., & d'Andrea, F. (2020a). How do ocean warm anomalies favor the aggregation of deep convective clouds? *Journal of the Atmospheric Sciences*, *77*(11), 3733–3745.

Shamekh, S., Muller, C., Duvel, J.-P., & d'Andrea, F. (2020b). Self-aggregation of convective clouds with interactive sea surface temperature. *Journal of Advances in Modeling Earth Systems*, *12*(11), e2020MS002164.

Shi, X., & Bretherton, C. S. (2014). Large-scale character of an atmosphere in rotating radiative-convective equilibrium. *Journal of Advances in Modeling Earth Systems*, *6*(3), 616–629.

Short, E., Vincent, C. L., & Lane, T. P. (2019). Diurnal cycle of surface winds in the maritime continent observed through satellite scatterometry. *Monthly Weather Review*, *147*(6), 2023 – 2044.

Showman, A. P., & Polvani, L. M. (2010). The Matsuno-Gill model and equatorial superrotation. *Geophysical Research Letters*, *37*(18).

Showman, A. P., & Polvani, L. M. (2011). Equatorial superrotation on tidally locked exoplanets. *The Astrophysical Journal*, *738*(1), 71.

Si, W., Liu, H., Zhang, X., & Zhang, M. (2021). Double intertropical convergence zones in coupled ocean-atmosphere models: Progress in cmip6. *Geophysical Research Letters*, *48*(23), e2021GL094779.

Siebesma, A. P., Bretherton, C., Brown, A., Chlond, A., Cuxart, J., Duynkerke, P. G., Jiang, H. L., Khairoutdinov, M., Lewellen, D., Moeng, C. H., Sanchez, E., Stevens, B., & Stevens, D. E. (2003). A large eddy simulation intercomparison study of shallow cumulus convection. *Journal of the Atmospheric Sciences*, *60*, 1201–1219.

Singh, M. S. (2019). Limits on the extent of the solsticial hadley cell: The role of planetary rotation. *Journal of the Atmospheric Sciences*, *76*(7), 1989 – 2004.

Singh, M. S., & Kuang, Z. (2016). Exploring the role of eddy momentum fluxes in determining the characteristics of the equinoctial hadley circulation: Fixed-sst simulations. *Journal of the Atmospheric Sciences*, *73*(6), 2427 – 2444.

Singh, M. S., & Neogi, S. (2022). On the interaction between moist convection and large-scale ascent in the tropics. *Journal of Climate*, (pp. 1 – 47).

Smith, R. B., Schafer, P., Kirshbaum, D. J., & Regina, E. (2009). Orographic precipitation in the tropics: Experiments in dominica. *Journal of the atmospheric sciences*, *66*(6), 1698–1716.

Sobel, A., Maloney, E., Bellon, G., & Frierson, D. (2008). The role of surface heat fluxes in tropical intraseasonal oscillations. *Nature Geoscience*, *1*(10), 653–657.

Sobel, A., Maloney, E., Bellon, G., & Frierson, D. (2010). Surface fluxes and tropical intraseasonal variability: a reassessment. *Journal of Advances in Modeling Earth Systems*, *2*.

Sobel, A., Wang, S., & Kim, D. (2014). Moist static energy budget of the mjo during dynamo. *Journal of the Atmospheric Sciences*, *71*(11), 4276 – 4291.

Sobel, A. H., & Bellon, G. (2009). The effect of imposed drying on parameterized deep convection. *Journal of the Atmospheric Sciences*, *66*, 2085–2096.

Sobel, A. H., Bellon, G., & Bacmeister, J. T. (2007). Multiple equilibria in a single-column model of the tropical atmosphere. *Geophysical Research Letters*, *34*, L22804.

Sobel, A. H., & Bretherton, C. S. (2000). Modeling tropical precipitation in a single column. *Journal of Climate*, *13*(24), 4378 – 4392.

Sobel, A. H., Burleyson, C. D., & Yuter, S. E. (2011). Rain on small tropical islands. *Journal of Geophysical Research Atmospheres*, *116*(8), 1–15.

Sobel, A. H., & Gildor, H. (2003). A simple time-dependent model of SST hot spots. *Journal of Climate*, *16*, 3978–3992.

Sobel, A. H., & Maloney, E. (2012). An Idealized Semi-Empirical Framework for Modeling the Madden–Julian Oscillation. *Journal of the Atmospheric Sciences*, *69*(5), 1691–1705.

Sobel, A. H., & Maloney, E. (2013). Moisture modes and the eastward propagation of the MJO. *Journal of the Atmospheric Sciences*, *70*(1), 187–192.

Sobel, A. H., & Neelin, J. D. (2006). The boundary layer contribution to intertropical convergence zones in the quasi-equilibrium tropical circulation model framework. *Theoretical and Computational Fluid Dynamics*, *20*, 323–350.

Sobel, A. H., Nilsson, J., & Polvani, L. M. (2001). The weak temperature gradient approximation and balanced tropical moisture waves. *Journal of the atmospheric sciences*, *58*(23), 3650–3665.

Song, X., & Zhang, G. J. (2018). The roles of convection parameterization in the formation of double ITCZ syndrome in the NCAR CESM: I. atmospheric processes. *Journal of Advances in Modeling Earth Systems*, *10*(3), 842–866.

Specq, D., Bellon, G., Peltier, A., Lefèvre, J., & Menkes, C. (2020). Influence of subseasonal variability on the diurnal cycle of precipitation on a mountainous island: The case of new caledonia. *Monthly Weather Review*, *148*(1), 333 – 351.

Staten, P. W., Lu, J., Grise, K. M., Davis, S. M., & Birner, T. (2018). Re-examining tropical expansion. *Nature Climate Change*, *8*(9), 768–775.

Stephens, G. L., Hakuba, M. Z., Hawcroft, M., Haywood, J. M., Behrangi, A., Kay, J. E., & Webster, P. J. (2016). The curious nature of the hemispheric symmetry of the earth's water and energy balances. *Current Climate Change Reports*, *2*(4), 135–147.

Stevens, B. (2005). Atmospheric moist convection. *Annu. Rev. Earth Planet. Sci.*, *33*, 605–643.

Stevens, B., Duan, J., McWilliams, J. C., Munnich, M., & Neelin, J. D. (2002). Entrainment, Rayleigh friction, and boundary layer winds over the tropical Pacific. *Journal of Climate*, *15*, 30–44.

Su, H., Jiang, J. H., Neelin, J. D., Shen, T. J., Zhai, C., Yue, Q., Wang, Z., Huang, L., Choi, Y.-S., Stephens, G. L., et al. (2017). Tightening of tropical ascent and high clouds key to precipitation change in a warmer climate. *Nature communications*, *8*(1), 1–9.

Sugiyama, M. (2009). The moisture mode in the quasi-equilibrium tropical circulation model. part i: Analysis based on the weak temperature gradient approximation. *Journal of the atmospheric sciences*, *66*(6), 1507–1523.

Takahashi, K., & Battisti, D. S. (2006). Processes controlling the mean tropical Pacific precipitation pattern: I. the Andes and the eastern Pacific ITCZ. *Journal of Climate*, *20*, 3434–3451.

Thual, S., Majda, A. J., & Stechmann, S. N. (2014). A stochastic skeleton model for the MJO. *Journal of the Atmospheric Sciences*, *71*(2), 697 – 715.

Tian, B., & Dong, X. (2020). The double-itcz bias in cmip3, cmip5, and cmip6 models based on annual mean precipitation. *Geophysical Research Letters*, *47*(8), e2020GL087232.

Tobin, I., Bony, S., & Roca, R. (2012). Observational evidence for relationships between the degree of aggregation of deep convection, water vapor, surface fluxes, and radiation. *Journal of Climate*, *25*(20), 6885 – 6904.

Tompkins, A. M. (2001). Organization of tropical convection in low vertical wind shears: The role of cold pools. *Journal of the Atmospheric Sciences*, *58*(13), 1650–1672.

Tompkins, A. M., & Craig, G. C. (1998). Radiative–convective equilibrium in a three-dimensional cloud-ensemble model. *Quarterly Journal of the Royal Meteorological Society*, *124*(550), 2073–2097.

Tompkins, A. M., & Semie, A. G. (2017). Organization of tropical convection in low vertical wind shears: Role of updraft entrainment. *Journal of Advances in Modeling Earth Systems*, *9*(2), 1046–1068.

Tompkins, A. M., & Semie, A. G. (2021). Impact of a mixed ocean layer and the diurnal cycle on convective aggregation. *Journal of Advances in Modeling Earth Systems*, (p. e2020MS002186).

Ulrich, M., & Bellon, G. (2019). Superenhancement of precipitation at the center of tropical islands. *Geophysical Research Letters*, *46*(24), 14872–14880.

Vecchi, G. A., & Harrison, D. E. (2002). Monsoon break and subseasonal sea surface temperature variability in the bay of bengal. *Journal of Climate*, *15*, 1485–1493.

Vincent, C. L., & Lane, T. P. (2016). Evolution of the diurnal precipitation cycle with the passage of a madden–julian oscillation event through the maritime continent. *Monthly Weather Review*, *144*(5), 1983 – 2005.

Vincent, C. L., Lane, T. P., & Wheeler, M. C. (2016). A local index of maritime continent intraseasonal variability based on rain rates over the land and sea. *Geophysical Research Letters*, *43*(17), 9306–9314.

Waliser, D. E., & Somerville, R. C. J. (1994). The preferred latitudes of the intertropical convergence zone. *Journal of the Atmospheric Sciences*, *51*, 1619–1639.

Walker, C. C., & Schneider, T. (2006). Eddy influences on hadley circulations: Simulations with an idealized gcm. *Journal of the Atmospheric Sciences*, *63*(12), 3333 – 3350.

Wang, B., & Chen, G. (2017). A general theoretical framework for understanding essential dynamics of madden–julian oscillation. *Climate Dynamics*, *49*(7), 2309–2328.

Wang, B., Liu, F., & Chen, G. (2016a). A trio-interaction theory for madden–julian oscillation. *Geoscience Letters*, *3*(1), 1–16.

Wang, S., & Sobel, A. H. (2017). Factors controlling rain on small tropical islands: Diurnal cycle, large-scale wind speed, and topography. *Journal of the Atmospheric Sciences*, *74*(11), 3515–3532.

Wang, S., & Sobel, A. H. (2022). A unified moisture mode theory for the madden–julian oscillation and the boreal summer intraseasonal oscillation. *Journal of Climate*, *35*(4), 1267–1291.

Wang, S., Sobel, A. H., & Kuang, Z. (2013). Cloud-resolving simulation of toga-coare using parameterized large-scale dynamics. *Journal of Geophysical Research: Atmospheres*, *118*(12), 6290–6301.

Wang, S., Sobel, A. H., & Nie, J. (2016b). Modeling the MJO in a cloud-resolving model with parameterized large-scale dynamics: Vertical structure, radiation, and horizontal advection of dry air. *Journal of Advances in Modeling Earth Systems*, *8*(1), 121–139.

Watterson, I. G., & Syktus, J. (2007). The influence of air-sea interaction on the Madden-Julian oscillation: the role of the seasonal mean state. *Climate Dynamics*, *28*, 703–722.

Wheeler, M., & Kiladis, G. N. (1999). Convectively Coupled Equatorial Waves: Analysis of Clouds and Temperature in the Wavenumber–Frequency Domain. *Journal of the Atmospheric Sciences*, *56*(3), 374–399.

Wheeler, M. C., & Hendon, H. H. (2004). An all-season real-time multivariate MJO index: Development of an index for monitoring and prediction. *Monthly weather review*, *132*(8), 1917–1932.

Williamson, D. L., Blackburn, M., Nakajima, K., Ohfuchi, W., Takahashi, Y. O., Hayashi, Y.-Y., Nakamura, H., Ishiwatari, M., McGREGOR, J. L., Borth, H., et al. (2013). The aqua-planet experiment (ape): response to changed meridional sst profile. *Journal of the Meteorological Society of Japan. Ser. II*, *91*, 57–89.

Wing, A. A., Camargo, S. J., & Sobel, A. H. (2016). Role of radiative–convective feedbacks in spontaneous tropical cyclogenesis in idealized numerical simulations. *Journal of the Atmospheric Sciences*, *73*(7), 2633 – 2642.

Wing, A. A., & Cronin, T. W. (2016). Self-aggregation of convection in long channel geometry. *Quarterly Journal of the Royal Meteorological Society*, *142*(694), 1–15.

Wing, A. A., Emanuel, K., Holloway, C. E., & Muller, C. (2018). Convective self-aggregation in numerical simulations: A review. In R. Pincus, D. Winker, S. Bony, & B. Stevens (Eds.) *Shallow Clouds, Water Vapor, Circulation, and Climate Sensitivity*, (pp. 1–25). Cham: Springer International Publishing.

Wing, A. A., & Emanuel, K. A. (2014). Physical mechanisms controlling self-aggregation of convection in idealized numerical modeling simulations. *Journal of Advances in Modeling Earth Systems*, *6*(1), 59–74.

Wing, A. A., Stauffer, C. L., Becker, T., Reed, K. A., Ahn, M.-S., Arnold, N. P., Bony, S., Branson, M., Bryan, G. H., Chaboureau, J.-P., De Roode, S. R., Gayatri, K., Hohenegger, C., Hu, I.-K., Jansson, F., Jones, T. R., Khairoutdinov, M., Kim, D., Martin, Z. K., Matsugishi, S., Medeiros, B., Miura, H., Moon, Y., Müller, S. K., Ohno, T., Popp, M., Prabhakaran, T., Randall, D., Rios-Berrios, R., Rochetin, N., Roehrig, R., Romps, D. M., Ruppert, J. H. J., Satoh, M., Silvers, L. G., Singh, M. S., Stevens, B., Tomassini, L., van Heerwaarden, C. C., Wang, S., & Zhao, M. (2020). Clouds and convective self-aggregation in a multimodel ensemble of radiative-convective equilibrium simulations. *Journal of Advances in Modeling Earth Systems*, *12*(9), e2020MS002138.

Woolnough, S. J., Slingo, J. M., & Hoskins, B. J. (2000). The relationship between convection and sea surface temperature on intraseasonal timescales. *Journal of Climate*, *13*, 2086–2104.

Wunsch, C., & Gill, A. (1976). Observations of equatorially trapped waves in pacific sea level variations. *Deep Sea Research and Oceanographic Abstracts*, *23*(5), 371–390.

Wyant, M. C., Bretherton, C. S., Chlond, A., Griffin, B. M., Kitagawa, H., Lappen, C. L., Larson, V. E., Lock, A., Park, S., De Roode, S. R., Uchida, J., Zhao, M., & Ackerman, A. S. (2007). A single-column model intercomparison of a heavily drizzling stratocumulus-topped boundary layer. *Journal of Geophysical Research - Atmospheres*, *112*, D24204.

Xiang, B., Zhao, M., Held, I. M., & Golaz, J.-C. (2017). Predicting the severity of spurious "double ITCZ" problem in CMIP5 coupled models from AMIP simulations. *Geophysical Research Letters*, *44*(3), 1520–1527.

Xie, S.-P. (2005). The shape of continents, air-sea interaction, and the rising branch of the Hadley circulation. In H. Diaz, & R. Bradley (Eds.) *The Hadley Circulation: Past, Present and Future*, (pp. 489–511). Cambridge University Press.

Xie, S.-P., & Seki, M. (1997). Causes of equatorial asymmetry in sea surface temperature over the eastern Pacific. *Geophysical Research Letters*, *24*, 2581–2584.

Xu, H. M., Wang, Y. Q., & Xie, S. P. (2004). Effects of the Andes on eastern Pacific climate: A regional atmospheric model study. *Journal of Climate*, *17*, 589–602.

Yanai, M., & Maruyama, T. (1966). Stratospheric wave disturbances propagating over the equatorial pacific. *Journal of the Meteorological Society of Japan. Ser. II*, *44*(5), 291–294.

Yanase, A., Yasunaga, K., & Masunaga, H. (2017). Relationship between the direction of diurnal rainfall migration and the ambient wind over the southern sumatra island. *Earth and Space Science*, *4*(3), 117–127.

Yang, D. (2018a). Boundary layer diabatic processes, the virtual effect, and convective self-aggregation. *Journal of Advances in Modeling Earth Systems*, *10*(9), 2163–2176.

Yang, D. (2018b). Boundary layer height and buoyancy determine the horizontal scale of convective self-aggregation. *Journal of the Atmospheric Sciences*, *75*(2), 469 – 478.

Yang, D. (2021). A shallow-water model for convective self-aggregation. *Journal of the Atmospheric Sciences*, *78*(2), 571 – 582.

Yang, D., & Ingersoll, A. P. (2013). Triggered convection, gravity waves, and the MJO: A shallow-water model. *Journal of the atmospheric sciences*, *70*(8), 2476–2486.

Yang, D., & Ingersoll, A. P. (2014). A theory of the MJO horizontal scale. *Geophysical Research Letters*, *41*(3), 1059–1064.

Yano, J.-I., & Bonazzola, M. (2009). Scale analysis for large-scale tropical atmospheric dynamics. *Journal of the Atmospheric Sciences*, *66*(1), 159 – 172.

Yano, J.-I., Liu, C., & Moncrieff, M. W. (2012). Self-organized criticality and homeostasis in atmospheric convective organization. *Journal of the Atmospheric Sciences*, *69*(12), 3449 – 3462.

Yano, J. I., & Plant, R. S. (2012). Convective quasi-equilibrium. *Reviews of Geophysics*, *50*(4).

Yano, J.-I., & Tribbia, J. J. (2017). Tropical Atmospheric Madden–Julian Oscillation: A Strongly Nonlinear Free Solitary Rossby Wave? *Journal of the Atmospheric Sciences*, *74*(10), 3473–3489.

Yokoi, S., Mori, S., Katsumata, M., Geng, B., Yasunaga, K., Syamsudin, F., Nurhayati, & Yoneyama, K. (2017). Diurnal cycle of precipitation observed in the western coastal area of sumatra island: Offshore preconditioning by gravity waves. *Monthly Weather Review*, *145*(9), 3745 – 3761.

Zhang, C. (2001). Double itczs. *Journal of Geophysical Research: Atmospheres*, *106*(D11), 11785–11792.

Zhang, C. (2005). Madden-Julian Oscillation. *Reviews of Geophysics*, *43*(2), RG2003.

Zhang, C., Adames, Á. F., Khouider, B., Wang, B., & Yang, D. (2020). Four theories of the Madden-Julian Oscillation. *Reviews of Geophysics*, *58*(3).

Zhang, C., Mapes, B. E., & Soden, B. J. (2003). Bimodality in tropical water vapour. *Quarterly Journal of the Royal Meteorological Society*, *129*, 2849–2866.

Zhang, C., McGauley, M., & Bond, N. A. (2004). Shallow meridional circulation in the tropical eastern pacific. *Journal of climate*, *17*(1), 133–139.

Zhang, C., Nolan, D. S., Thorncroft, C. D., & Nguyen, H. (2008). Shallow meridional circulations in the tropical atmosphere. *Journal of Climate*, *21*(14), 3453 – 3470.

Zhang, X., Liu, H., & Zhang, M. (2015). Double itcz in coupled ocean-atmosphere models: From cmip3 to cmip5. *Geophysical Research Letters*, *42*(20), 8651–8659.

Zhou, L., & Wang, Y. (2006). Tropical rainfall measuring mission observation and regional model study of precipitation diurnal cycle in the new guinean region. *Journal of Geophysical Research: Atmospheres*, *111*(D17).

Zhou, W., Held, I. M., & Garner, S. T. (2014). Parameter study of tropical cyclones in rotating radiative–convective equilibrium with column physics and resolution of a 25-km GCM. *Journal of the Atmospheric Sciences*, *71*(3), 1058 – 1069.

Zhu, H., & Sobel, A. H. (2012). Comparison of a single-column model in weak temperature gradient mode to its parent AGCM. *Quarterly Journal of the Royal Meteorological Society*, *138*(665), 1025–1034.

Zhu, L., Meng, Z., Zhang, F., & Markowski, P. M. (2017). The influence of sea-and land-breeze circulations on the diurnal variability in precipitation over a tropical island. *Atmospheric Chemistry and Physics*, *17*(21), 13213–13232.